MEDIUM POWER STABLE LASERS FOR HIGH PRECISION METROLOGY

by

David Ottaway

Thesis submitted for the degree of

Doctor of Philosophy

in

The University of Adelaide

(Department of Physics and Mathematical Physics)

December, 1998

This work contains no material which has been accepted for the award of any other degree or diploma in any university or other tertiary institution and, to the best of my knowledge and belief, contains no material previously published or written by another person, except where due reference has been made in the text. All electronic circuitry described in this thesis was designed and constructed by myself unless otherwise stated.

I give consent to this copy of my thesis, when deposited in the University Library, being available for loan and photocopying.

DATE: 16/2/99

Supervisors: Dr. P. Veitch, Dr. M. Hamilton and Prof. J. Munch

Acknowledgments

Throughout the course of my graduate education there have been many people who have shared my joy when things have been going well and have cheered me up when things were not going to plan.

Firstly I would like to thank my parents, Ric and Libby Ottaway who were always there for support and advice. Toward the end they were a constant source of 'encouragement', when they could be relied upon to regularly ask "when on earth will that PhD be finished?".

To my supervisors: Dr Peter Veitch who has been my supervisor since I joined the group in Honours, he has been a constant source of encouragement and guidance. Dr Murray Hamilton who has helped me to understand various aspects of laser physics. Prof. Jesper Munch who will hopefully one day heed my advice and just go out and buy that yacht he always talks about. His constant pushing to improve my results and presentation has greatly enhanced the quality of this work.

To Jim Richard from DSTO, inventor of the CPFS laser. His excitement for the development of these laser systems is infectious and he was a great source of ideas. I would also like to thank Alisdair McInnes also from DSTO for his helpful input to this work.

The members of the Optics group: Patrick Klovekorn who suffered many of the problems one year ahead of me, if only I had taken more notice of the forewarning. Kerry Corbett who suffered many of the same problems at the same time as me and was a great source of support whilst writing up. Damien Mudge whose work had many similarities to my own and was a great person to share ideas with. Blair Middlemiss, the optics group technician extraordinaire whose technical ability and advice saved me a great deal of time and frustration. Chris Hollit whose electrical engineering abilities and advice was invaluable. Yuri, Geoff, Petar, Peter Foster, Alex (Bill) , Shu, Thulan, Tim, Laurence, Renus, Rob, Heather, Mary and the rest of optics group who made the optics group a very pleasant and interesting place to work. Also thanks to Neville Wild, Mike Shorthose, Bob Hurn and John Smith for

technical assistance.

To my many friends at the Adelaide Uni dive club and the skipper and crew of the yacht RAGER who provided me with a very enjoyable and positive distraction to my graduate studies. To my many other friends who have supported me when the going got tough, in paticular all the Daves, Squid, John, Sarah and Grant.

Finally I would like to express by gratitude to two very important friends: Firstly, Nick Vandegraaff who has always known the "exact" time to drag me off to the pub and help me to understand many of lifes problem. Juanita Cabot who has been a constant source of love and understanding and has an inexhaustible supply of listening ability when I really needed it.

The research presented in this thesis has been supported by the Australian Research Council (ARC) and in part by DSTO. I have also been the fortunate recipient of a University of Adelaide postgraduate scholarship.

Abstract

Medium power (5-10W) single frequency lasers with low intensity and frequency noise, plus good beam quality are required for a range of high precision metrology applications. Examples of such applications include laser interferometric detection of gravitational waves and long range vibrometry. In this thesis I will describe the development of a compact and efficient, single frequency, injection-locked, 5 W Nd:YAG laser. The laser output is close to diffraction limited with M^2 values of 1.0 and 1.2 in the horizontal and vertical planes respectively.

The slave laser is a diode pumped slab laser based on the co-planar pumped folded zig-zag slab laser geometry. The slab is side pumped using a single twenty watt laser diode array collimated by a Doric fibre lens. The slab is tranversely cooled using Peltier cells that are air cooled.

We use injection-locking to force single frequency operation and to transfer the frequency stability of the monolithic Non Planar Ring Oscillator (NPRO) master laser to the output of our slave laser. The inherrent stability of the slave laser allows injection-locking for periods of up to 30 s without the use of servo control. We achieve long term injection-locking by controlling the slave laser resonator using a Pound Drever Hall frequency control servo system.

A heterodyne technique is used to study the phase fidelity of our injection-locked laser compared to that of our master laser. We show that the slave laser contribution to the frequency noise of our injection-locked laser is negligible compared with the frequency noise of the free running master laser. This is in good agreement with theory.

The relative intensity noise of the injection-locked slave has also been measured and is less than $10^{-5}/\sqrt{Hz}$ at low frequencies. Further intensity noise reduction, in excess of an order of magnitude at low frequencies, has been achieved by electronic feedback to the slave laser pump source (a high power multi-emitter diode linear array). The laser is shot-noise limited above 5 MHz for 6 mA of detected photo-current.

List of Symbols

$G(s)$	...	Gain of a system
$\Delta\nu_l$	...	The full injection-locking range
$\Delta\nu_c$	...	The cold cavity linewidth of the slave laser resonator
FSR	...	Free spectral range of the slave laser resonator
T	...	Transmission of the output coupler of the slave laser
P_m	...	Power of the master laser
P_s	...	Power of the slave laser
L_{total}	...	Round trip loss of a resonator excluding output coupler loss
$g_0 l$	...	Small signal gain-length product
$\Delta\phi(t)$	...	Phase difference between the master and the injection-locked slave
γ_e	...	Cavity decay rate due to the output coupler
γ_c	...	Total cavity decay rate
γ_m	...	Rate of growth of the cavity field due to the saturated laser gain
γ_2	...	Rate of depopulation of the upper lasing state due to spontaneous emission
τ_c	...	Cavity round trip time
$H_m(\omega)$	...	Transfer fuction for master laser frequency noise to injection-locked laser frequency noise
$H_s(\omega)$	...	Transfer fuction for slave laser frequency noise to injection-locked laser frequency noise
$S_{f,m}(\omega)$	...	Spectral density of master laser frequency noise
$S_{f,fr(slave)}(\omega)$	...	Spectral density of slave laser frequency noise
$S_{f,servo}(\omega)$	...	Spectral density function of slave laser frequency noise with servo loop noise reduction
$S_{f,il(slave)}(\omega)$	...	Spectral density of the slave laser contribution to the injection-locked laser frequency noise

Contents

Chapter 1

Introduction

Building lasers that are multi-watt, single frequency and user-friendly is a complex problem. Such lasers are required for a range of applications, including high precision interferometry and field based vibrometry. An extremely demanding application is their use in the detection of gravitational radiation. This thesis discusses the development of a new, more compact and efficient, 5 Watt, diode pumped, single frequency Nd:YAG laser.

In Chapter 1 I will review the progress in the field of medium to high power, single frequency, diffraction limited solid-state lasers and a few of their applications. In Chapter 2 the design of the slave laser that is an optimum mix of efficiency and inherent stability will be examined. In Chapter 3 the injection locking experiments will be discussed, and in Chapter 4 intensity and frequency noise of the injection-locked laser will be discussed.

I will begin this chapter with an overview of the techniques of obtaining multi-watt single frequency solid state lasers Then I will discuss the particular use of these lasers in the interferometric detection of gravitational waves and field based vibrometry. The laser performance criteria for these applications will also be discussed. In the design of stable laser systems active control of various parameters is required. I will therefore finish this section with a general introduction to control theory, providing the necessary theoretical background to design the various stabilization systems used in this work.

1.1 Multi-watt single frequency solid-state lasers

Early work on frequency stabilized lasers was done predominantly for gas and dye lasers[1][2][3][4] [5][6][7][8][9] [10][11][12] Lamp pumped solid-state laser systems were unattractive for stable laser applications due to the large amount of noise generated by the inefficiency of lamp pumping. More recently, advances in diode laser pumping enabled solid state lasers to be attractive for stabilization.

In 1986 Kane and Byer [13] invented a monolithic Non Planar Ring Oscillator (NPRO) solid state laser. This monolithic laser uses a magnetic field applied to the Nd:YAG medium to produce Faraday rotation of the resonator mode polarization. The out of plane resonator geometry provides polarization rotation that cancels the Faraday rotation in one direction and exacerbates it in the other. Hence uni-directional lasing in the monolithic ring oscillator is generated. The uni-directional ring nature of the laser enables a travelling laser mode to be produced which reduces the effects of spatial holeburning compared with standing wave lasers. The laser resonator is also compact, ensuring a large spacing between the axial modes and thus limiting the number of these modes within the Nd:YAG linewidth. This along with the significant reduction in spatial holeburning effects results in a single frequency output. The monolithic resonator significantly reduces the effects of environmental technical noise on the laser, and this laser is thus one of the most inherently frequency stable lasers available [14]. Further, the uni-directional nature of the laser significantly reduces its sensitivity to output being scattered back into the laser resonator. This is a major cause of instability in standing wave lasers.

The free running frequency stability of these solid-state NPRO lasers has been measured using a heterodyne beat experiment between two independent oscillators [14]. The resulting beat note linewidth was found to be less than 3kHz for a 100mS measurement time. Further work by Fritschel et al. [15] showed that the frequency noise of these lasers approached the fundamental Schawlow and Townes limit above 80kHz. For frequencies below 80 kHz, the frequency noise is limited by pump amplitude fluctuations[16]. These pump fluctuations perturb the optical path length of the laser, which produces excess frequency noise. Another measure of the frequency stability is the coherence length which is greater than 1500 km [17].

The frequency of monolithic NPRO lasers has been actively stabilized by locking the lasers to a high finesse Fabry-Perot reference cavity[18] [19][16][20][21][22][23][24][25][26] [28], using the Pound-Drever-Hall technique[10][29]. Day et al.[16] demonstrated that the beatnote between two stabilized monolithic NPRO lasers had a linewidth of 330 mHz. This result was achieved by locking the two lasers to adjacent axial modes of a single high finesse cavity. Using a single reference cavity enabled common-mode rejection of reference cavity noise. However, the width of the beatnote is larger than the predicted shot-noise-limited performance. Even with the common-mode rejection of reference cavity noise, it was thought that the locked laser stability and the beatnote width were limited by the stability of the reference cavity.

Later experiments improved the stability of the reference cavity using passive noise reduction techniques (such as acoustic and vibration isolation) [23][24][26][28]. Sandford and Antil[25] locked two lasers to adjacent axial modes of a reference cavity and the beat signal between the two lasers was then compared to a stable microwave source. The error signal was then used to actively stabilize the high finesse reference cavity and a beatnote with a linewidth of less than 4mHz was achieved. Uehara and Ueda[22] increased the detected reference power by combining the output of several photodiodes and hence reduced the shot-noise limit. A shot-noise-limited frequency stability at 100 Hz of $4.2\times10^{-5}Hz/\sqrt{Hz}$ relative to the reference cavity was achieved. Even better stability may be achieved when narrower linewidth cavities are used, such as the pre-stabilization cavities that will be used on the laser interferometric gravitational wave detectors. Indeed, the use of a 10m reference cavity enabled an argon ion laser to be stabilized to a relative stability of a few $\times\ 10^{-5}\ Hz/\sqrt{Hz}$[30], even though such lasers have orders of magnitude more frequency noise than monolithic NPROs when free running [30]. To achieve absolute long term stability a monolithic NPRO was frequency doubled and its frequency was then compared and locked to a hyperfine transition in molecular iodine[31].

Although the monolithic NPRO laser is extremely stable and efficient, its end-pumped architecture limits the maximum available output power from a single device. The highest published output power of a monolithic NPRO is 1.8 Watts[32].

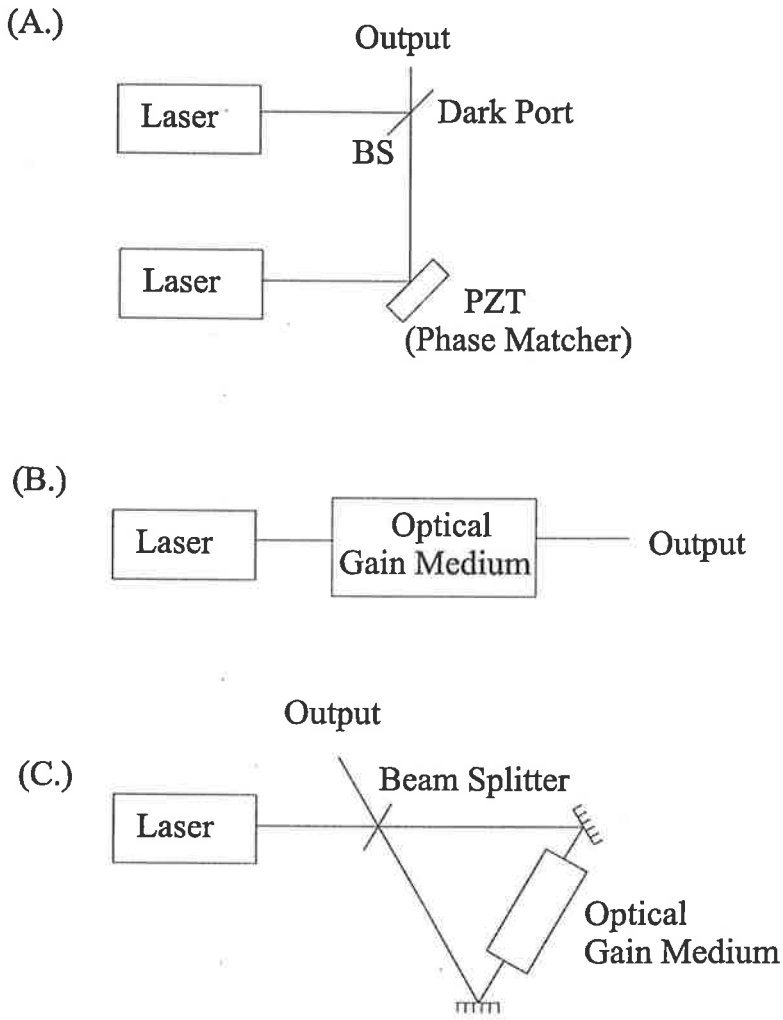

Figure 1.1: Schematic of (A) Coherrent addition, (B) Optical amplifier and (C) Injection locking or below threshold regenerative amplification depending on the reflectivity of the beam splitter

To increase the power and maintain the stability of the monolithic laser, there are 4 possible choices, as illustrated in Figure 1.1.

- Coherent addition of the outputs from several lasers
- Master Oscillator Power Amplifier (MOPA)
- Below threshold regenerative amplification
- Injection-locking of a high power laser oscillator

Coherent addition of several laser sources has been demonstrated for Argon-ion lasers[33][34], HeNe lasers[35], diode lasers[36] and diode pumped Nd:YAG lasers[37][38].

This technique spatially overlaps a series of laser beams using binary phase gratings [38][36][35]or beam splitters [33][34]. To achieve good efficiency, the lasers that are combined must have high mutual coherence and be phase matched at the point of combination. Mutual coherence is achieved by the electronic locking of one laser resonator to another[33] or by deliberate leakage of the light field from one laser into the resonators of the other lasers (injection locking)[33][34], or multiple beams sharing the same resonator[36] . Phase matching is often achieved by path length adjustment, sometimes using active control involving a piezo electric transducer (PZT) [33][34][38]. Very high efficiencies have been reported; Menard et al.[37] report coherent addition of two diode-pumped Nd:YAG lasers with an efficiency of 96.8%. Veldkamp et al. [35] performed a proof of principle experiment, recombining seven laser beams originally split from the same laser beam with an efficiency of 75%. Although this method can be efficient, it would be quite complicated to combine enough monolithic NPROs using this method to generate significant power levels.

An alternative means of increasing the output power of a low power single frequency monolithic NPRO is to use an optical power amplifier. One means of doing this is the Master Oscillator Power Amplifier (MOPA) scheme. This technique is best used in high power systems where the amplifiers can be well saturated. However a cw MOPA laser [39]developed by Lightwave Electronics Corporation was recently manufactured for the Laser Interferometer Gravitational-Wave Observatory (LIGO) project[40]. This laser amplifies a 1 W master laser using four double-passed amplifier stages, producing 10 Watts of output power. The optical amplifiers used in MOPA systems are broadband devices and hence accurate control of the frequency response of the device is not required. However, at the 1 W input power level it is difficult to fully saturate the amplifier gain medium. This has two undesirable effects; firstly, the amplifier adds excess noise to the master oscillator beam because of amplified spontaneous emission (ASE) due to unsaturated gain. Secondly, unsaturated gain leads to poor power extraction from the gain medium leading to reduced efficiency. An additional problem with amplifiers is the possibility of wave-front distortion which leads to a reduction in beam quality.

Below-threshold regenerative amplification involves putting a resonator around

the optical amplifer as illustrated in Figure 1.1. This provides positive feedback to the amplifier for frequencies around the resonant frequencies of the resonator and hence the gain is increased with a corresponding reduction in bandwidth. The feedback is chosen such that the regenerative amplifier is just below threshold and hence does not self oscillate. This scheme has the advantage of increased power gain from normally low gain Nd:YAG amplifiers and hence increased energy extraction from the optical gain medium. The obvious trade-off for this increase in gain is the need to keep the resonator resonant at the master laser frequency. Hence the additional complication of servo control of the resonator of the regenerative amplifier is required. Very little work has been done in developing this approach, possibly because of the greater energy extraction available with injection-locking and the simplicity of the optical amplifier approach.

Injection-locking involves injecting light from a single-frequency master laser into a usually more powerful slave laser. The light is regeneratively amplified and if the master laser frequency is sufficiently close to that of a free-running slave laser mode, then the free-running modes of the slave are extinguished and replaced with an amplified version of the master. Hence a high power slave laser is controlled by a low power master laser. This method has the advantage that it splits the burden of efficient production of high powers and frequency stability into two laser systems. It also bridges the gap in size and efficiency between amplifiers and oscillators [41]. In an injection-locked laser the slave laser gain is well saturated and mode discrimination is provided predominantly by the slave laser resonator. Injection locking has been demonstrated for many laser systems, including helium-neon[42], CO_2[43][41], diode [44], argon ion [34][33], and Nd:YAG lasers [38][45][46][47] [48][49][50]. The work done on injection locking of medium power Nd:YAG lasers will be discussed extensively in the next few paragraphs.

A great deal of effort has been applied world wide to demonstrate multi-watt injection-locked lasers. Nabors *et al.*[45] demonstrated a 13 W injection-locked laser using a commercially available lamp-pumped rod gain medium, and showed that injection-locking could be used to force unidirectional operation in a 13 W ring laser without the use of an intracavity optical diode. Cregut *et al.*[50] produced

an 18 W, injection-locked, lamp-pumped, rod laser system that utilized two commercially available laser amplifiers as the gain medium. Freitag *et al.*[48] achieved 20 W of injection-locked laser power using 340 W of diode-laser pump power and a side-pumped rod architecture. The advantage of the rod laser architecture is that the output is rotationally symmetric. However, further power scaling of an injection-locked laser using such an architecture is expected to be limited by thermal birefringence.

Alternative pumping geometries include end-pumping and side-pumped slabs. Yang *et al.*[49] have demonstrated a 10 W injection locked laser that is extremely efficient and is thus advantaged by not requiring water cooling. However the laser is an end-pumped rod laser which is not scalable to higher powers. Farinas *et al.*[47] have demonstrated an injection-locked side-pumped slab laser that is scalable and efficient. The rectilinear cooling geometry of the slab laser overcomes the problems of increased cavity losses and polarization degradation caused by thermal birefringence.

We have developed a laser that will fulfill the requirements for gravitational wave astronomy, by improving the slab laser concept using the Co-planar Pumped Folded-zig-zag Slab (CPFS) architecture developed by Richards *et al.*[51]. The CPFS geometry was designed primarily to provide an inexpensive pulsed laser system for use in field-based laser ranging experiments. The CPFS geometry provides a gain path length that is twice as long as a conventional slab design [47] and nearly four times that of a rod for the same length of crystal. As it has higher gain it is less sensitive to resonator losses [52]. The folded zig-zag geometry ensures a good sweep out of the gain region in the horizontal plane and the collimated diode pump light enables a good match of the pumped region to the vertical extent of the mode. The efficient sweep out of the pumped region and the high gain enable the CPFS geometry to be one of the most efficient side-pumped lasers available. In standing wave configuration it produces over 6.4 W of cw multimode radiation from 18.3 W of pump light. The efficiency and the compactness of the CPFS laser suggested that it would make an ideal architecture for our slab laser system. Further work by Richards *et al.* [53] has demonstrated 14 W of multimode power and over 10 W of TEM_{00} radiation when the laser is pumped by two 20 W diodes. Recent work by Mudge *et al.*[54] has

suggested that a modified version of the CPFS laser system may be scaled to over the 100 W output power level using a stable/unstable laser resonator.

The intensity noise of the laser is often required to be very low if it is to be used in the forementioned experiments. At low to medium frequencies the intensity noise of solid state lasers is generally limited by pump intensity fluctuations. These fluctuations can be reduced by detecting a sample of the laser field and using it to apply an electronic feedback correction to the laser pump source[55][56][57][58]. At higher frequencies intensity noise is often limited by the Resonant Relaxation Oscillation (RRO) which usually occurs between 100-500 kHz. Negative feedback may be used to suppress the RRO [59][55][56]. Injection locking can also be used to suppress RRO as the process effectively overdamps the relaxation oscillation [60][61] [62][58].

Intensity noise suppression of lasers may also be achieved by feeding back to a modulator that is external to the laser cavity[63]. This method is quite simple, enables high noise reduction at low frequencies and has the advantage that being external to the laser. However, the external modulator approach to intensity noise reduction does not enable enough noise reduction at higher frequencies, and thus can't suppress the RRO of solid state lasers using a single, simple feedback loop [64]. At frequencies beyond a few MHz solid state lasers are often shot or quantum noise limited [65][66].

1.2 Interferometric Detection of Gravitational Waves

The existence of gravitational waves was predicted over 75 years ago as a consequence of Einstein's General Theory of Relativity [67][40][30]. Gravitational waves interact extremely weakly with matter, and thus the detection of these waves will open a new window to the universe, as well as verifying an important prediction of General Relativity. When a gravitational wave passes through space it distorts space-time. Hence to detect them one must detect the strain in space created by their passage. One means of doing this is to use a Michelson interferometer, which detects the change of length of one arm with respect to the other. However, the predicted

strain $(\frac{\Delta L}{L})$due to a galactic event that occurs with sufficient regularity to stand a reasonable chance of being detected is estimated to be 10^{-21}. Thus, the aim of the first generation of laser interferometric gravitational wave detectors is to achieve a spectral strain sensitivity of $\tilde{}3\times10^{-23}/\sqrt{Hz}$ at 200 Hz.

To achieve the required sensitivity, some extremely tight specifications are placed on the laser system[30]:

- Output power $\geqslant$10 Watts
- Frequency noise of $\leqslant10^{-6}\text{Hz}/\sqrt{\text{Hz}}$ at 1 kHz
- Relative intensity noise of $\leqslant5\ 10^{-8}/\sqrt{\text{Hz}}$ at 1kHz
- Reliability
- Low beam jitter

For the second stage interferometers the power of the laser will need to be increased to around 100 W.

The frequency noise is some 7 orders of magnitude less than that of the monolithic NPRO. However, as was discussed earlier, monolithic NPROs have been actively stabilized to within less than two orders of magnitude of this level and the required loop gains have been demonstrated in stabilized argon ion lasers. Further more, in the case of the monolithic NPRO, the stabilization was limited by the shot noise limit set by the amount of power that was detected and the linewidth of the reference cavity. This limit will be reduced for the gravitational wave detector as extremely narrow linewidth reference cavities will be used.

The relative intensity noise of a monolithic NPRO has been reduced to $6\times10^{-8}/\sqrt{Hz}$ at 1 kHz[57] by direct feedback to the lasers pump source drive current. External shutters, such as acousto-optic modulators, can also be used as convenient external noise eaters, with large noise reduction possible at low frequencies[63].

The laser must be reliable as the gravitational wave detectors will run continuously for long periods and must not be limited by laser failures.

The minimum specifications for the un-stabilized laser required for LIGO stage 1 are[68]:

- $>$ 10 W in a circular TEM_{00} mode

  $<$1 W total in all non-TEM_{00} modes

- Relative power fluctuations $< 10^{-5}/\sqrt{Hz}$ between 100 Hz and 10 kHz

- Within 2 dB of the shot noise limit for 10mA of photodetector current

  ($7\times10^{-9}/\sqrt{Hz}$) above 24.5 MHz

- Frequency fluctuations $< 500 \times (100/\mathrm{f})\ Hz/\sqrt{Hz}$ from100 Hz to 10 kHz

- Relative pointing angle fluctuations $< 3 \times 10^{-6}\ /\sqrt{Hz}$ above 150 Hz

The injection-locked laser we have developed is a 5 W device; the power was limited by the number of pump diodes we had available. As was mentioned earlier the CPFS laser design has already be shown to be capable of producing in excess of 10W of TEM_{00} mode radiation. We have measured the beam quality of our laser and have found it to be very close to diffraction limited. The frequency noise of our injection-locked laser system is limited by the frequency noise of the NPRO master laser, and thus easily meets the LIGO stage 1 specifications. The free running intensity noise of the injection locked laser satisfies LIGO stage 1 specifications. It is even further improved by using a simple feedback loop to the pump diode driver. It is then suppressed to more than an order of magnitude below the required specifications. The laser is shot noise limited for frequencies above 5 MHz for 6mA of photocurrent.

For LIGO stage 2 approximately 100 W of laser power will be required. To achieve this the University of Adelaide Optics Group has proposed to injection-lock a fibre-coupled diode pumped, unstable/stable ring resonator [54]. The block diagram for this system is illustrated as Fig 1.2. The proposed experiment uses two stages to amplify the low power monolithic master to the 100 W level. To ensure reliable injection-locking of the 100W laser, its master laser will be the medium power laser presented here.

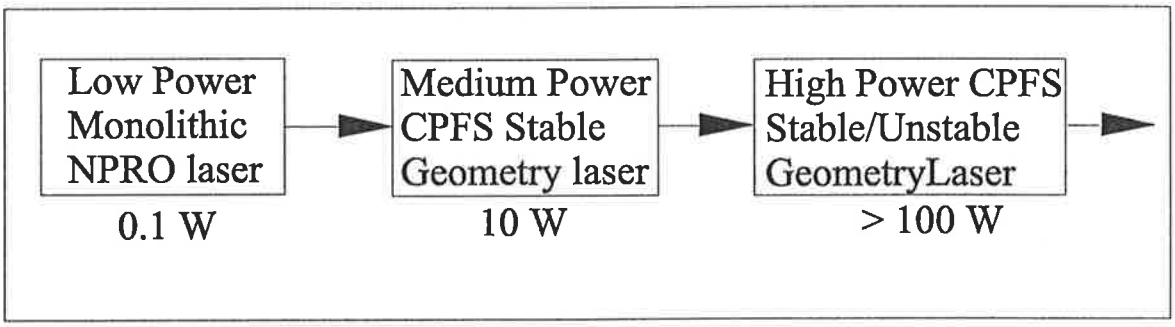

Figure 1.2: Schematic of the three stage injection-locking scheme

1.3 Field Based Laser Vibrometry

Field based laser vibrometry is another form of coherent laser radar. All mechanical objects have a vibration signature which if measured, can be used to identify them[69]. This is of particular interest if the vehicle is obscured or camourflaged.

A proposed laser vibrometry experiment is shown as Fig 1.3. The laser is used to illuminate the target. The Doppler shifted return from the target (vibrating object) is interfered with a frequency shifted sample of the original beam, and the beat signal is detected with a fast, low noise photodiode. The beat signal is then fed into a discriminator (frequency to voltage converter). The output voltage of the discriminator is proportional to the instantaneous velocity of the vibrating object and can be analyzed using fast Fourier transform techniques.

A possible discriminator is shown as Fig 1.4. This discriminator is just the RF equivalent of a non-path-matched Michelson interferometer. An alternative form of frequency discriminator is a phase locked loop, such as is used in an FM radio receiver.

The laser requirements for field based vibrometry are significantly less demanding than those required for laser interferometric gravitational wave detection. Ideally the laser must have:

- Single frequency operation
- Shot noise limited intensity noise at heterodyne frequency
- Compactness, robustness and portability

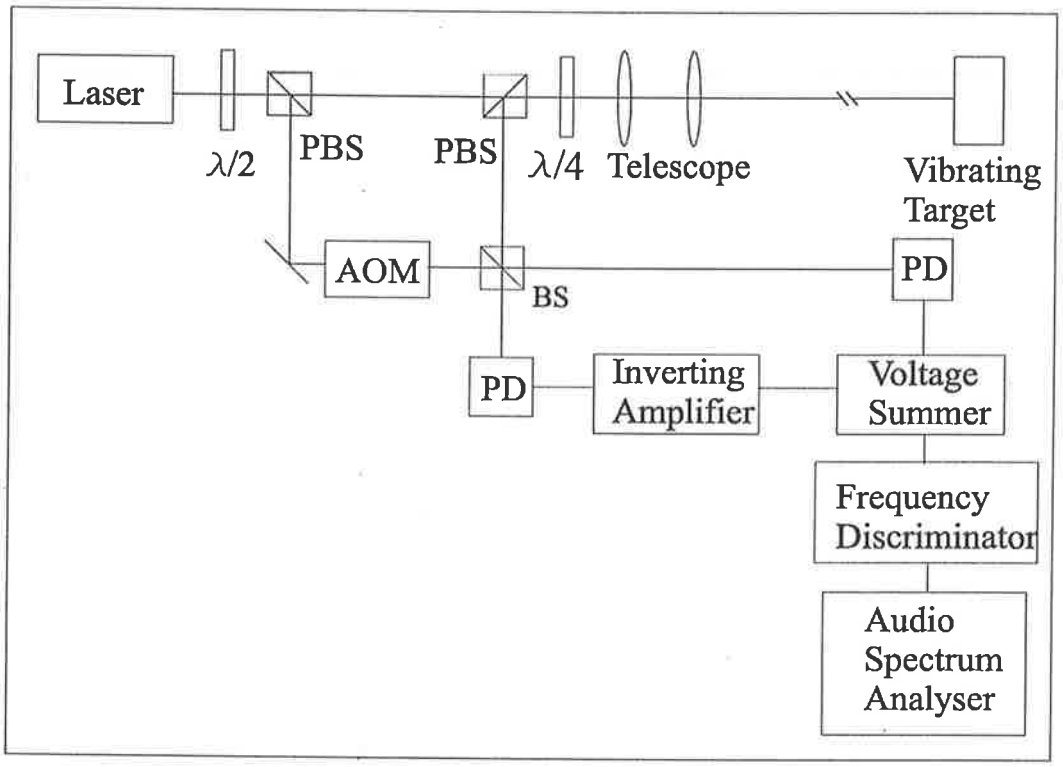

Figure 1.3: Schematic of the proposed laser vibrometry experiment

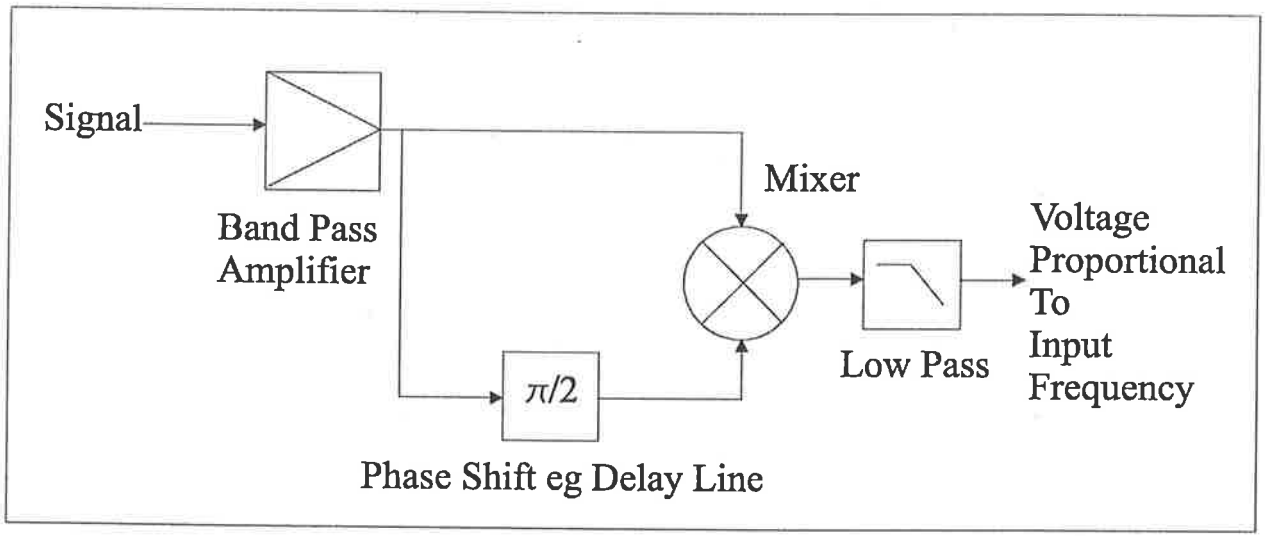

Figure 1.4: Schematic of a possible frequency discriminator of laser vibrometry

- Linearly polarized output
- Long coherence length
- Eye safe wavelength

The medium power laser presented here meets most of the above specifications easily as they are less stringent than the requirements for LIGO stage 1. The laser is efficient and thus it would be easy to convert it to an air-cooled unit, which along with its compactness, would enable good field portability. To make the laser eye safe the wavelength of the laser would need to be shifted from $1\mu m$ to approximately $1.5\mu m$. This could be done using a Optical Parametric Oscillator (OPO)[70].

1.4 Introduction to Control Theory

In the work described in this thesis feedback is used to control various system parameters. Examples include the Nd:YAG slab laser temperature controller, and servo control of the slave laser frequency so that it remains sufficiently close to the frequency of the master laser to enable reliable injection locking.

Systems that do not use feedback are known as open loop systems. Control theory texts [71][72] often use block diagrams to illustrate systems and a block diagram of an open loop control system is illustrated as Fig 1.5. In systems where the output must be well controlled, open loop systems require a very stable input and a well defined gain that does not change with time. For extremely stable applications, often the best components are not sufficiently stable and some form of negative feedback is required. A block diagram of a system with feedback is also illustrated as Fig 1.5

The equation relating the output $C_{ol}(s)$ to the input R(s) for an open loop system is

$$C_{ol}(s) = G(s)R(s) \tag{1.1}$$

where s is the Laplace transform variable and $G(s)$ is the open loop gain of the system. The output of a closed loop $C_{cl}(s)$ system is related to the input by[71]

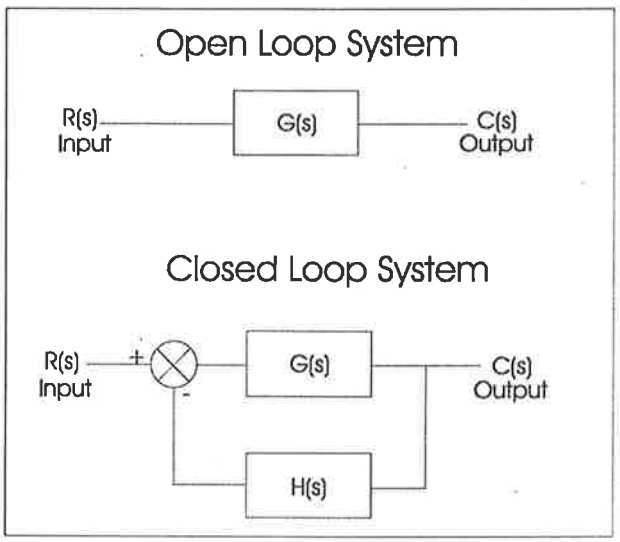

Figure 1.5: A block diagram of an open loop and close loop system

$$C_{cl}(s) = \frac{G(s)}{1+G(s)H(s)}R(s) = \frac{C_{ol}(s)}{1+G(s)H(s)} \tag{1.2}$$

It can be seen from Equations 1.1 and 1.2 that one of the main advantages of a closed loop system compared with an open loop system is the reduction of the effect of the input (noise) by $1 + G(s)H(s)$. The term $G(s)H(s)$ is called the loop gain of the system. To achieve good noise reduction the value of the loop gain must be high for the values of s where noise reduction is desired.

Care must be taken when designing feedback loops, because the system will become unstable if the feedback is positive. The most likely outcome of this is that the system will oscillate. In some applications this is a not a bad thing, for example lasers and RF oscillators rely on self oscillation for their outputs. However in control systems oscillations result in large unwanted output fluctuations.

In the work undertaken in this thesis the stability of control systems has been determined using frequency based methods in which the Laplace variable s is replaced by Iω where ω is the angular frequency . Certain elements of the servo loops used in this work do not have accurate mathematical descriptions of their behavior. Frequency response methods are particularly useful in these applications as experimentally determined responses can be used in place of results derived from

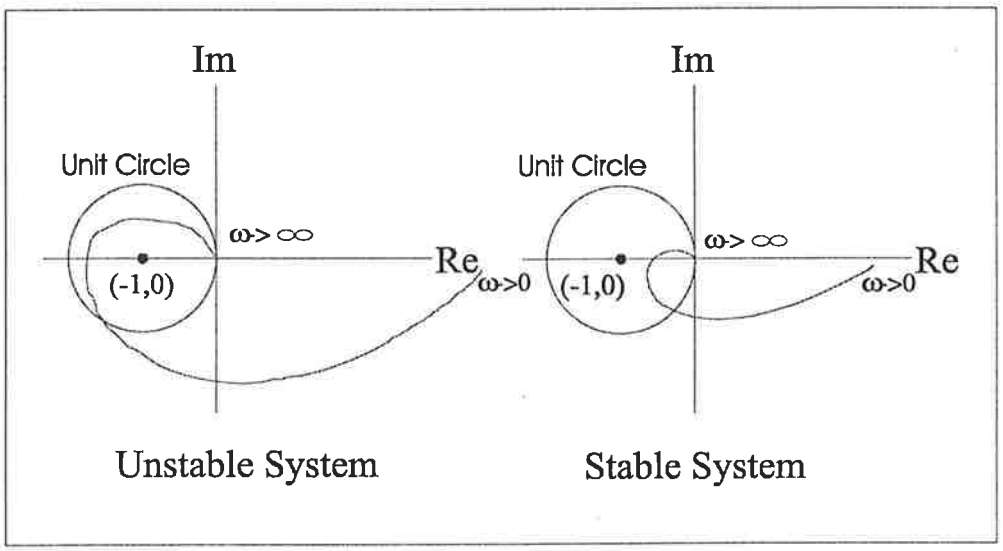

Figure 1.6: A sample Nyquist diagram for a stable and unstable feedback system

models.

One method for determining the stability of a system is the Nyquist's stability criterion[71]. To utilize the Nyquist stability criterion a contour plot of {Re[G(Iω)H(Iω)], Im[G(Iω)H(Iω)] } as the parameter ω is varied from 0->∞ must be obtained. In the cases relevant for this thesis the Nyquist stability criterion states that a feedback system is stable if and only if the contour does not encircle the point (-1,0) in a clockwise direction as ω increases. Fig 1.6 illustrates this for a typical stable and unstable feedback system. Also shown on this diagram is the unit circle centered on the point (-1,0). For frequencies where the Nyquist contour falls within this circle the output noise is amplified rather than being suppressed.

Another graphical tool that is used to study feedback loops is the Bode diagram[71]. A Bode diagram is actually two plots, one of the magnitude (in dB) of the loop gain vs log of frequency, the other of the phase of the loop gain vs log frequency. An example of a Bode plot is shown as Fig 1.7 . Two different magnitude curves are shown for the same phase response. The Nyquist stability criterion implies that a feedback system is stable if the loop gain magnitude passes through unity gain when the loop gain phase is greater than -180 degrees. The phase margin is the phase of the loop gain at the unity gain point minus 180 degrees. These terms are illustrated in Fig 1.7 , where trace A has negative phase margin and is hence unstable, while

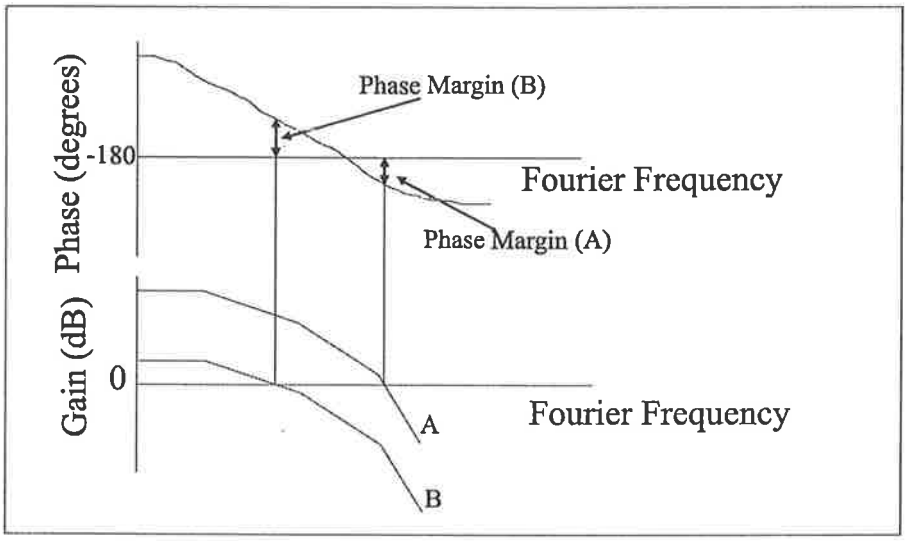

Figure 1.7: A sample bode stability diagram showing an unstable system (A) and stable system (B)

trace B has positive phase margin and is stable. These cases demonstrate a common type of servo system where an unstable system can be made stable by reducing the loop gain. However as the output noise reducing properties of a feedback system are nearly proportional to the loop gain it is not always desirable to simply reduce the gain.

A Bode plot can be obtained by applying a sinusoidal modulation to the input of a system and measuring the resulting phase and magnitude of the output relative to the input. This is done throughout the frequency range of interest. It should be noted that the input signal needs to be larger than the effective input noise, but not so large that non-linear effects are significant.

Chapter 2

The Slave Laser

2.1 Introduction

In an injection-locked laser, the slave laser is used to amplify the power of a master laser while maintaining the superior frequency noise characteristics of the master laser. To facilitate this and ensure that the injection-locked laser has good intensity noise performance and reliability the slave laser should, as will be discussed below, have the following properties:

- Single transverse mode operation (near diffraction limited output)
- Efficient
- Compact
- Low intensity noise
- Low frequency noise
- Linearly polarized
- Ring resonator architecture

If the slave laser fulfills these requirements as closely as possible, the engineering required to enable the injection-locked laser to be a portable, reliable and stable laser source will be relaxed.

The slave laser defines the transverse mode structure of the injection-locked laser output, although a small amount of mode discrimination can be provided by the master laser if it is correctly mode matched to the fundamental mode of the slave resonator. It is therefore important that the slave laser runs in a TEM_{00} mode. Further, if the injection-locked laser has a well defined spatial mode then its output can easily be mode matched into other resonant cavities, such as the mode cleaners and frequency stabilization cavities that will be used on the gravitational wave interferometers.

Efficiency is generally a desirable feature for a laser system. If the power of the master laser is small compared with that of the slave, the output power and hence the efficiency of the injection-locked laser is set by the slave laser. To facilitate portability for use in field-based remote sensing, it would be desirable to cool the laser diodes using air cooled heatsinks. The problem of accurately regulating the temperature of the laser diodes using air cooled heatsinks is made far easier when the heat energy required to be removed is small. Further, at present the pump laser diodes are among the most expensive components of a diode pumped solid state laser especially when the costs of laser diode drivers and cooling systems are considered. Therefore if the injection-locked laser is to be an elegant solution to the problem of a medium power single frequency stable laser, the slave laser must be as efficient as possible.

To achieve injection locking the frequency of one of the free-running axial modes of the slave laser must be sufficiently close to the frequency of the master laser. The maximum frequency difference between the master and the slave laser mode for which injection locking will occur is given by half the locking range($\Delta\nu_l$)[73]

$$\Delta\nu_l = \Delta\nu_c\sqrt{\frac{P_m}{P_s}} \cong \frac{T.FSR}{\pi}\sqrt{\frac{P_m}{P_s}} \tag{2.1}$$

where $\Delta\nu_c$ is the cold cavity linewidth of the slave laser, P_m/P_s is the ratio of the power of the master to that of the slave, T is the transmission of the slave's output coupler and FSR is the free spectral range of the slave laser resonator.

Active control of the frequency of the free running slave is required to obtain long term injection locking. To simplify the design of the servo system needed to

achieve this, the resonator of the slave laser should be as stable and therefore compact as possible. The temperature of the laser crystal should be tightly controlled as temperature drifts cause refractive index variations which in turn cause slave laser frequency drifts. This helps to relax the requirement of the dynamic range of the servo. Compactness and rigidity of the slave resonator help to reduce higher frequency noise and hence reduce the requirements on the bandwidth of the frequency control servo.

The intensity noise of the pump source is efficiently coupled into the intensity noise of the injection-locked laser for frequencies below about 100 kHz [74]. It is well known that the intensity noise of laser diode pump sources is up to three orders of magnitude quieter than that of arc-lamp pumping[74]. Further, laser diodes provide a more reliable and efficient pump source. Therefore, the use of laser diodes as pump source for highly stable, reliable, medium power lasers is indispensable. If the pump diodes are to be quiet as possible, the drive current must be well regulated. The coupling optics must also be rigidly mounted so that they do not introduce additional pump fluctuations.

Injection-locking presents a mechanism for slave laser frequency noise to be coupled into the intensity noise spectrum of the injection locked slave if the natural frequency of the slave and the master laser are not matched[75][61][60]. Hence the slave laser frequency should be controlled such that it is as close to the master laser frequency as possible, so that the intensity noise of the slave is not degraded. This will be considered in greater detail in Chapters 3 and 4.

A well defined polarization state is necessary to maximize the injection locking range, as this readily enables polarization matching between the slave and the master laser. For interferometric gravitational wave detection the laser source should ideally be linearly polarized as this would give the best fringe visibility when the laser light is matched into the high finesse reference cavities used in LIGO.

In an injection-locked laser the master laser must be isolated from the slave laser. If the output of the slave laser is allowed to leak back into the master laser, the slave laser could injection lock the master laser, hence imposing its poor frequency stability on the master. Further, if large amounts of the slave laser field are incident

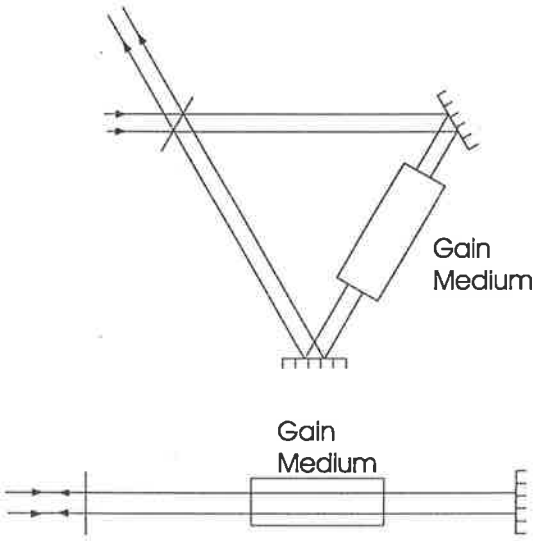

Figure 2.1: A schematic illustrating an odd numbered mirror ring laser (top) and a linear or standing wave cavity (bottom)

on the master laser, irreparable damage may result. Figure 2.1 illustrates the ring laser resonator and the linear resonator (standing wave) laser. The ring laser has a significant advantage over the standing wave laser configuration for laser systems that utilize an externally injected signal. By virtue of the laser geometry the input and the output are spatially separated, hence providing inherent isolation of the master laser from the slave laser.

Also, in a linear resonator geometry, a standing wave is produced in the resonator which causes spatial hole burning in the gain medium. A ring resonator removes this problem as the slave laser mode is a travelling wave. This is a significant advantage for high power single frequency applications.

An additional advantage of an odd-number mirror planar ring resonator is that it is relatively insensitive to mirror misalignment in the plane of the ring laser[73]. This is because the ring laser mode can always find a closed self consistent path around the resonator and a reduction in output power will result only when the resulting mode does not take the optimal path through the gain medium.

A disadvantage of a ring laser as opposed to a standing wave laser is that the laser gain medium is usually traversed only once per round trip and hence the laser has a reduced signal gain and is therefore more sensitive to losses[73]. An additional

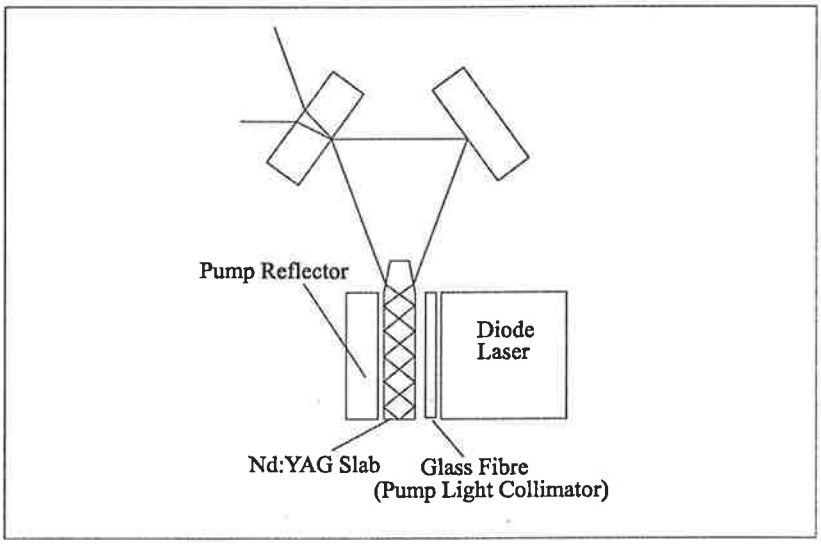

Figure 2.2: Top view of the slave laser

disadvantage is the increased complexity in alignment compared with a standing wave resonator. Overall, the advantages of ring lasers outweigh the disadvantages and make them the preferred choice for medium to high power injection-locked lasers.

Our slave laser, which utilizes the CPFS laser head architecture, admirably meets all of the forementioned criteria. A schematic of the laser is shown as Fig 2.2. As discussed in Chapter 1, it is one of the most efficient side pumped architectures. It produces five watts of linearly polarized light when pumped by a single 20W diode, and has excellent beam quality with M^2 values very close to unity. The laser is compact and if required could be air cooled. The laser has a high level of intrinsic frequency stability and inherently low intensity noise.

These results were achieved using a 20 Watt Opto-Power Corporation [76] (OPC-CS Series) pump diode with a spectral linewidth of 2nm. This was collimated using a Doric graded index fibre lens[77] of focal length 0.685mm. The crystal that was used was manufactured by British Aerospace Australia[78] and had a surface quality of 10-5 (Scratch/Dig) to MIL-0-13830. The total internal reflection sides of the crystal were parralel to within 1 minute. The crystal was doped to 1.1 Atomic %.

The realization of such an efficient and stable laser will be described in this chapter. As discussed earlier, the resonator should be temperature controlled. I will

therefore describe in the next section, the mounting and cooling of the slab laser. Careful design was necessary to enable a high inherent stability of the slave laser system. Next I will discuss the measurements of the crystal losses and the small signal gain of the fully pumped slab, which enabled us to understand the optimum laser output coupling in the ring configuration. Results of the standing wave experiments are presented next, these enable an understanding of how to achieve the optimum mode size for efficient TEM_{00} mode operation using the CPFS laser geometry. Further, the results discussed here are immediately applicable to the ring laser geometry. I will then discuss the interferometric tests performed to examine the laser crystals which, combined with the crystal loss measurement, increased our knowledge of the quality of the laser crystals. These experiments and the standing wave experiments enabled us to gain a significant understanding of the slab lensing in the horizontal plane. I will conclude this section by presenting the results obtained for the ring laser.

2.2 Diode and Slab Temperature Control

In the original CPFS laser design both the slab and the pump laser diode were cooled by mounting them on a single copper block, which was water cooled. During the initial work we reproduced this arrangement in our laboratory. However, early frequency stability experiments clearly demonstrated that the noise of the laser was limited by vibrations driven by the cooling water. This is not surprising as the CPFS laser geometry utilizes the slab as one of the mirrors in a three-mirror resonator. Hence, any movement of the slab relative to the other mirrors in the resonator directly adds frequency noise to the output of the laser. It is therefore extremely important that the slab is rigidly mounted and is decoupled from any water cooling vibrations.

The temperature of the slab should be tightly controlled as temperature changes of the slab cause changes of the optical length of the resonator, mostly because of the dependence of the refractive index of the gain medium on temperature. Variations in the optical length of the resonator directly alter the lasing frequency. To control

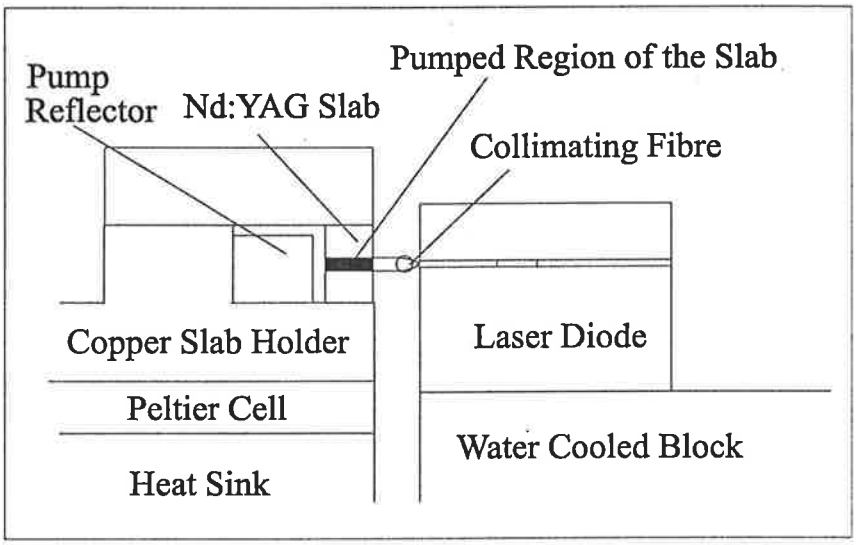

Figure 2.3: End view of the slave laser pump geometry clearly illustrating the cooling systems

the temperature of the slab we use active temperature stabilization. A schematic of the slave laser cooling architecture is shown in Fig 2.3. The slab is held by a copper mount, which has its temperature controlled by a Peltier Cell. Copper was chosen for the holder material because of its high thermal conductivity. The Peltier cell is cooled by a heatsink using natural convection. For ease of construction the laser diode is mounted on a separate water cooled copper block. For field-based work both the slab and the laser diode could be cooled by Peliter cells which are cooled by forced air convection.

A Peltier cell is a solid-state heat pump which transports heat from one side to the other upon application of a voltage across its terminals[79]. This creates a hot and a cold side. The cold side can be used to cool a small heat load (generally less than 1kW). Like all heat pumps, Peltier Cells obey the laws of thermodynamics and cannot destroy heat, only move it from one place to another. Hence to prevent the Peltier cell from over-heating, the hot side must be cooled, and this is usually done by mounting it on a heatsink.

The laws of thermodynamics tell us that to move heat energy from a cold surface to a hot surface requires work to be done. The amount of work required to transport the heat energy depends on the gradient over which the heat is to be transported

and the amount of heat energy that must be moved. In the case of the Peltier cell the work is provided by the electrical supply. The work done in transporting the heat also adds to the heat energy load that must be dissipated by the heat sink. The size of the temperature gradient depends on the temperature of the hot side of the Peltier cell. This is determined by the thermal resistance of the heat sink and the ambient temperature of the room in which the system is to operate. These quantities are related by the following equation

$$T_{hotside} = T_{room} + R_{therm}Q_{total}$$

where Q_{total} is the total heat to be dissipated by the heat sink and R_{therm} is the thermal resistance of the heatsink, a quantity defined as the rise in temperature above ambient per watt of power dissipated by the heatsink. Typical values of thermal resistance of heatsinks are $(0.5 - 10)$ $\circ$C/W for natural convection cooling to $(0.02 - 0.5)$ $\circ$C/W for forced convection cooling.

Determining the temperature of the hot side is an iterative process as Q_{total} depends on the temperature of the hot side of the Peltier Cell. As the heat load to be transported increases, the value of Q_{total} increases which increases the temperature gradient which in turn increases the work done to transport the heat. Hence as the heat load increases the engineering difficulties increase significantly. It is therefore important to minimizes parasitic increases in the thermal load, due to thermal short-circuits between the hot and the cold side.

The heat load deposited in the slab is approximately 7 W when the slab is pumped with 20 W of diode laser pump power. Care must be taken with the design of the clamps that are used to secure the slab holder to the Peltier cell and the Peltier cell to the heatsink as these may increase the parasitic heat load. If aluminium clamps are used, the resulting thermal short circuit may increase the effective heat load by 10 W. To overcome this problem we used stainless steel clamps with thermally insulating mica pads between the clamps and the slab holder.

As the ambient temperature and heat loads change, the temperature of the slab will change unless feedback is used to stabilize the temperature of the slab mount and hence the slab. A block diagram for the thermal servo system is shown in Fig

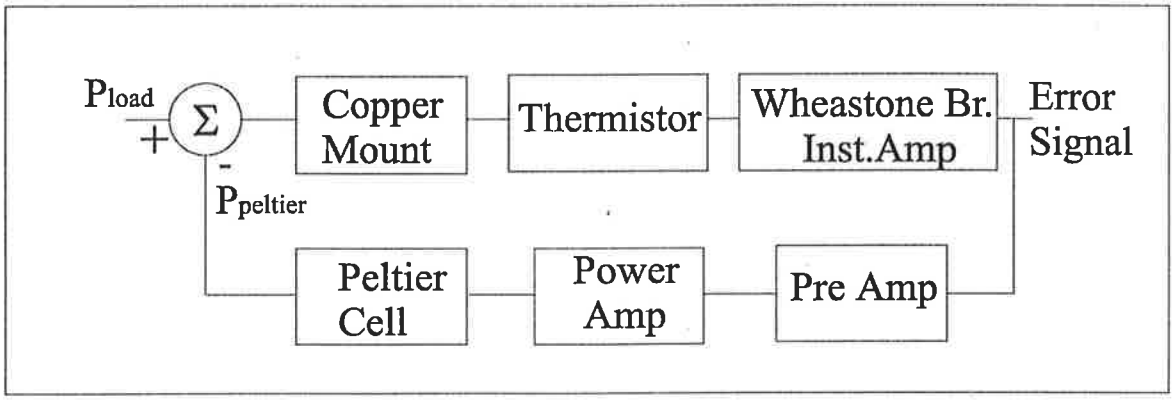

Figure 2.4: Block diagram of the slab temperature control servo system

2.4. To regulate the temperature of the slab as tightly as possible it is important to place the temperature sensor of the servo as close to the slab as possible. In our system we have placed the temperature sensor immediately below the slab.

The temperature sensor is a thermistor whose resistance is related to its temperature by the equation

$$R_{Thermistor} = R_0 e^{B/T} \tag{2.2}$$

where B and R_0 are constants. The value of its resistance is interrogated using a Wheatstone bridge circuit. An instrumentation amplifier is used to amplify the voltage difference between the two sides of the bridge. The slope of the Wheastone bridge temperature error signal is derived in Appendix A1 and is given by

$$\frac{\Delta V_{instr.amp.}}{\Delta T} = -\frac{T^{-2} B R_0 e^{B/T} V_s G_{instr}}{(R_0 e^{B/T} + R_{ref})^2} \tag{2.3}$$

where G_{instr} is the gain on the instrumentation amplifier, V_s is the voltage supplied to the bridge and R_{ref} is the resistance of the reference resistor in the same arm of the Wheatstone bridge as the thermistor.

The transfer function which relates the voltage applied to the Peltier cell to the temperature of the thermistor is the hardest to determine theoretically as it is combination of various physical processes. In the limit of a small modulation of applied voltage, the power removed from the copper is linearly related (1st term in a Tay-

lor's expansion) to the applied voltage. If it is assumed that the Peltier cell and the thermistor response time are fast and the thermal conductivity of copper is large, then the forementioned transfer function would simply be that of an integrator. An integrator transfer function has a 1/f roll-off in amplitude and a constant ninety degree phase lag. The transfer function of the Peltier cell applied voltage to thermistor temperature was measured and is shown as Fig 2.5. The transfer function tends towards the ideal integrator at very low frequencies but deviates from this model at higher frequencies.

It can be shown that the thermal response time of a thin slab of material for a change in the set temperature of its boundary is given by the relationship [80]

$$\tau = \frac{c\rho}{k}\left(\frac{t}{\pi}\right)^2 \tag{2.4}$$

where$t$ is the thickness of the material, c is the specific heat of the material,k is the thermal conductivity of the material and ρ is the density of the material. Using Equation 2.4 it can be shown that the thermal response time of a 5mm thick piece of copper is 0.02 seconds. Hence the thermal reaction time of the copper block is too fast to explain the additional phase lag that occurs at higher frequencies. The quoted response time of the thermistor is 10s and this is the most likely cause of the additional phase lag.

The copper slab holder is exposed to fluctuating external conditions such as room temperature variations. Therefore it is useful for the temperature servo to have as fast a transient response as possible. Also the slave laser frequency may be tuned by varying the slab temperature, which would be made easier if the slab temperature control had a reasonable transient response. It is well known that a servo system achieves its fastest settling time if it is critically damped for a given bandwidth [71], which requires a phase margin of 70 degrees. Unfortunately due to the loss of phase illustrated in Fig 2.5 this is not possible without a significant decrease in the unity gain frequency.

To increase the phase margin at unity gain we use a Proportional, Integration and Differentiation (PID) compensation circuit as a preamp. The transfer function of the pre-amp is shown as Fig 2.6. The signal from the pre-amp is buffered by a

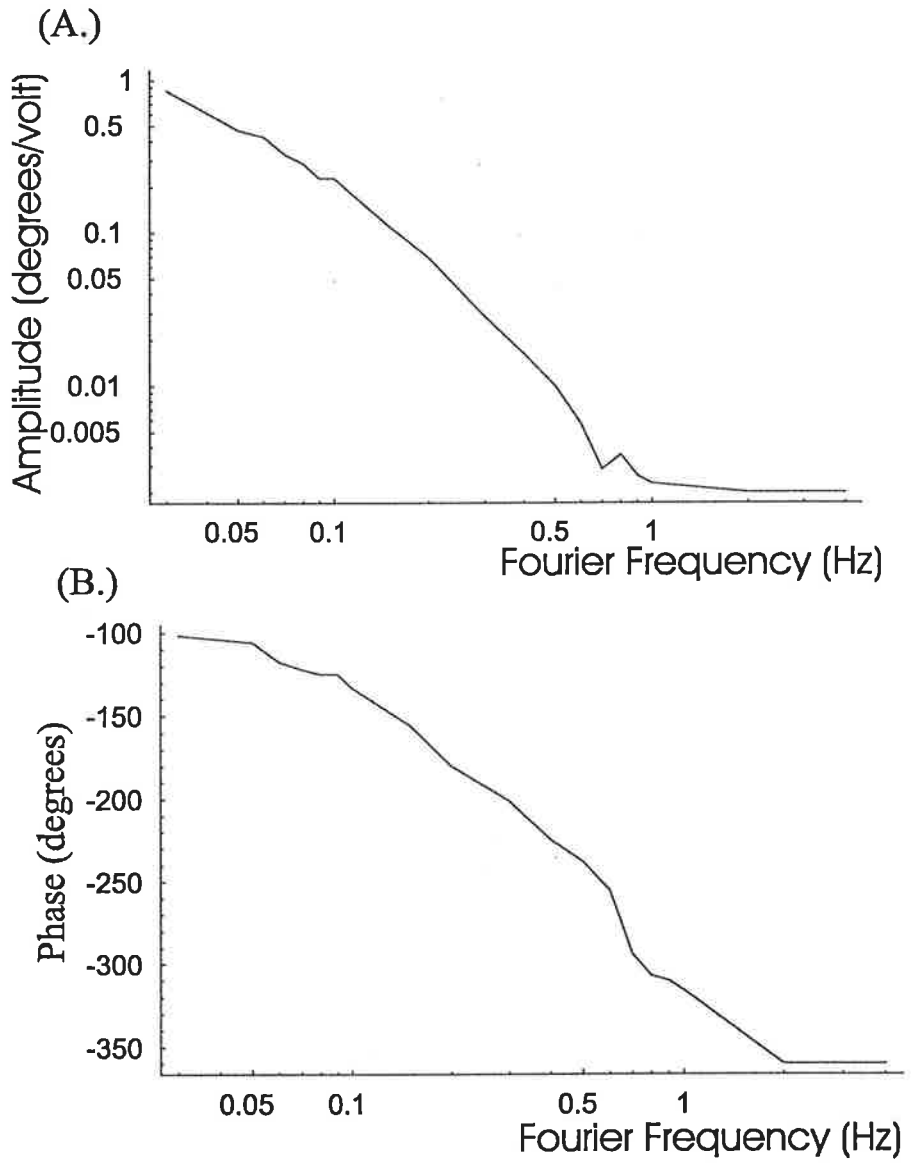

Figure 2.5: The frequency response of the temperature of the thermistor to fluctuations in the applied Peltier cell voltage

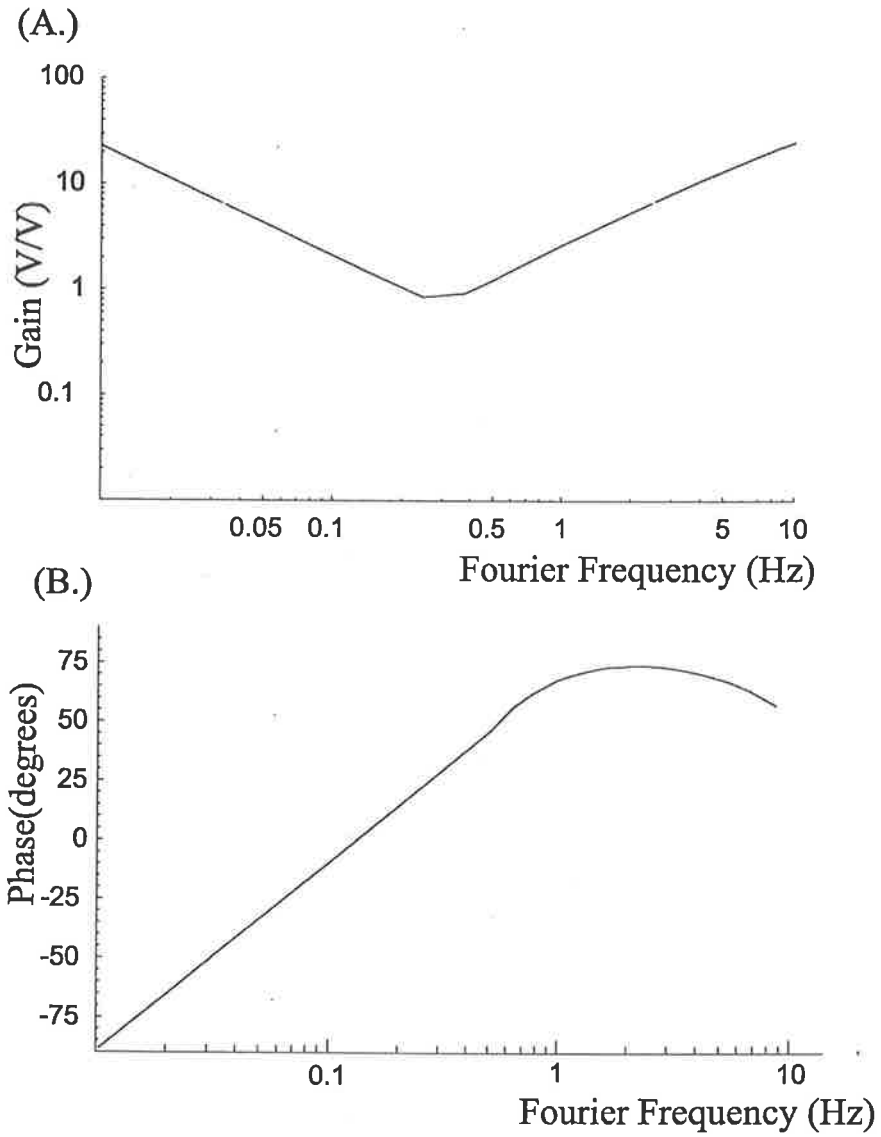

Figure 2.6: Frequency response of the thermal system Pre-Amp

power op-amp with a gain of five, whose output drives the Peltier Cell. A circuit diagram for pre-amp and the power op-amp are shown in Appendix B1 and B2. The open loop gain of the servo is shown as Fig 2.7; it has a unity gain frequency of 0.3 Hz is and a phase margin of 45 degrees. The transient response of the servo after turn on is illustrated as Fig 2.8. The error signal indicates that the stability of the system is better than 5mK. This is only an estimate of the stability as the parameters of the discriminator may change and alter the set-point hence giving a false reading.

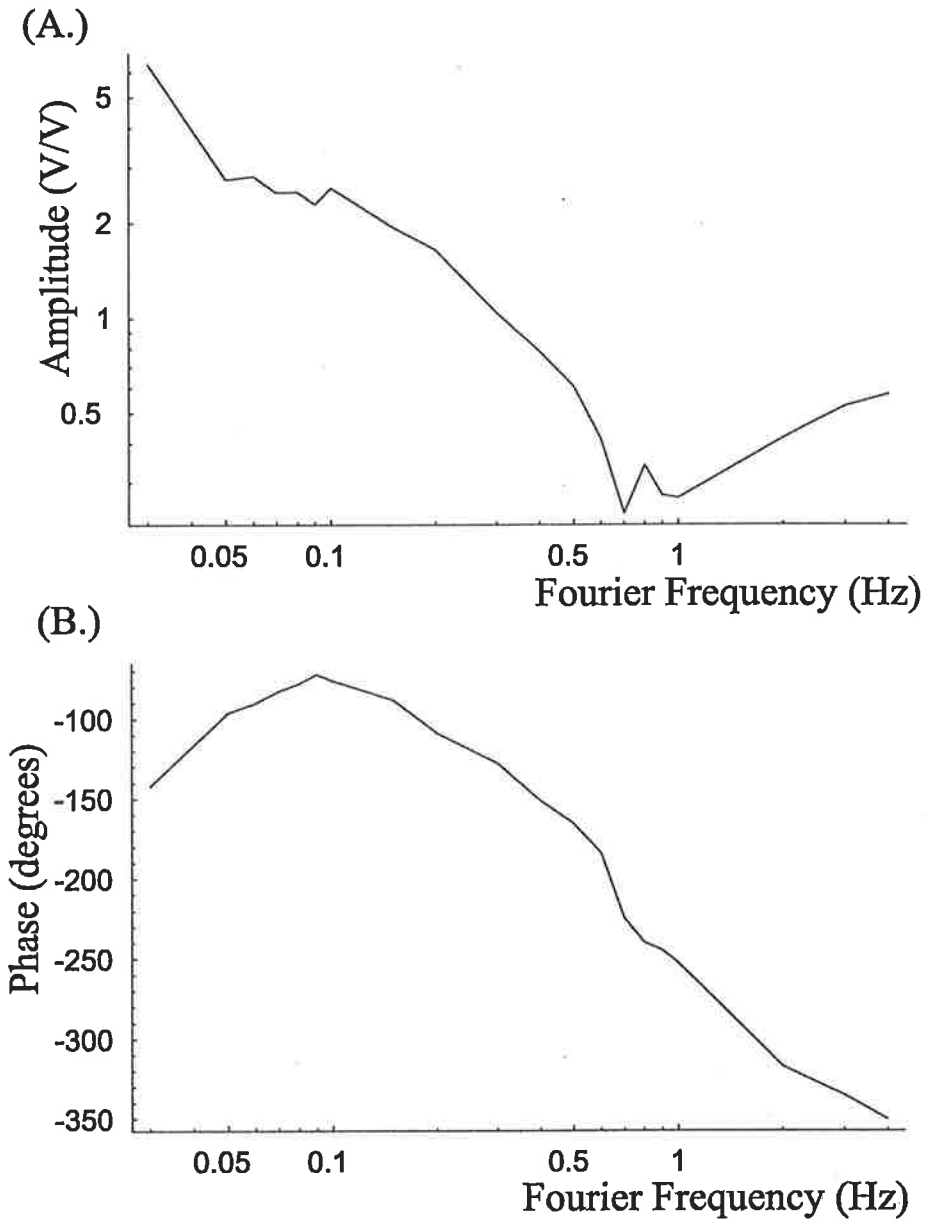

Figure 2.7: A Bode diagram for the loop gain of the thermal servo

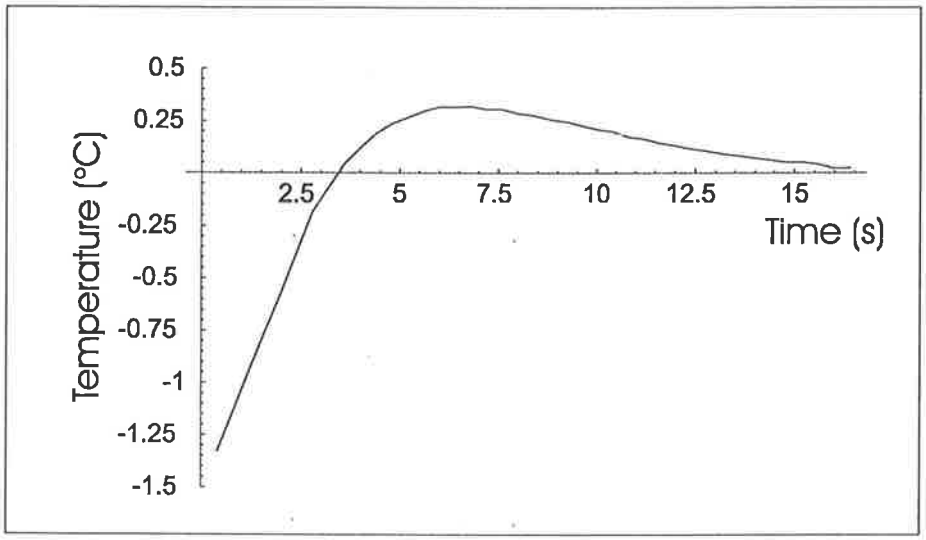

Figure 2.8: The transient response of the thermal system to a setpoint change

The drift in the frequency of the slave laser due to a change in the Nd:YAG crystal temperature can be evaluated as follows. A change in temperature ΔT, in the laser crystal changes the optical path length by

$$\Delta L = \frac{dn}{dT} \Delta T \; L \tag{2.5}$$

where L is the distance that the laser mode propagates through the crystal and $\frac{dn}{dT}$ is the change in refractive index per unit temperature change. A perturbation of the optical path length by ΔL causes a corresponding change in the frequency of the laser $\Delta\nu$ given by

$$\Delta\nu = -\frac{\Delta L}{\lambda} FSR \tag{2.6}$$

where FSR is the free spectral range of the resonator and λ is the wavelength of laser light. Hence the change in frequency $\Delta\nu$, for a change in temperature ΔT of the laser crystal is given by

$$\Delta\nu = -\frac{\frac{dn}{dT} \Delta T \; L \; FSR}{\lambda} \tag{2.7}$$

For a temperature change of 5mK, Equation 2.7 gives a frequency stability of 2.2 MHz given L=40mm, $\frac{dn}{dT}$=7.3 10^{-6} $/C$ and a FSR of 1.5 GHz. For the injection

locking experiments reported in this thesis, the typical injection locking ranges are 10 MHz. Hence the crystal temperature induced frequency changes are sufficiently small to enable long term injection locking.

Equation 2.7 can be rearranged to give the frequency tuning coefficient $\frac{\Delta\nu}{\Delta T}$ for the laser. For the parameters listed above, this is 440 MHz/°C, and thus a temperature change of 3.4 degrees is required to sweep the frequency of the laser through a full spectral range.

2.3 Slab Laser Loss and Gain Measurements

The small signal gain of the fully pumped slab crystals and the losses of the crystals were investigated. This was done to determine the optimum output coupling. Also, measurement of the losses and interferograms of the crystal surfaces (discussed in Section 2.5), enabled us to gain an insight into the quality of our locally manufactured laser crystals.

2.3.1 Crystal Loss Measurements

The losses of the slab laser are quite difficult to measure accurately. The expected bulk scatter loss for transmission through a 40mm length of Nd:YAG is between 0.8 and 1.6% [52]. For the multiple bounce path used in the CPFS geometry, a higher loss value can be expected due to imperfections in the surfaces used for total internal reflection.

A schematic of the set up used to measure the crystal losses is shown as Fig 2.9. The probe laser used in this experiment was a 400 mW NPRO manufactured by Laser Zentrum Hannover (LZH). The polarizing beam splitter and the half wave plate were used to set the input polarization of the probe laser beam. To measure the slab losses with an accuracy of 10%, the power of the probe laser beam must be measured to one part to 10^3. To achieve this we chopped the laser beam and detected the signal using a transimpedance photodiode circuit and a lock-in amplifier. The lock-in detection technique has the advantage that any DC-offset errors due to the photodiodes or background radiation are removed. Using this chopped detection

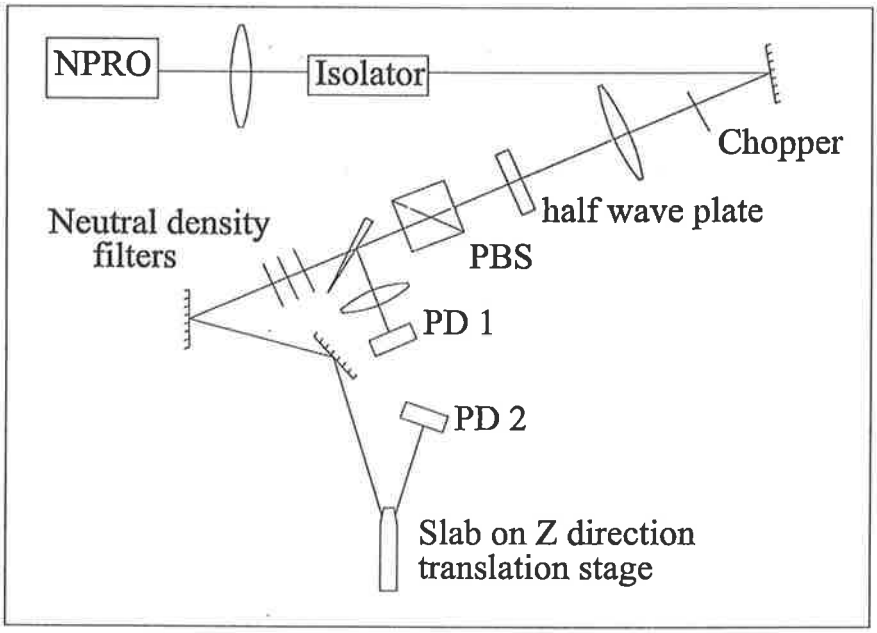

Figure 2.9: Schematic of the set-up used to accurately measure crystal loss

method the light intensity incident on the photodiodes (PD 1 and PD 2) can be measured to 1 part in 10^4. To calibrate the measurement accurately, the light power incident on the crystal was measured by removing the crystal and placing photodiode PD 2 in the path of the beam. During the calibration procedure only the photodiode was moved as spatial variations in the beam steering mirror reflectivity could easily exceed a few parts in 10^4. The photodiode was mounted on an xy translation stage that enabled the lateral position of the photodiode to be varied such that the signal voltage was always maximized. The intensity of the NPRO laser was monitored during the whole process by PD 1 to ensure that it remained constant to the level required for the experiment.

It was found that NPRO had significant beam jitter immediately after turn on. The beam jitter was converted into intensity variation due to spatial imperfections in the transmission of the neutral density filters, which could degrade the maximum achievable accuracy of the loss measurement. However, the pointing stability of the NPRO improved significantly half an hour after turn. After this time the intensity of the probe beam transmitted through the neutral density filters was stable to 1 part in 10^3.

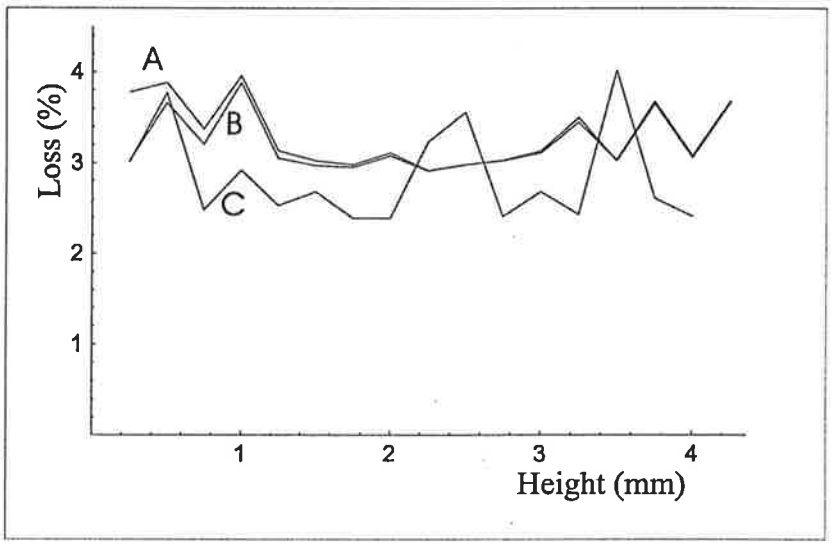

Figure 2.10: Slab vertical loss profiles

The slab laser was mounted on a translation stage that enabled its vertical position to be manipulated. Hence a vertical loss profile could be established. The results for slab #2 are shown as Fig 2.10. Traces A and B were obtained from a vertical scan in one direction and then a following scan in the opposite direction. This demonstrates that the translation of the crystal in the vertical direction produces reproducible results and shows that there are significant variations in the losses in the crystal with changes in height. The third trace was obtained when the experimental setup was dismantled and reassembled. There appears to be little correlation between the two curves, this suggests that the losses in the crystal are spatially dependent with variations of up to the ±0.5 %.

The output power of a laser is described by the equation[52]

$$\mathrm{P}_{out} = \left(\frac{T}{T + L_{total}}\right) AI_s g_0 l - \frac{TAI_s}{2} \tag{2.8}$$

where T is the transmission of the output coupler, L is the roundtrip losses of the resonator excluding the contribution due to the output coupler, A is the area of the lasing mode, I_s is the saturation power of the gain medium and $g_0 l$ is the gain-length product for the gain medium. It can be seen from Equation 2.8 that for lasers operating well above threshold ($\mathrm{g}_0 l \gg \mathrm{T}+\mathrm{L}_{Total}$), the laser power output

is proportional to $\frac{T}{T+L}$. Hence variations in the loss at the one percent level with a 10% output coupler will result in a 10% variation in the output power of the laser. The spatial variations in the loss could therefore account for the output variations between different assemblies of the same laser system which were about 5%. In general the losses of the laser crystals used were about 3% per pass. This figure is higher than the quoted bulk scatter loss which is at most 1.6% for this laser material and path length[52], and therefore scatter at the 11 total internal reflection surfaces and 2 Brewster faces must contribute a loss of approximately 1.5% or 0.15% per bounce.

2.3.2 Small Signal Gain Measurements

The small signal gain of the pumped crystal was measured using the experiment illustrated as Fig 2.11. The elliptically polarized laser light from the NPRO is plane polarized by the Faraday effect isolator. The half wave plate and the polarizing beam splitter are used to vary the intensity of the master light that is incident on the slave laser crystal without altering its propagation characteristics, ie spot size and radius of curvature. The lens immediately before the half-wave plate is used to form a waist of size 0.15mm at the first Brewster window of the slab. The results are shown as Fig 2.12

Identical results were obtained when half the probe laser power was used. Hence the results are independent of the probe laser power and therefore this is a true measure of the small signal gain. The gain was maximum, when the diode cooling water temperature was set to 11 °C.

2.3.3 Optimum Output Coupling.

The optimum output coupling fraction for a laser operating in standing wave configuration can be determined using the following equation [52]

$$T_{opt} = \left(\sqrt{\frac{2g_0 l}{L_{total}}} - 1 \right) L_{total} \tag{2.9}$$

where L_{total} is the fraction of the total power lost in a single roundtrip to sources

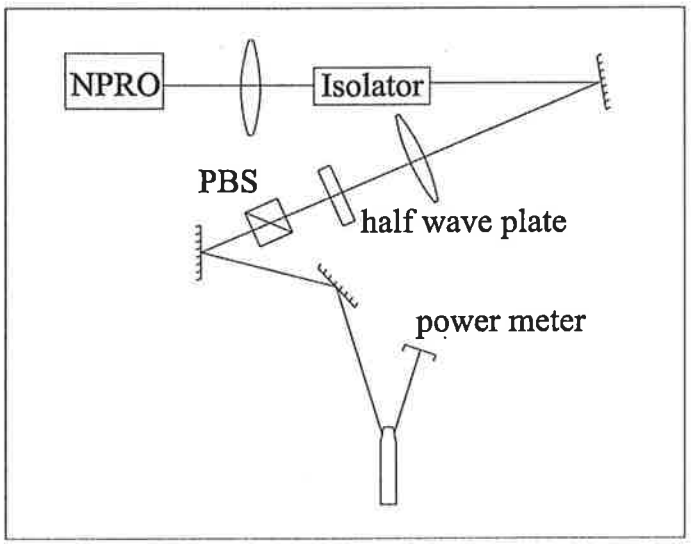

Figure 2.11: CPFS slab laser head gain measuring experiment

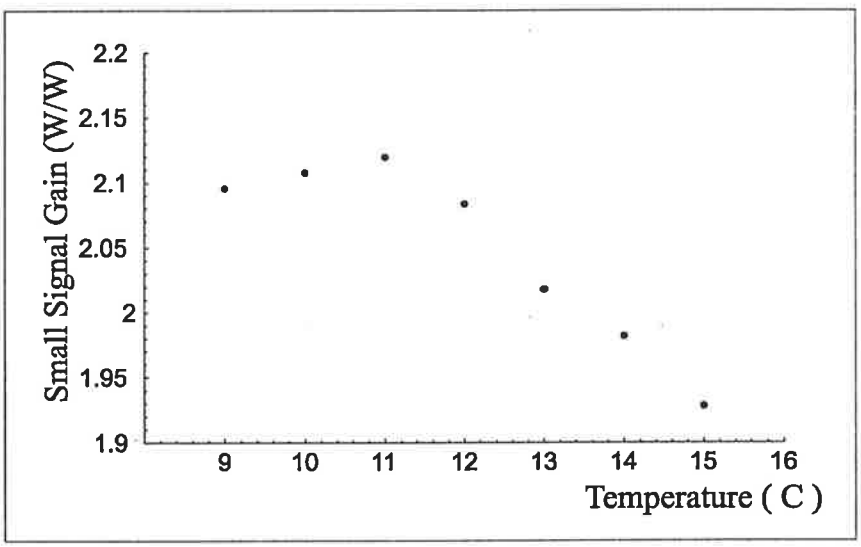

Figure 2.12: The small signal gain of the CPFS gain medium vs the temperature of pump diode. The CPFS gain medium was pumped using a single 20 W diode running at 20 W

of loss other than useful output coupling. For ring resonators the term $2g_0l$ is replaced by g_0l , to account for the gain medium being traversed only once. For a standing wave resonator with losses of L_{total}=6% (assumes two passes through the gain medium and negligible HR mirror loss) and g_0l=0.75, the predicted optimum value of output coupler transmission is T_{opt}=24%. For a ring resonator with losses of L_{total}=3.5% (assumes single pass through the gain medium and 0.5% HR mirror loss) and g_0l=0.75, the predicted optimum value of output coupler transmission is T_{opt}=13%.

The output power of the CPFS laser in standing wave configuration (see Fig 2.13) was measured for three different output coupler reflectivities. This was done with the resonator mirrors extremely close to the slab so that the laser ran in multiple transverse modes. The results are

Output Coupler Transmission (%)	40	20	10
Output Power (W)	3.4	6.3	6.1

These results demonstrate that the optimum output coupling fraction for the standing wave resonator is close to 20%, which is in reasonable agreement with the theoretical prediction. It can therefore be assumed with confidence that an output coupling fraction of 10% for the ring resonator will give close to optimum results.

2.4 Efficiency and Mode Confinement

The efficiency and mode confinement of a ring laser which used flat mirrors were investigated by using the CPFS pump geometry in a standing wave configuration. It is simpler to analyze the output of a standing wave laser than a bi-directional ring, as it has only one output.

In a standing wave resonator with flat end mirrors, waists are located on both end mirrors. Therefore if a standing wave resonator is constructed with end mirrors placed at the same distance from the Brewster angle windows as the waist in a ring laser, the transverse mode properties of the two resonators will be identical.

To obtain the highest output power from a CPFS slab laser the diverging pump

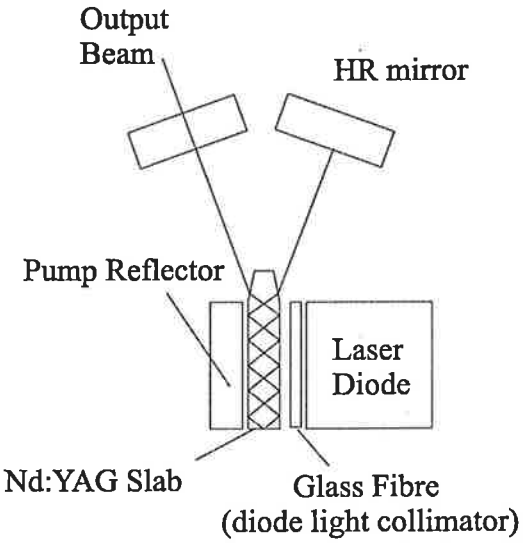

Figure 2.13: A schematic of the CPFS laser in a standing wave configuration

light must be collimated in the vertical direction. This could be done using a simple optical fibre as a cylindrical lens, however the best results were obtained by collimating the laser diode using a 1mm diameter AR-coated Doric lens that had a focal length of 0.685 mm. A Doric lens is a graded index optical fibre specifically manufactured to collimate laser diodes[77].

Using flat mirrors, an output coupler reflectivity of 20% and a slab to mirror distance of 20mm, an output power of 6.7 W was obtained from 20W of incident pump power with a slope efficiency of 50%. The resulting laser beam consists of multiple transverse modes.

The confinement of the slave laser mode is provided by lensing in the slab. Transverse mode control in the horizontal plane is provided by the Brewster-angle windows (see Fig 2.14). These provide an aperture of effective width 1.0 mm to the beam propagating outside the slab. A small amount of positive lensing is required in the horizontal plane to ensure stability. However in practice when a short cavity with flat mirrors is used and the output power is maximized the laser runs in multiple transverse horizontal modes. This suggests that the slab laser has sufficient horizontal lensing not only to ensure stability but also to reduce the size of the fundamental mode such that the apertures formed by the Brewster windows are no longer small enough to ensure fundamental mode operation. One of the initial papers written on

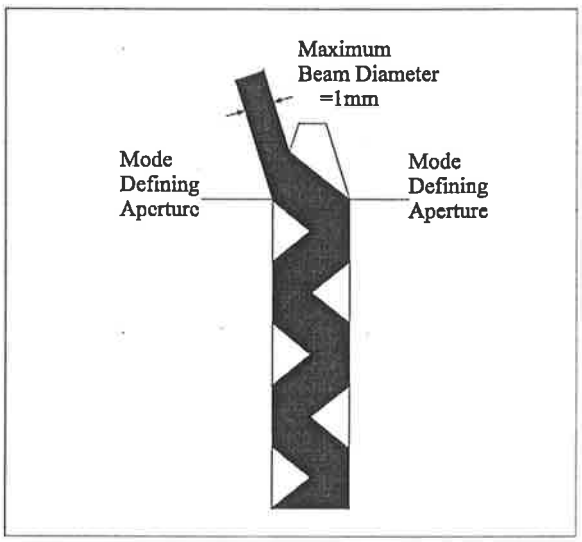

Figure 2.14: Schematic illustrating the horizontal mode defining apertures and the maximum extent of the slab laser mode in the horizontal direction.

the lensing behavior of CPFS slabs[51] suggested that the horizontal lensing was a thermal effect caused by end effects. However it was noticed by both us and workers at DSTO[53] that the ease with which CPFS slab lasers could be made to run in a fundamental mode varied between crystals. We have performed a test which conclusively shows that the lensing in the horizontal plane is independent of pump power, thus eliminating thermal lensing as a possible cause of the horizontal lensing. This test consisted of using a short (25mm slab to mirror distance) standing wave cavity. An extra intra-cavity edge was used to provide an additional aperture in the horizontal plane to force the resulting laser to run in a single transverse mode. The size and the M^2 of the mode were then determined, using a Spiricon beam profiler, for varying diode drive currents. The results are as follows:

Drive Current	Diode Power	Laser Power	Laser Power(apertured)	w_{0h} (mm)
30 Amps	19.0 W	6.0 W	5.1 W	0.32±0.02
26 Amps	16.0 W	4.6 W	3.8 W	0.31±0.02
22 Amps	12.7 W	2.9 W	2.5 W	0.31±0.02
18 Amps	9.3 W	1.3 W	1.1 W	0.31±0.02
15 Amps	6.8 W	30 mW		0.31±0.02

where w_{0h} is the measured size of the fundamental waist in the cavity. It is clear from these results that the size of the fundamental mode in the horizontal plane is independent of pump power and hence the lensing in that plane is not a thermal effect. We believe that the lensing in the horizontal plane is caused by residual curvature of the slab sides. Due to the multiple internal reflections and the off-normal angle of incidence reflections, even a slight curvature on the side faces results in the slab acting like a lens with focal length of the order of one metre. This will be discussed in greater detail in the following sections.

The mode confinement in the vertical plane is predominantly provided by thermal lensing. Since the slab is cooled by conduction through its top and bottom faces, a strong lens in the vertical plane is expected. It has been predicted[81] that the lens in the vertical plane can have a focal length as short as 40 mm for a 0.25 mm half-height pump distribution. This value agrees well with what we observed. For a cavity with a 45 mm slab-to-mirror distance, a 40 mm thermal lens should produce a fundamental waist size of 0.12mm, which is in excellent agreement with the experimentally determined value of 0.12±0.01 mm. As the thermal lens in the vertical plane is strong, laser cavities have to be kept short when using flat mirrors to ensure stability.

Fundamental mode operation in the vertical plane is realized by adjusting the distance between the Doric lens and the diode. This alters the collimation of the pump light and the height of the gain region, and hence the available gain for different transverse modes. As the height of the pumped region is reduced, the power of the thermal lens is increased[81] and the size of the fundamental waist is reduced. Fortunately the reduction in waist size occurs more slowly than the reduction in the height of the pumped region and hence transverse mode control may be achieved by reducing the height of the pumped region. We found that for lasers which use a 1mm diameter Doric lens this technique is effective in producing beams that have an $M^2 \cong 1$ for standing wave cavities whose slab to mirror distance is greater or equal to 45 mm. For cavities shorter than this, the height of the fundamental mode is too small for the pump light to be matched.

To demonstrate the effect of varying the fibre position on the vertical transverse

mode, a resonator was set up using flat mirrors and a slab to mirror separation of 45mm. For various horizontal positions of the Doric lens relative to the pump diode, the output power was recorded and the shape of the beam and M^2 was analyzed using a Spiricon Laser Beam Profiler. The results are shown in the following table and Fig 2.15.

Fibre position (mm)	M_v^2	Output Power
0.85	1.0	4.7 W
0.80	1.7	5.2 W
0.69.	2.2	5.4 W
0.65	2.9	5.2 W

where the fibre position is the distance between the laser diode and the centre of the Doric lens. To make the vertical behavior clearer, the horizontal plane was externally apertured such that the laser ran in a single horizontal transverse mode, which reduced the laser output power. These results demonstrate that good beam quality can be obtained for a small reduction in output power by adjusting the fibre position.

2.5 Slab Interferograms

To gain a greater understanding of the lensing in the horizontal plane the slabs were studied using an interferometric technique. The experimental setup used is illustrated as Fig 2.16. The HeNe beam was passed through a spatial filter. The re-collimated enlarged beam was then used to illuminate the side faces of the slab. The reflections from the front and back surfaces were passed through a beam reducer that also imaged the crystal onto the a CCD array. The interferograms, illustrated as Fig 2.17, indicate the degree to which the slab faces are out of parallel, and the degree to which the slab sides are curved relative to each other. This is also the curvature which the slave laser mode experiences as it bounces between them.

Four interferograms are shown. The long thin slab (Slab D) was purchased from Litton. It was designed for the high power laser project [54] and had very

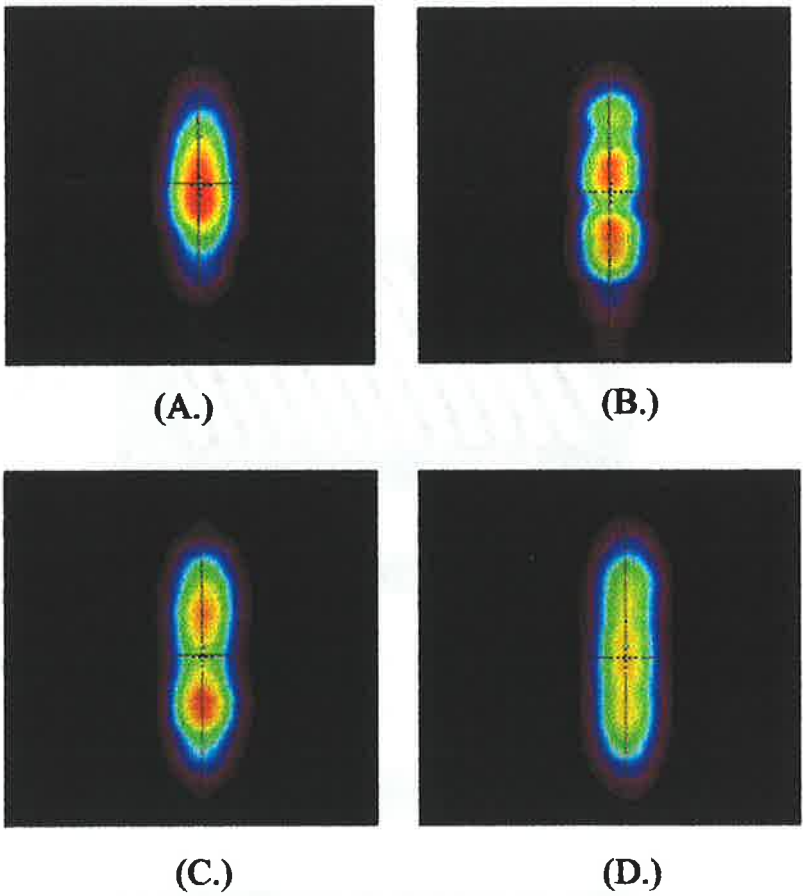

Figure 2.15: Vertical mode profiles for various diode to Doric lens distances (A) 0.85mm (B) 0.80mm, (C) 0.69mm and (D) 0.65mm

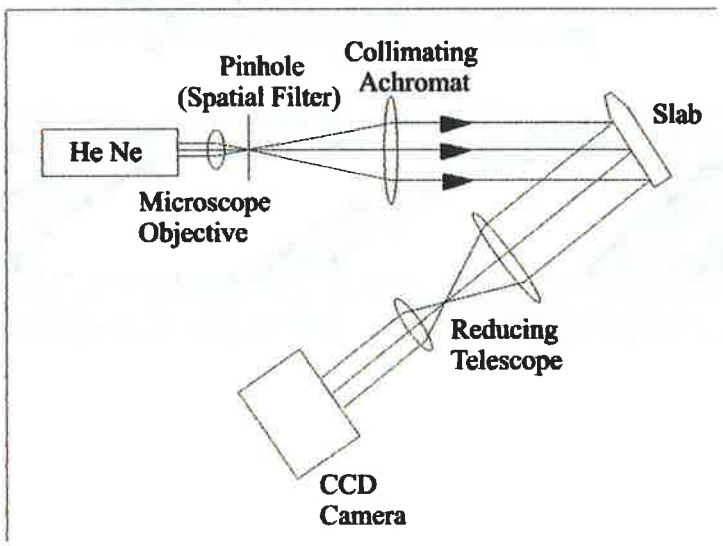

Figure 2.16: The set-up used to interferometrical test the relative quality and parrallelism of the slab side

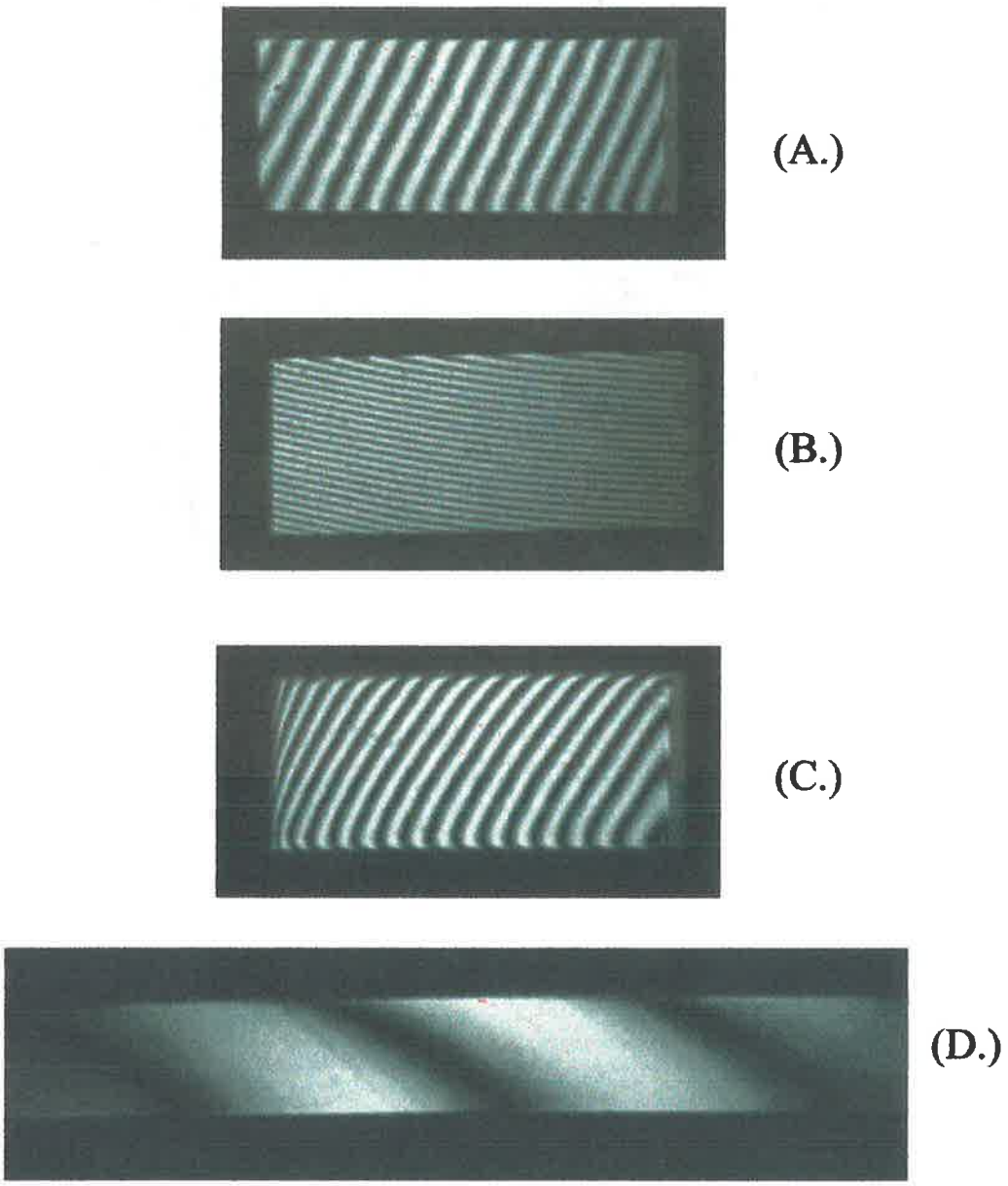

Figure 2.17: Interferograms of the the laser crystal used in this work

tight manufacturing tolerances specified. The inteferogram of this crystal is shown for comparison. Slab A has demonstrated good output power and good transverse mode properties and was used for the majority of the results presented in this thesis.

Slab B was the first crystal used in the slave laser development until it was damaged. Initially it was thought that for the slave laser to produce high output power the side faces of the slab had to be extremely parallel to avoid walk-off of the laser mode out of the pump plane. However Slab B produced excellent results with output powers comparable to that of Slab A for similar pump powers. It is clear from the interferogram that its side faces are not parallel in the vertical direction, in fact it has in excess of twenty waves of error over 5mm. The strong curvature of the side faces in the vertical direction under pump load obviously provides the stability required to avoid the walk off problem and hence the tolerance prescribed on the parallelness of the side faces in the vertical plane can possibly be relaxed.

Slab C was bought as a replacement for the damaged initial slab. Unfortunately, although the output power it produced was comparable to the other two slabs, its beam quality was not comparable for equivalent output power. Using a laser resonator similar to that used with the other two slabs, it produced a much smaller fundamental mode in the horizontal plane. This required a smaller aperture to enable it to run in a single transverse mode with a corresponding drop in output power. The extra curvature of the slab sides present in the horizontal plane is clear from the interferogram, where spacing of the fringes changes considerably from one end of the slab to the other. A conclusion from this work is the slab laser is particularly sensitive to any residual curvature in the horizontal plane. Some curvature is necessary to provide stability as there is no thermal lensing in the horizontal plane. If the curvature is insufficient and the fundamental mode is thus large then aperture clipping losses will significantly reduce the laser efficiency. However, one can always provide additional mode confinement by using a concave mirror. If the curvature is too great then the mode size will be small and the fundamental mode will not couple to the available gain efficiently.

The combination of the requirement of a relatively large mode in the horizontal direction and the eleven-bounce geometry which compounds the effect of side cur-

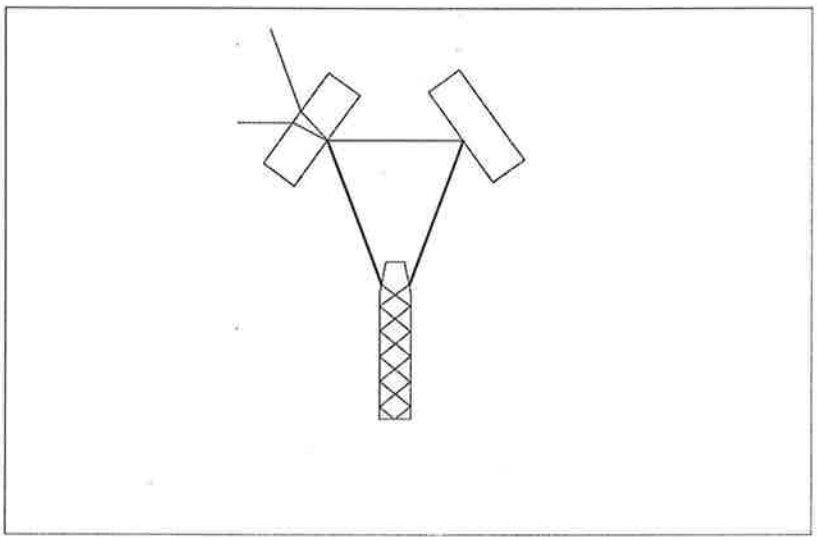

Figure 2.18: A schematic of the ring laser resonator with the out-of-slab cavity length shown as the bold line

vature, means that a tight tolerance on surface curvature is required. To restrict lasing to a single transverse mode, a spot size of 0.360 mm is required. In a symetric standing wave cavity in which the slab to mirror distance is 45mm, this requires a radius of curvature of 220m. In practice, flatness at this level is very difficult to achieve. However, this specification could be somewhat relaxed if a dynamically stable resonator [82] was designed for the horizontal plane. Such a resonator would be insensitive to small changes in horizontal curvature. This would be quite useful if many of these lasers were to be manufactured. However, this is quite a complex procedure when vertical stability requirements also need to be met. Further, additional resonator elements can degrade both the efficiency and the stability of the laser resonator and toroidal elements are usually of very low quality. We have found that simple compensation for the slab horizontal lensing can be achieved by changing the flat maxR mirror to a slightly convex or concave mirror, depending on the lensing present. This can compensate for the curvature in a particular crystal and will be discussed in greater detail in the following section.

2.6 Ring Resonator Results

As was mentioned in the previous section, crystals that had minimal surface curvature still had significant lensing in the horizontal plane. The lensing was large enough that when these crystals were used in flat-flat resonators in which the vertical height of the fundamental mode was correct, the horizontal waist size was too small to enable single transverse mode operation. To increase the size of the mode in the horizontal plane, a convex mirror was used as the HR mirror. Using Slab A and an out-of-slab cavity length (see Fig 2.18) of 85mm the best results were achieved using a 3 m or 5 m convex spherical mirror. The waist sizes and M^2 values for the horizontal and vertical planes at a pump power of 19 W are shown in the following table. Shown for comparison, are the results obtained using two flat mirrors, although it should be noted that single transverse mode operation in the horizontal plane was only achieved with an additional aperture inserted into the resonator. Also shown are the results for a slightly larger ring (slab-slab length of 105mm) where single transverse mode operation in the horizontal plane was achieved by misaligning the slave cavity in that plane. This has the effect of shifting the laser mode closer to one side of a Brewster-window aperture. Note that almost identical powers are achieved for flat -flat resonators, in which single transverse mode operation is obtained using either an intra-cavity aperture or mirror misalignment.

Mirror Radius (m)	Power	w_{oh}	w_{ov}	M_h^2	M_v^2
3m	5.0 W	380±30	155±15	0.99±0.1	1.20±0.1
5m	5.0 W	353±30	150±15	0.95±0.1	1.14±0.1
Flat (apertured)	4.4W	340±30	160±16	0.94±0.1	1.14±0.1
Flat (misaligned)	4.5W	345±30	160±16	0.95±0.1	1.10±0.1

The M^2 and waist sizes were measured using a Spiricon M^2 beam analyzer. This device uses a lens to create an artificial waist. The beam size is measured at various places at and around the artificial waist. The internal algorithm of the beam profiler then fits Equation 2.10 to the data, using a weighting system to favor those points closest to the artificial waist.

$$W^2(z) = W_1^2 + \Theta_1^2 (z - Z)^2 \tag{2.10}$$

where $W(z)$ is the diameter of the laser beam at point z, W_1 is the width of the beam at the artificial waist, Θ_1 is the far field divergence angle for the beam from the artificial waist and Z is the position of the artificial waist.

The values of W_1 and Θ_1 that give the best fit of Equation 2.10 to the data are then used to determine the M^2 of the laser using

$$M^2 = \frac{W_1 \Theta_1 \pi}{4\lambda} \tag{2.11}$$

where the λ is the wavelength of the laser light. The waist sizes in the laser under test are then calculated using the Gaussian beam propagation formula and the focal length of the lens used to create the artificial waist.

The artificial waist size data are shown in Fig 2.19 for the resonators that used the 3m and 5m radii of curvature, convex, max-R mirrors. The fits are very good. In the horizontal plane the M^2 error range includes values that are less than 1. It should be noted that theoretically M^2 values cannot be less than 1. Therefore the likely value of the true M^2 value in the horizontal plane is marginally more than 1. Hence the resulting beam is extremely close to diffraction limited in both the vertical and horizontal planes. When a 1m convex mirror was used as the max-R reflector, the laser had an output power of less than 3 Watts and a poor quality beam.

Using a flat-flat ring resonator a total output power of 5.0 W was obtained with 19 W of diode pump power and no external aperture. When a geometrically equivalent standing wave resonator was set up, the maximum power that obtained was 5.2 W. These two values are sufficiently close to assume that the choice of a 90% output coupler was correct and that there are no alignment problems with the ring resonator.

The directional discrimination that enables the laser to operate in a single direction is provided by injection locking. When the ring laser is free running it operates in both directions with up to eight longitudinal modes. Mode competition between

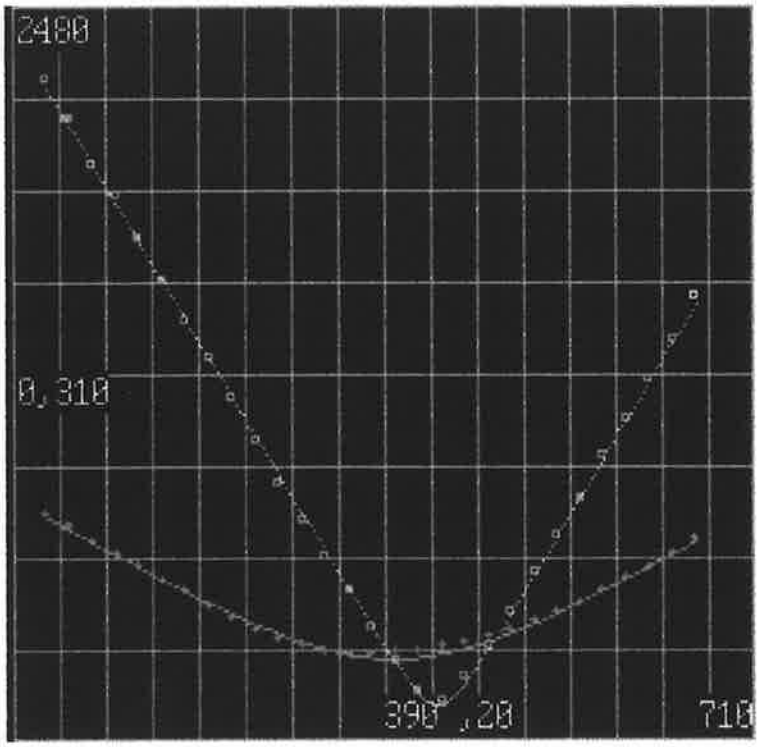

(A.)

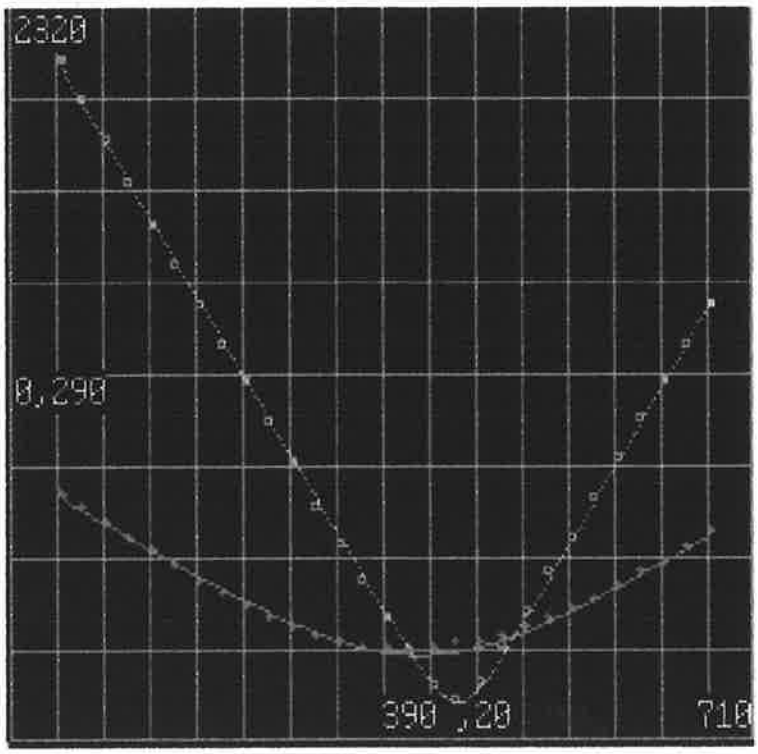

(B.)

Figure 2.19: The artificial waist data for M^2 analysis of ring resonators utilising convex mirrors of radius of curvature (A) 5m (B) 3m. The blue curves are for the vertical and the red curves are for the horizontal plain.

counter-propagating modes causes rapid fluctuations of the intensities in the two directions. By adjusting the horizontal tilt of one of the mirrors, one direction can average up to ten times more power than the other. This effective reverse-wave suppression is caused by an asymmetry in the light scattered by the Brewster windows, combined with the greater acceptance angle of a diverging mode than a converging mode. The maximum total output power for a flat-flat resonator is obtained when the average power in the two counter propagating modes are approximately equal. The difference in the output powers between the two counter propagating modes means the output power of both directions must be measured during alignment to achieve the maximum total output power. This is usually done by using a beam steering mirror to guide the two outputs onto the same power meter.

Chapter 3

Injection Locking of the Slave Laser

3.1 Introduction

Injection-locking is a well known technique for synchronizing two laser or maser systems. The first comprehensive work on the theory of injection-locking was done by Adler[83] for microwave masers. This first demonstration of the injection-locking of lasers was performed by Stover and Steier of Bell Telephone laboratories in 1966 using two single frequency helium neon lasers[42].

Most common examples of injection locking use the technique to transfer the intensity and frequency characteristics of a stable master laser to a much higher power, noisier slave laser. The low power master "captures" the mode of the noisy high power slave. Several authors have discussed the classical theory of injection locking [41][43][84]. A particularly useful account which enables some physical insight to be gained is given by Siegman[73]. From this account it becomes possible to appreciate such concepts as the injection locking range and the physical mechanism by which the free running slave laser mode can be extinguished and replaced by an amplified version of the master laser. Siegman also presents a semi-classical rate equation analysis of injection-locking. This theory is the basis of later works which use the semi-classical theories of injection locking to predict the effect of noise sources that are well above the quantum limit[75][62]. To describe the output of an

injection locked laser with a quantum noise limited master and pump laser it is necessary to use a fully quantum mechanical model such as that presented by Ralph et al[61] [60][85]. At present these models have concentrated on and provided analytical transfer functions for the intensity noise only. To gain an understanding of the contributions to the frequency noise of the injection locked laser, it is necessary to refer to the semi-classical model presented by Farinas et al[62] and Barrilet et al[75]. A summary of the noise transfer theory will be provided at the start of Chapter 4.

I will summarize the injection locking theory provided by Siegman and its extension by other authors in the next section. In subsequent sections I will describe parameters that were optimized to provide stable injection-locking and single mode operation. The performance of the injection locked laser without a servo system will be described. I will then describe the design of a servo system that was constructed to provide long term injection locking. I will finish this chapter by analyzing the performance of the servo system and show that its performance is in good agreement with the that predicted by control theory.

3.2 Theory of Injection Locking

A laser with the pump level set just below threshold for laser oscillation can be used as an optical amplifier (normally called a regenerative amplifier). If the laser is set up as shown in Fig 3.1 the input field (E_{inc}) is related to the output field (E_{out}) by

$$E_{out}(\omega) = \frac{1}{\sqrt{R}} \frac{R - G_{rt}(\omega)}{1 - G_{rt}(\omega)} E_{inc} \tag{3.1}$$

where $G_{rt}(\omega) = G(\omega)e^{-j\phi(\omega)}, \phi(\omega) = \omega p/c$ is the round-trip phase shift, R is the reflectivity of the laser output coupler, p is the optical round trip length of the resonator and $G(\omega)$ is the magnitude of the net round trip amplitude gain including losses and output coupling. This equation is derived in Appendix A2.

The resonator is simply a mechanism for providing positive feedback to an amplifier, hence trading bandwidth for gain. Using this assumption, in the highly regenerative limit (ie $G(\omega) \rightarrow 1$) Equation 3.2 can be simplified to

$$E_{out}(\omega) \cong -\frac{1-R}{1-G+jG\tau_c(\omega-\omega_c))}\frac{E_{inc}(\omega)}{\sqrt{R}} \tag{3.2}$$

where ω_c is the frequency of one of the lasers free running modes and τ_c is the cavity round trip time. It can be seen in the limit as $G \rightarrow 1$ the gain tends to infinity at frequencies equal to the slave resonator modes.

When the magnitude of the round trip gain (G) exceeds 1, the optical amplifier becomes unstable and oscillation or lasing occurs. Gain saturation then clamps the magnitude of the round trip gain at unity for the lasing wavelength. If a laser is oscillating and a small signal is injected into the laser cavity at a frequency slightly different from a free running mode of the laser, the signal may be amplified, with almost no effect on the free running modes of the slave laser. As the frequency of the injected signal is tuned closer to that of the free running modes of the laser, the small injected signal will be amplified more strongly. When the magnitude of the amplified injected signal approaches that of the free running slave mode, the amplified signal begins to saturate the gain and rob the free running mode of gain. Eventually the free running mode is extinguished and only the amplified incident signal remains.

The above discussion illustrates that for a small injected signal to gain control of the laser, its frequency must be sufficiently close to one of the modes of the free running laser. The range of frequencies for which this occurs is defined as the injection locking range. The theory described below will show that it is given by the following equation:

$$\Delta\nu_l = \Delta\nu_c\sqrt{\frac{P_m}{P_s}} \cong \frac{T.FSR}{\pi}\sqrt{\frac{P_m}{P_s}} \tag{3.3}$$

where $\Delta\nu_c$ is the slave laser cold cavity linewidth, P_m is the power incident on the output coupler that is mode matched into the spatial mode of the slave laser, P_s is the output power of the slave laser, T is the transmission of the slave laser's output coupler and FSR is the free spectral range of the slave laser resonator. A compact resonator will have a larger free spectral range and hence a larger locking range.

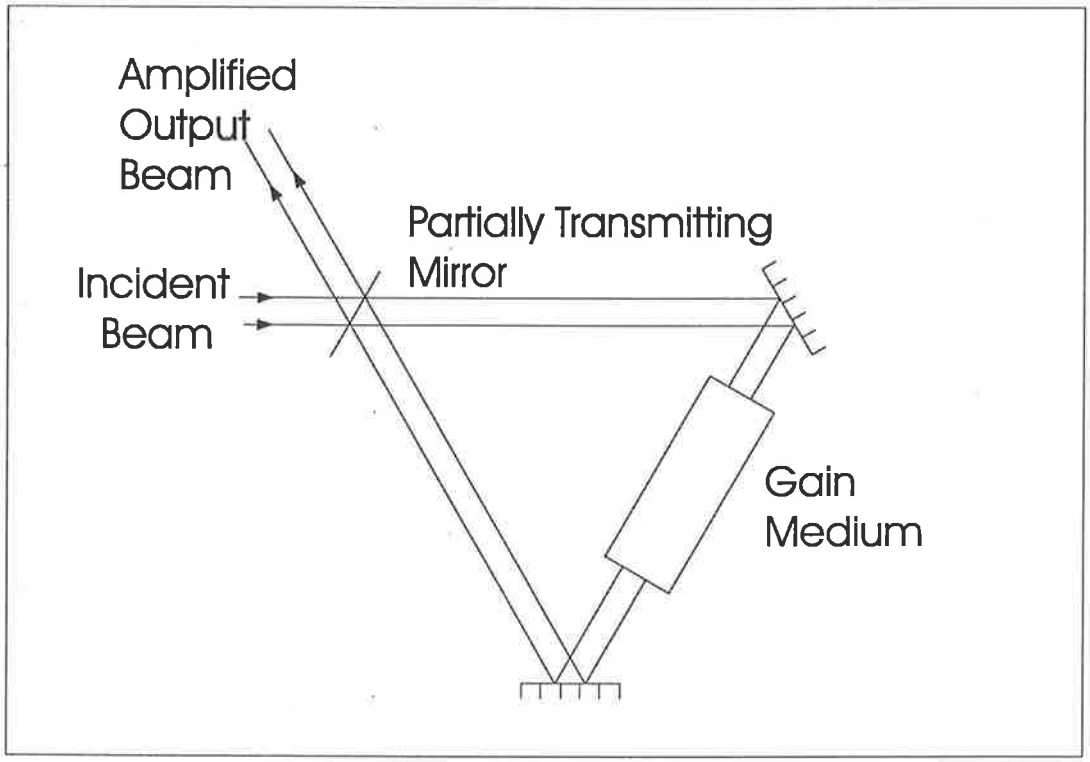

Figure 3.1: A laser resonator used as a narrow band amplifier

A more advanced model of injection locking based on laser dynamic equations is also presented by Siegman and has been extended by Farinas *et al.* [62]. The laser dynamics are described by three differential equations that make use of the slowly varying envelope approximation; the rate of change in amplitude and phase is slow compared with the inverse of the frequency of the laser light:

$$\frac{d\,\bar{E}(t)}{dt} + [\gamma_c/2 + j(\omega - \omega_c)]\,\bar{E}(t) = -j\frac{\omega}{2\epsilon}\,\bar{P}(t) + \left(\frac{2\gamma_e}{\epsilon V_c}\right)^{1/2}\bar{E}_m(t) \tag{3.4}$$

$$\frac{d\,\bar{P}(t)}{dt} + [\Delta\omega_a/2 + j(\omega - \omega_a)]\,\bar{P}(t) = -j\frac{\kappa}{2\omega V_c}\Delta N(t)\,\bar{E}(t) \tag{3.5}$$

$$\frac{d\Delta N(t)}{dt} + \gamma_2 \Delta N(t) + R_p(t) = j\frac{V_c}{4h}\left[\bar{E}^*(t)\bar{P}(t) - \bar{E}(t)\bar{P}^*(t)\right] \tag{3.6}$$

where $\bar{E}$ is the complex cavity mode amplitude, $\bar{E}_m$is the amplitude of the in-

jected signal, P is the atomic polarization, ΔN is the atomic population difference, R_p is the pumping rate, ω_a is the atomic transition frequency with an linewidth of $\Delta\omega_a$, κ is the cavity signal to cavity polarization coupling coefficient, V_c is the mode volume of the resonator,γ_c is the total photon cavity decay rate, γ_e is the cavity decay rate due to the output coupler and γ_2 is the spontaneous emission decay rate of the upper state.

These equations may be solved[73] using the assumption that the atomic polarization relaxes much faster than the electric field or the atomic population. Using this approximation and assuming that the injected master field and the slave laser field, can be written respectively in the form $\bar{E}_m(t) = E_m(t)\exp[j\phi_m(t)]$ and $\bar{E}(t) = E(t)\exp[j\phi(t)]$, the following equations can be derived.

$$\frac{dE(t)}{dt} + \frac{\gamma_c - \gamma_m}{2}E(t) = -\gamma_e E_m(t)\cos[\phi(t) - \phi_m(t)] \tag{3.7}$$

$$\frac{d\phi(t)}{dt} + \omega_m - \omega_s(t) = -\gamma_e \frac{E_m(t)}{E(t)}\sin[\phi(t) - \phi_m(t)] \tag{3.8}$$

where γ_m is the rate of growth of the cavity field of the slave laser due to the saturated gain and $E_m$and E are the fields measured just outside the slave laser output coupler. Equations 3.7 and 3.8 describe the time evolution of the phase and amplitude of the injection-locked laser.

If it is assumed that the intensity of the master laser is much less than the intensity of the slave, ie $E(t) \simeq E_s(t)$ then Equation 3.8 can be written as

$$\frac{d\phi(t)}{dt} + \omega_m - \omega_s(t) = -\gamma_e \frac{E_m(t)}{E_s(t)}\sin[\phi(t) - \phi_m(t)] = -\omega_{lock}\sin[\phi(t) - \phi_m(t)] \tag{3.9}$$

where $\omega_{lock} \equiv \gamma_e \frac{E_m(t)}{E_s(t)}$. Equation 3.9 is the well known Adler equation that was first derived for microwave oscillators[83]. For steady state locked behavior, when $\frac{d\phi(t)}{dt} = 0$,

$$\phi(t) - \phi_m(t) = Arc\sin\left[\frac{\omega_m - \omega_s(t)}{\omega_{lock}}\right] \tag{3.10}$$

The steady state phase difference between the master and the slave is dependent on the relative difference in frequency between the free-running slave laser and the master. Equation 3.10 shows that the steady state phase difference is real only if $-\omega_{lock} \leq \omega_m - \omega_s(t) \leq \omega_{lock}$. The range of slave laser frequencies for which injection locking will occur is thus given by Equation 3.3. For the parameters used in thesis the locking range is of the order of 10 MHz.

The detection of the above phase shift forms the basis of two types of discriminators [10][45][86] used to provide the error signal for feedback control of the slave laser resonator to ensure that the free-running frequency of one of its modes falls within the injection locking bandwidth.

It is well known that injection locking can force a laser that is oscillating in multiple axial (longitudinal) modes to oscillate at a single frequency[45]. The reason is that the injected signal is amplified to such a level that it saturates the gain further than it would be in free-running operation. Therefore it does not have enough gain to support any of the other free running modes. The level of gain saturation can be determined by solving Equations 3.7, to give

$$\gamma_c - \gamma_m = \frac{2\gamma_e E_1}{E} \cos\left[\phi(t) - \phi_m(t)\right] = \omega_{lock} \cos\left[\Delta\phi(t)\right] \tag{3.11}$$

For a free-running laser the rate at which lasing light is added to the cavity by stimulated emission exactly equals the rate at which light is lost due to output coupling and other losses, and thus $\gamma_c - \gamma_m = 0$. However Equation 3.11 shows that in an injection locked laser, the slave laser gain is saturated to such an extent that the round trip gain (ie $Exp[(\gamma_c - \gamma_m)\tau_c]$) is less than one and hence a free-running laser mode is not possible. The slave laser becomes a regenerative amplifier with its power gain limited by the saturation properties of the slave laser gain. Equation 3.11 also shows that round trip gain of the resonator is reduced as the difference in frequency between the free running mode of the slave laser and the master laser is made smaller. Hence higher suppression of spurious modes is achieved when the frequency of the slave is tightly locked to that of the master. This is particularly relevant when effects such as spatial hole-burning are present in the resonator.

3.3 Passive Injection Locking Performance

The compactness and rigid construction of the slave laser resonator enables excellent free-running performance: injection-locking was maintained for periods of up to thirty seconds without the use of servo control. In this section on passive injection locking I will describe the mode matching of the master light to the slave laser resonator and the temperature matching of the crystals of slave and master lasers. Temperature matching of the master and slave lasers' crystals was found necessary to ensure that the frequency where the maximum gain of the slave and the master occurred was matched.

3.3.1 Mode Matching and Alignment

When an arbitrary TEM_{00} mode is incident upon a resonant structure, its field with be coupled into the various transverse modes of the resonator. Mode matching is required to ensure that all of the incident field is coupled into the fundamental mode of the resonator. In the case of injection locking, incorrect mode matching manifests itself as a reduction of the locking range.

The types of mismatch between the master field and the fundamental slave laser mode can be categorized into four types [87]:

- Waist size mismatch
- Waist position mismatch
- Angular misalignment
- Transverse displacement

The first two forms of mismatch occur when the waist and the radius of curvature of the master beam are not matched to the fundamental mode of the slave laser. The fundamental mode of the slave laser is elliptical which makes accurate mode matching of the master laser to this mode more complicated. Initially we decided to simply focus the master laser to a circular spot, with its size in between the sizes of the slave laser mode in the vertical and the horizontal planes. A simple extension

of the formula presented by Siegman[73] enables theoretical coupling efficiency to be calculated, the result is

$$\frac{P_{coupled}}{P_{incident}} = \frac{4}{w_{mx}w_{sx}w_{my}w_{sy}\sqrt{\left(\frac{1}{w_{mx}^2}+\frac{1}{w_{sx}^2}\right)^2+\frac{k^2}{4R_{sx}^2}}\sqrt{\left(\frac{1}{w_{my}^2}+\frac{1}{w_{sy}^2}\right)^2+\frac{k^2}{4R_{sy}^2}}} \tag{3.12}$$

where $k = \frac{2\pi}{\lambda}, w_{mx}$, w_{my} is the master waist size in the horizontal and vertical planes respectively within the slave resonator; w_{sx}, w_{sy} is the spot size of the slave laser measured at the location of the masters waist; R_{sx}, R_{sx} are the radii of curvature of the wavefront of the slave laser, also measured at the location of the master's waist. Equation 3.12 is derived in Appendix A3.

The master and slave laser's radius of curvature are closely matched and therefore any mis-match will be ignored. Using this approximation and assuming the slave waist size is (0.35mm, 0.15mm) and the master waist size is 0.2 mm, Equation 3.12 indicates that the fraction of the master power injected into the slave laser fundamental mode is 0.82. With 82% coupling efficiency the locking range should be 92% of the full range. We have measured the locking range by sweeping the frequency of the master laser by a known amount and determining the range of frequencies over which complete extinquishment of the reverse slave laser mode occurs. The reverse slave laser mode is the mode that propogates in the opposite direction around the slave laser ring resonator to the mode which we injection-lock. For the case of a master power of 80mW and a slave power of 4.0 W, the locking-range was found to be 8.5±1.0 MHz, compared with an optimum theoretical value of 8.7 MHz. We conclude from this that elaborate, exact matching of the master laser waist size is not necessary.

The optics for the modematching of the master laser field were designed using the simple modematching formula presented in the paper by Kogelnik and Li[88]. To match a waist size w_{in} to a waist size of w_{out} a simple thin lens can be used. If the lens is placed a distance d_1 from waist w_{in} and then the waist w_{out} will be found a distance d_2 from the lens where

$$d_1 = f \pm \frac{w_{in}}{w_{out}}\sqrt{f^2 - f_0^2} \tag{3.13}$$

$$d_2 = f \pm \frac{w_{out}}{w_{in}}\sqrt{f^2 - f_0^2}$$

$$f_0 = \frac{\pi w_{in} w_{out}}{\lambda} \tag{3.14}$$

where f is the focal length of the modematching lens. In our experience, accurate knowledge of the initial waist position is necessary to obtain accurate size matching. In our injection-locked laser scheme two lenses were necessary, the first one to guide the light through the EOM and the optical isolator without significant clipping loss, the second to modematch into the slave laser resonator.

The last two forms of mismatch occur due the master laser not being aligned with the optical axis of the slave resonator. Correct alignment of the master laser was achieved by first locating the slave laser beam using a pinhole and a CCD camera. The master laser was then aligned such that when it was reflected off the output coupler it matched the spatial position and orientation of the slave laser beam.

It was noticed that a slight mismatch in the alignment of the laser beam caused a significant reduction in the locking range. Both angular misalignment and transverse displacement predominantly couple light into the TEM_{01} mode of the slave laser resonator. The coupling coefficients for these effects have been derived by Andersen[87]. The amplitude coupling coefficient for angular misalignment is

$$c_{01(tilt)} = \alpha\frac{\pi w_0}{\lambda}$$

where w_0 is the waist size of the slave laser, α is the angle between the input master field and the slave laser measured at the waist of the slave laser and λ is the wavelength of the laser light. Note that this coupling coefficient assumes that there is no other form of misalignment. If the maximum reduction of the locking range is to be 10% and the slave waist size is 300μm, then $\alpha < 10^{-4}$ radians.

The amplitude coupling coefficient for transverse displacement is

$$c_{01(displacement)} = \frac{x_d}{w_0}$$

where x_d is the transverse displacement between the slave laser beam and the input master laser beam measured at the location of the waist. Like the other coupling formula, this coupling coefficient assumes that there is no other form of misalignment.

The mode-matching of the slave laser was limited by waist size mis-match and not by our alignment technique. However, over a period of weeks the locking range was found to decrease due to mirror misalignment. If an injection-locked laser is to be used for a long period, then rigid and stable mirror mounts must be used to guide the master laser.

3.3.2 Master and Slave Temperature Matching

For convenience, injection locking was often achieved by tuning the NPRO frequency to a dominant mode of the slave laser. When the master laser was sufficiently close to a slave laser mode, the frequency control servo of the slave would take over and adjust the slave frequency to be that of the master. It was done this way as the master frequency was very easy to tune by altering its temperature (tuning coefficient ~2 GHz/C).

However, the line center of the monolithic NPRO was found to be temperature dependent. Thus, if the slave and master lasers are not temperature matched, the master laser will injection-lock a slave laser mode that is far from the slave laser gain centre. The result of this is a reduction in the range of frequencies over which complete extinguishment of spurious slave laser modes occurs. If the temperature of the crystals were badly mis-matched (~20oC) complete extinguishment of the free running slave laser modes would not occur even if the frequency of master laser was exactly matched to an axial mode of the slave laser resonator.

3.4 Injection Locking Servo Design

To achieve long term injection locking, servo control of the slave laser resonator frequency is necessary. Further, if the slave laser frequency is different from that of the master but still within the locking range, frequency noise can be coupled into the intensity noise spectrum of the injection-locked laser[75]. Hence, to prevent degradation of the intensity noise spectrum of the injection locked laser, the slave laser frequency must be tightly servo controlled.

A schematic of the servo used to achieve long term injection locking is shown as Fig 3.2. A block diagram describing the servo is illustrated as Fig 3.3. The servo loop consists of four main parts: the discriminator, pre-amplifier, high voltage (HV) amplifier and actuator. The design and transfer functions of the discriminator, actuator and HV amp will be first discussed in detail and then the design of the pre-amp will be discussed. The pre-amp is designed to enable the optimum feedback loop performance given the limitations of the actuator, discriminator and HV amp. To minimize the effect of the electronic noise of the servo, the gain of the discriminator and the pre-amp must be as high as possible [71], even if this means reducing the gain of the actuator to ensure that the servo loop remains stable. A convenient way to minimize the effect of servo noise is to use the capacitance of the PZT actuator in a low pass filter.

3.4.1 The Discriminator

The discriminator uses the Pound-Drever-Hall technique[10] to derive an error signal. As was shown in Section 3.2, if the frequency of the slave does not exactly match that of the master laser then there will be a phase difference between the output of the injection-locked laser and the master laser. From Equation 3.10, this phase difference varies from $-\frac{\pi}{2}$ to $\frac{\pi}{2}$ as the slave laser resonator is scanned through the whole locking range. The Pound-Drever-Hall discriminator is an RF sideband technique that detects this phase difference by imposing phase-modulation sidebands on the master laser. This can be done using either an external electro-optic modulator (EOM) or by modulating the master laser directly at one of its natural crystal

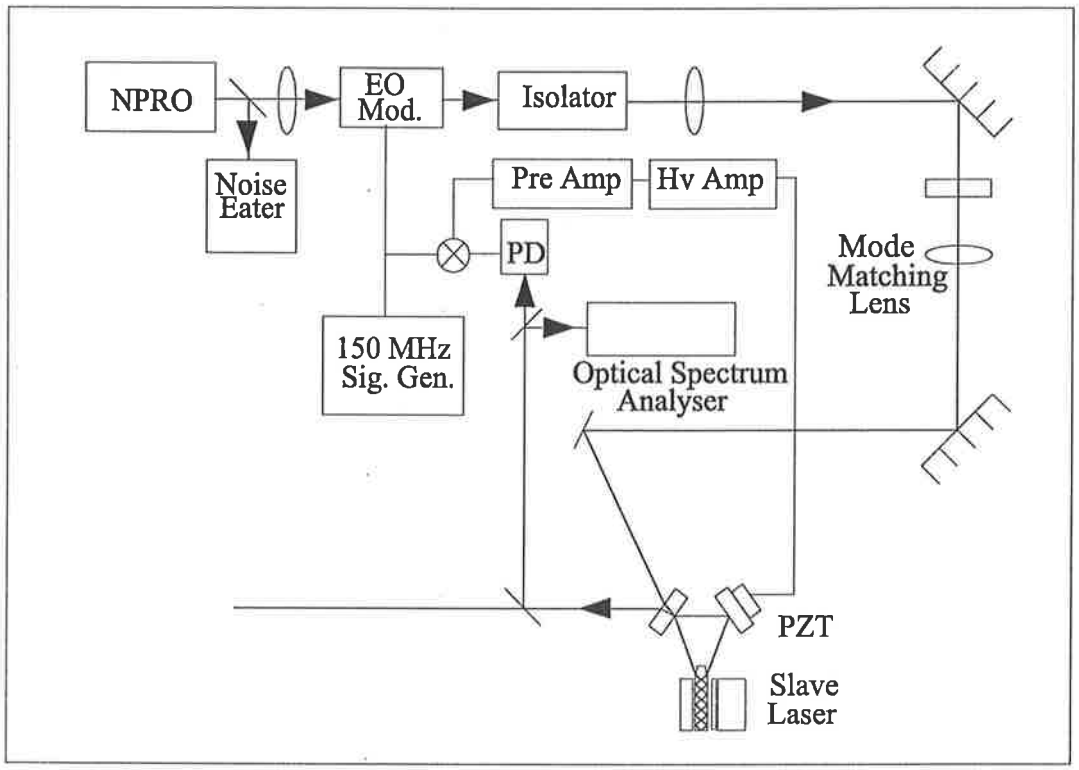

Figure 3.2: A schematic of the Pound Drever Hall servo system

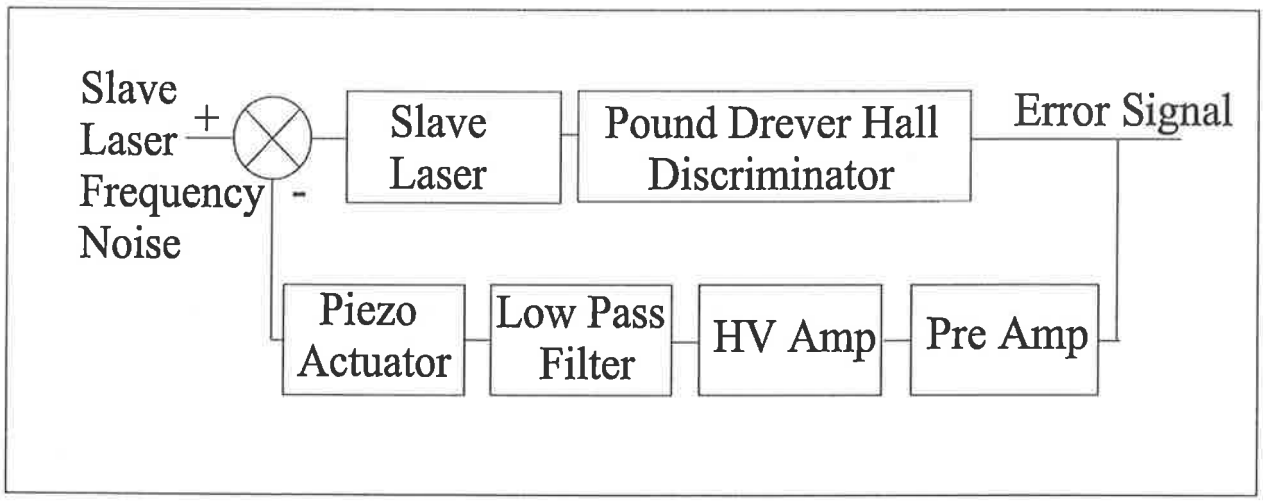

Figure 3.3: A block diagram of the Pound Drever Hall servo system

resonances using a PZT [89]. The phase-modulation frequency must greater than the cavity linewidth so the sidebands will be reflected by the output coupler with no change in phase. Our slave laser resonator is compact and hence its linewidth is large (~60 MHz). We therefore chose to use an 150 MHz tuned EOM to generate the phase-modulation sidebands. Note that the EOM is placed before the optical isolator so that it is protected from the optical power of the reverse wave of the free-running slave laser.

The slave laser light is mixed with the phase modulated master on a photodiode. If the free-running frequency of the slave laser is equal to that of the master laser, then the injection-locked laser light is in phase with the master laser light and thus no amplitude modulation will occur. However if a frequency difference is present, then the modulation products will not cancel and an amplitude modulation term will be produced. The magnitude of the amplitude modulation term is proportional to the sine of the phase difference. It is heterodyned to DC using a double balanced mixer with the local oscillator being provided by a sample of the EOM drive.

The discriminator sensitivity is derived in Appendix A4 and is given by

$$\frac{\Delta V(t)}{\Delta \omega(t)} = \frac{-2R_f \eta_d \eta_p \eta_{DBM} \sqrt{P_s P_m} J_1(\beta)}{\omega_{lock}} \tag{3.15}$$

where η_d is the sensitivity of the photodiode, η_p is the percentage of the total field measured by the photodiode, η_{DBM} is the efficiency of the double balanced mixer, R_f is the transimpedance gain of the photo-detector, P_m is the power of the master, P_s is the power of the slave and β is the phase modulation depth. The sensitivity of the discriminator is independent of frequency within the bandwidth of the servo (DC-10kHz).

3.4.2 The Actuator

A piezo-electric transducer (PZT) with a mirror bonded to it is used as the actuator. The actuator converts the feedback voltage to a frequency correction, by altering the optical path length of the slave resonator. Electo-mechanical actuators generally have lower resonant frequencies than purely electrical systems. Disc PZTs were found to have higher resonant frequencies than tube PZTs. However, greater

displacement per volt can be achieved for tube PZTs than for disc PZTs, unless many discs are bonded together. Often the maximum displacement obtainable by PZTs is limited by the high voltage amplifier used to drive them, as high voltage swings at high modulation frequencies (>10 kHz) can be difficult to achieve. Hence systems that make use of PZTs which have a greater displacement per volt often have a greater dynamic range. In summary disc PZTs have high bandwidth and a low dynamic range, whilst tube PZTs have a lower bandwidth and a higher dynamic range.

To achieve the conflicting goals of high bandwidth and high dynamic range other workers have found it necessary to use a split feedback[49] [75]. Split feedback systems utilizes two PZT actuators: a narrow bandwidth PZT with large dynamic range and a high bandwidth PZT with low dynamic range. To achieve the required loop gain with a single PZT actuator, the design becomes critical. After much experimentation it was decided that the best solution was to use a balanced disc PZT, as this enabled the largest servo bandwidth and the reduction in dynamic range was found not to be significant.

The configuration used consists of two annular PZT discs mounted 'back-to-back' with a thin sheet of copper shim sandwiched between them. The discs were made from Pz27[90] with 10mm thick, 10mm inside diameter and 25mm outside diameter. The disc PZT assembly was held by the mount in a balanced configuration, as shown in Fig 3.4. The HR mirror was mounted on one end of the PZT stack and a counter balance mass was mounted on the other. The PZT stack is held by the mirror mount at the plane of its centre of mass. This balance arrangement results in negligble reaction forces on the mount, and thus prevents low frequency resonances of the mount from adding parasitic resonances to the transfer function. Using two PZTs mounted back-to-back rather than a single balanced PZT doubles the dynamic range of the system, but halves the frequency of the lowest longitudinal resonance. The copper shim acted as an electrode and was grounded, the high voltage signal was applied to the other ends of the PZTs.

The transfer characteristics of the actuator are shown as Fig 3.5. These characteristics were measured by placing the actuator in a Mach-Zender interferometer

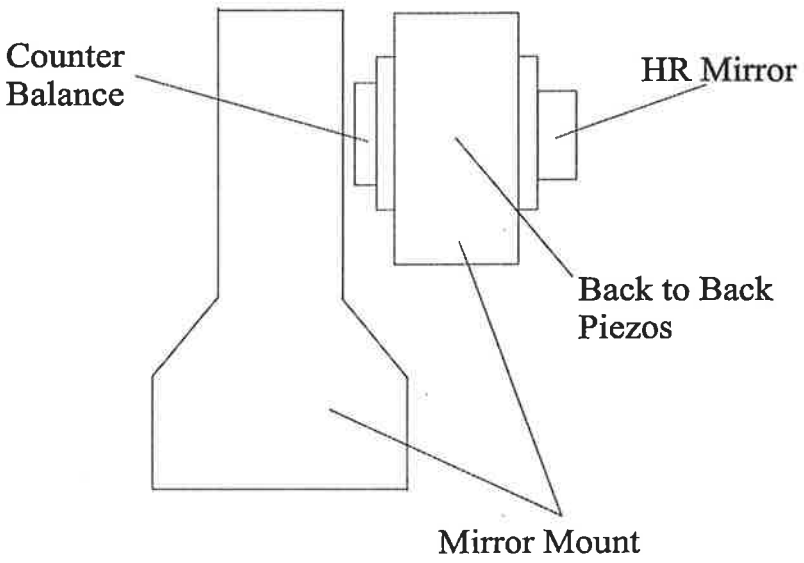

Figure 3.4: The balanced piezo actuator

as illustrated in Fig 3.6. This type of interferometer has an advantage over a conventional Michelson interferometer as reflections off the back face of the HR mirror do not degrade the fringe visibility. The interferometer was tuned by applying a DC voltage to the PZT such that the output of interferometer at the detector was midway between a dark fringe and a light fringe. A spectrum analyzer was used to provide a swept frequency signal that was amplified, AC coupled to the PZT. The response of the interferometer was then compared to a sample of the amplifed drive, giving the frequency response of the actuator.

The transfer function shows a longitudinal resonance at 42 kHz and a parasitic resonance at 27 kHz. The low frequency part of the transfer function is clear of any mount resonances, which illustrates the effectiveness of the balanced mounting system. Since the mass of the mirror is small compared with the mass of the PZT, the frequency of the lowest natural resonance of the PZT should be approximately that of the unloaded PZT. The fundamental resonant frequency of the unloaded PZT is the lowest frequency at which an acoustic standing wave will be established. For this resonance, the ends of a balanced PZT can be considered as free ends and the centre of the structure where the PZTs are joined can be considered a node. The acoustic wavelength required to establish the fundamental standing wave is therefore twice the length of the PZT. The fundamental resonance and frequency of the PZT

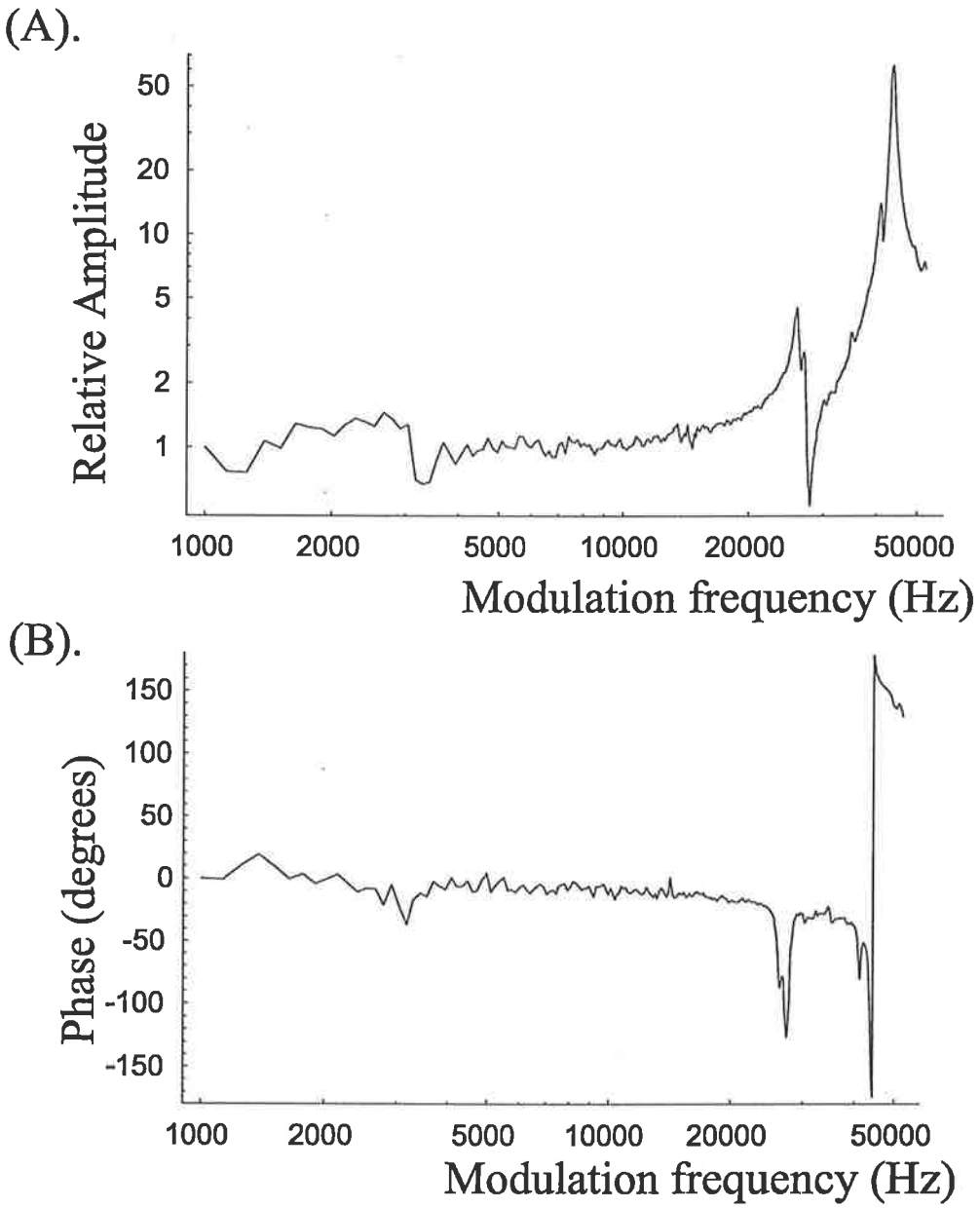

Figure 3.5: Transfer function for disc piezo (a) Amplitude (b) Phase

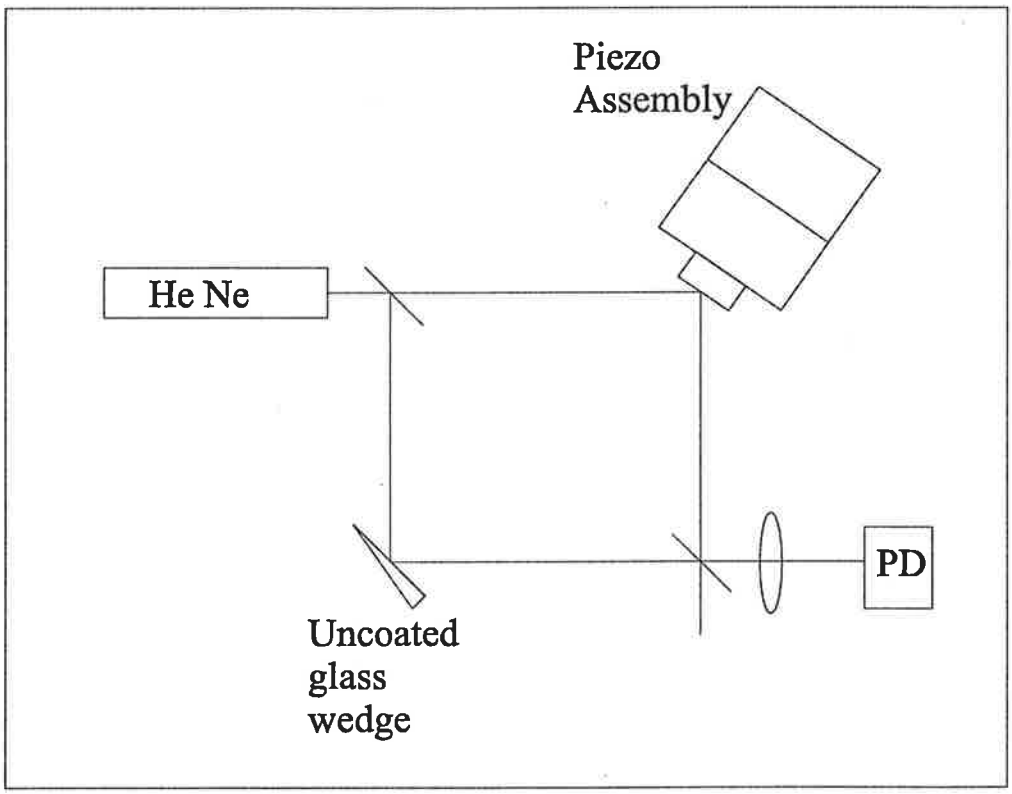

Figure 3.6: A Schematic of the optical set-up used to test the PZT actuator transfer characteristics

is thus given by

$$f = \frac{v_{sound}}{\lambda} = \frac{\sqrt{E/\rho}}{4L} \tag{3.16}$$

where E is the Young's modulus, ρ is the density of the PZT ceramic and L is the length of the PZT stack. Equation 3.16 assumes that the glue holding the PZT stack together is stiff.

It was found during the preliminary work that the lowest resonance of this system was always significantly less than the theoretical value of 65 kHz for the PZT stack as predicted by Equation 3.16. It was thought that the mirror mass and the glue holding the mirror to the PZT acted like a mass on a spring. This was verified when the lowest resonant frequency was increased by changing the glue from five minute epoxy to a much harder glue (Torrseal). Also, when a system with identical components was reassembled using a different gluing technique to attach the mirror to the PZT also using Torrseal, a lowest resonant frequency of 47kHz was obtained. This suggests that the frequency of the lowest resonance is still limited by the gluing technique even though a hard glue was used. To improve the bandwidth further a lighter mirror would be required.

The tube PZT actuator was also investigated. These PZTs work by applying an electric field perpendicular to the direction of desired length change and because the applied electric field contracts the piezo ceramic in the direction parallel to applied electric field it expands them in the other direction, or vice versa. The tubes that were used were made from PZT 5A[91] and had the dimensions of 25mm length, 25mm OD and 19mm ID. The transfer function for the balanced tube configuration is illustrated as Fig 3.7. The tube PZTs have higher dynamic range but their transfer functions were found to exhibit four large resonances at 28, 35, 42, 48 kHz and the loss of phase associated with these resonances limits the maximum bandwidth achievable. Stable injection locking was achieved using this PZT actuator, however the largest servo loop gain was obtained using the balanced disc PZT actuator.

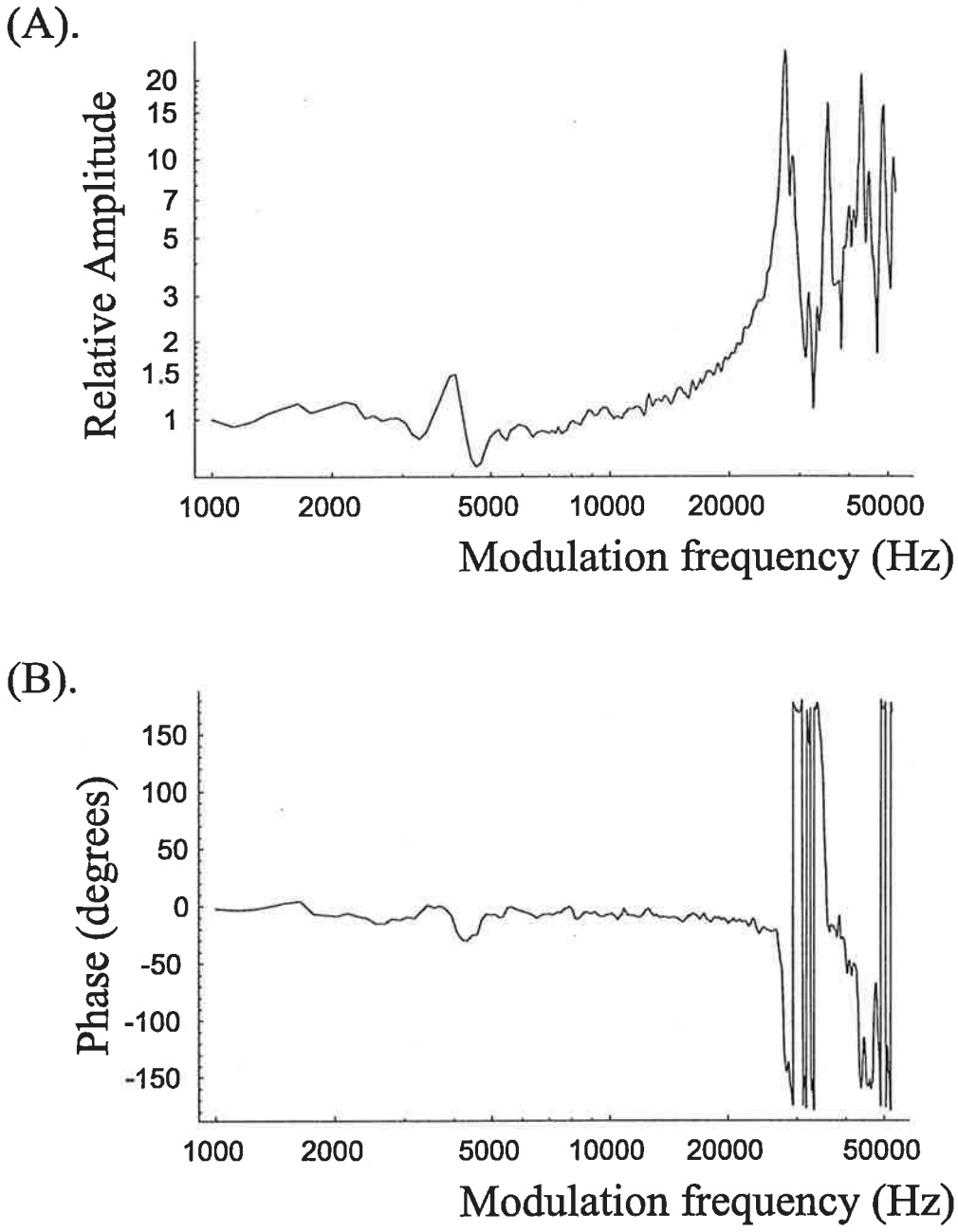

Figure 3.7: The tube Piezo transfer functions (a) Amplitude (b) Phase

3.4.3 High Voltage Amplifier

In the course of his PhD work Chris Hollitt designed and built a high voltage amplifier using a HV op-amp[92] recommended by the ANU quantum optics group. The HV amplifier had a maximum output voltage of 400 V and a voltage gain of 100. Its response was flat to 50 kHz and only 5 degrees of phase was lost over that bandwidth, as shown in Fig 3.8.

3.4.4 Pre-Amp Design and Loop Gain

The pre-amp is used to adjust the loop gain to compensate for imperfect elements, such as the actuator. This enables the loop gain and hence noise reduction to be maximized while ensuring that the servo remains stable and does not oscillate. A circuit diagram for the pre-amp is shown in Appendix B3. A plot of the calculated transfer function for the pre-amp is shown in Fig 3.9.

To maintain stability the phase margin of the loop gain must be positive as was explained in Section 1.4. The techniques of phase lag and phase lead compensation [71][72] were used to increase the gain at low frequencies and still ensure positive phase margin at unity gain. An integrator was used to provide increased loop gain at low frequencies. A phase-lead filter was then used so that positive phase margin was obtained as the loop gain passed through unity gain. To ensure that the resonances at 27 kHz and 42 kHz did not cause instability, an additional low pass filter with its corner frequency at 17 kHz was incorporated. This ensured that the phase was less than -180 degrees before the frequency of the two resonances was reached. Therefore, as shown in Fig 3.10, these two resonances occurred on the positive side of the real axis on the Nyquist diagram and hence did not cause encirclement of the point (-1,0). This low pass filter had the additional advantage that it added to the steep roll-off of the loop gain at high frequencies, which ensured that the loop gain at any higher frequency resonances did not exceed unity gain. The Bode Plot of the loop gain is shown in Fig 3.11.

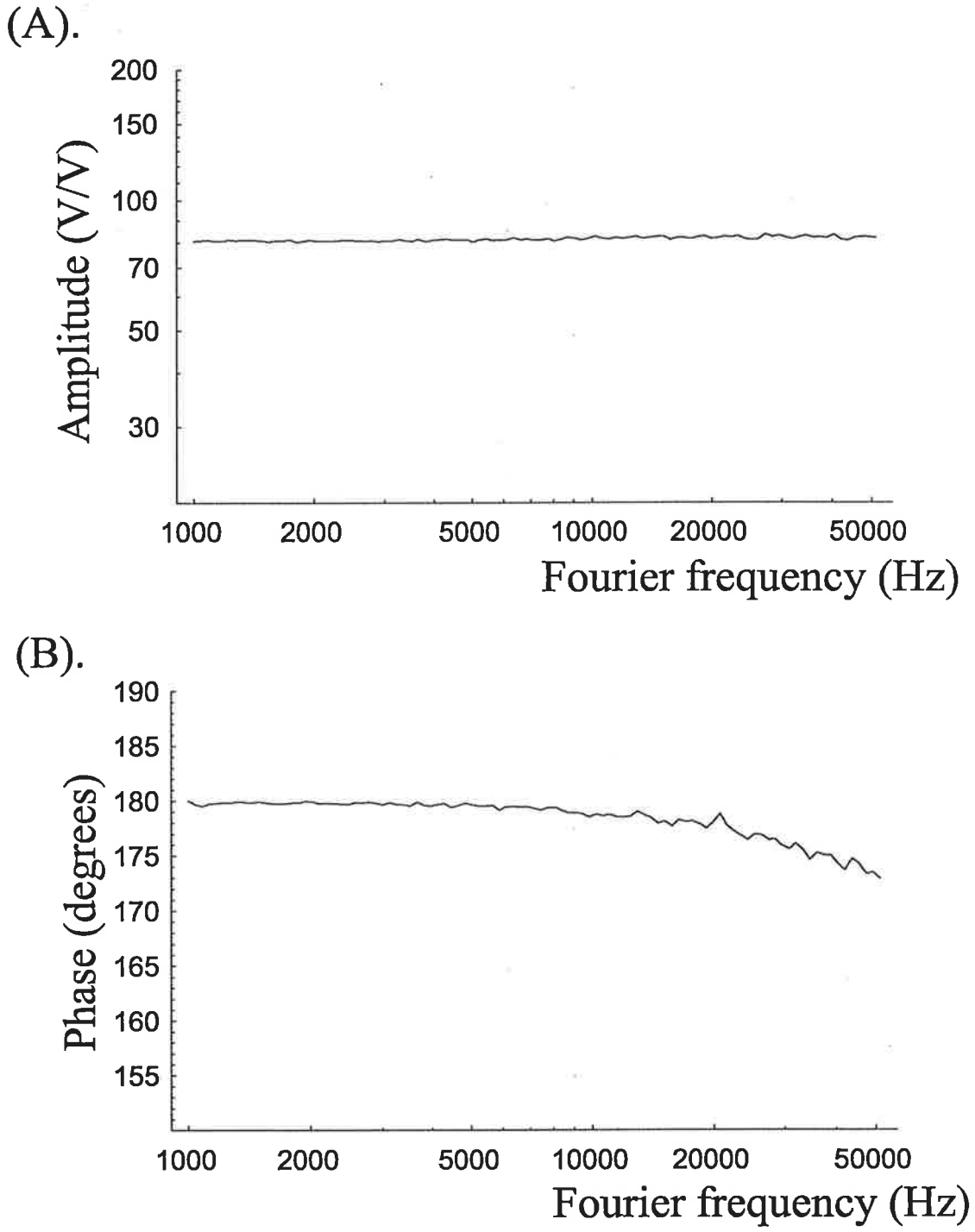

Figure 3.8: Transfer function for the high voltage amplifier (a) Amplitude (b) Phase

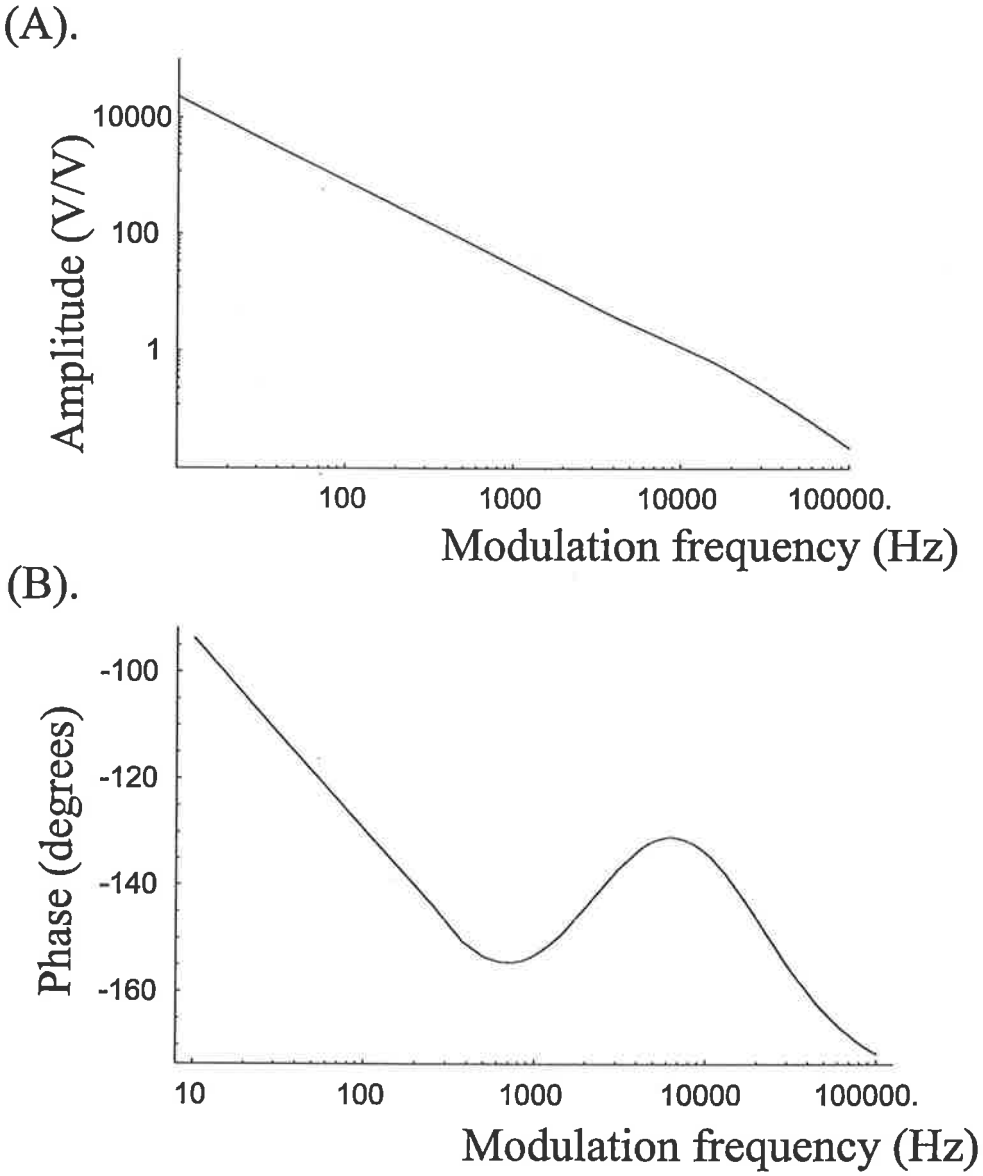

Figure 3.9: Transfer function for the servo pre-amp (a) Amplitude (b) Phase

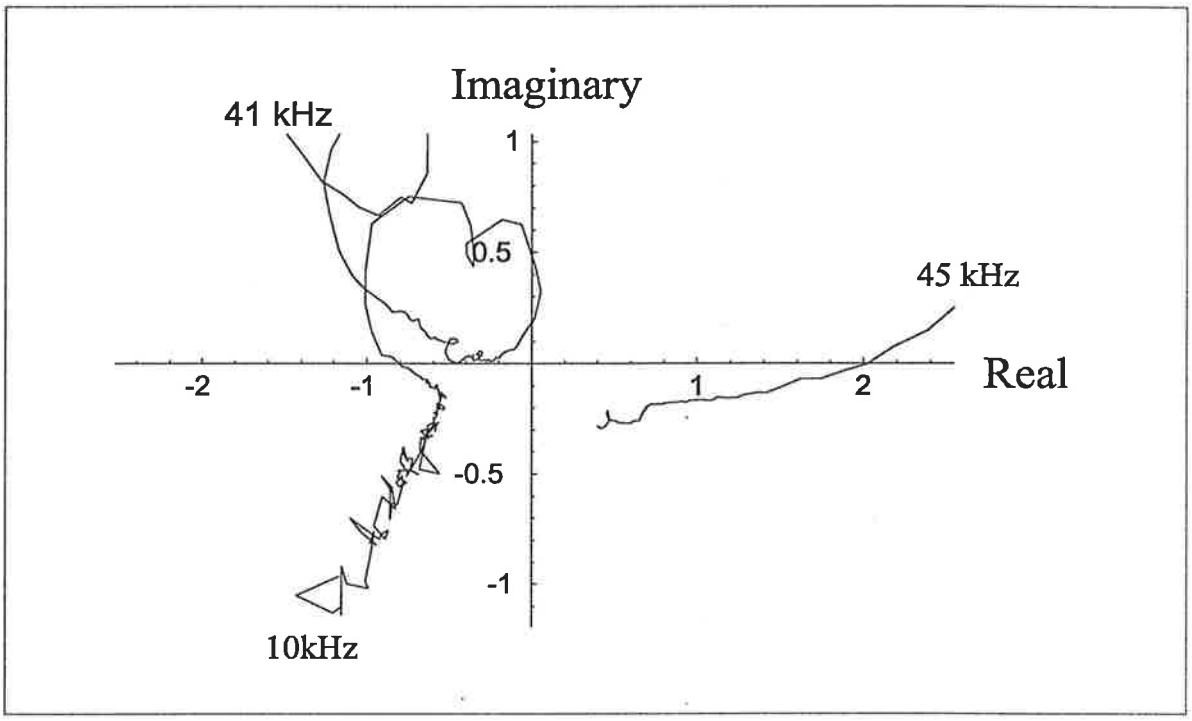

Figure 3.10: The Nyquist plot for the loop gain of the servo system

3.5 Slave Laser Frequency Noise

The signal from the discriminator can be used as a measure of the residual frequency noise if the signal is sufficiently far above the discriminator noise floor. The residual noise of the slave laser and the discriminator noise floor are shown in Fig 3.12. They were calibrated by slowly sweeping the frequency of the master by a known amount and measuring the slope of the error signal. The residual frequency noise of the laser is well above the noise floor of the discriminator. This demonstrates that the discriminator sensitivity is sufficiently high that it does not limit the noise reduction. The bright lines in the noise floor are caused by 50 Hz harmonic pick-up, with improved shielding of the experiment these would be removed. The shot noise limit for this system is below the electronic noise and hence does not limit the noise reduction either.

For frequencies at which the servo loop gain is high, the frequency correction applied to the PZT actuator is equal in magnitude but opposite in sign to the frequency noise of the slave resonator. Hence the free-running slave laser frequency

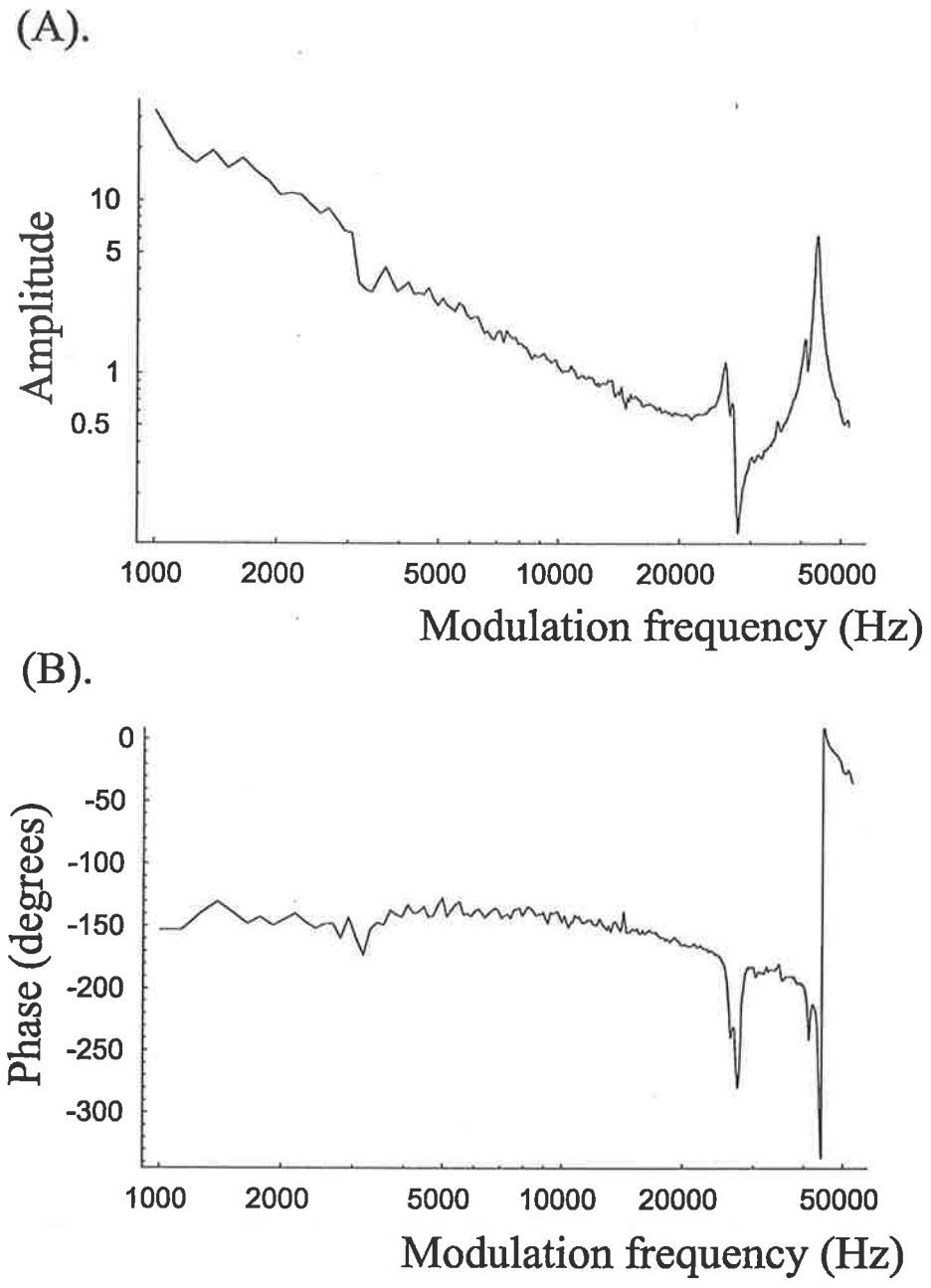

Figure 3.11: The transfer characteristics for the loop gain of the servo system

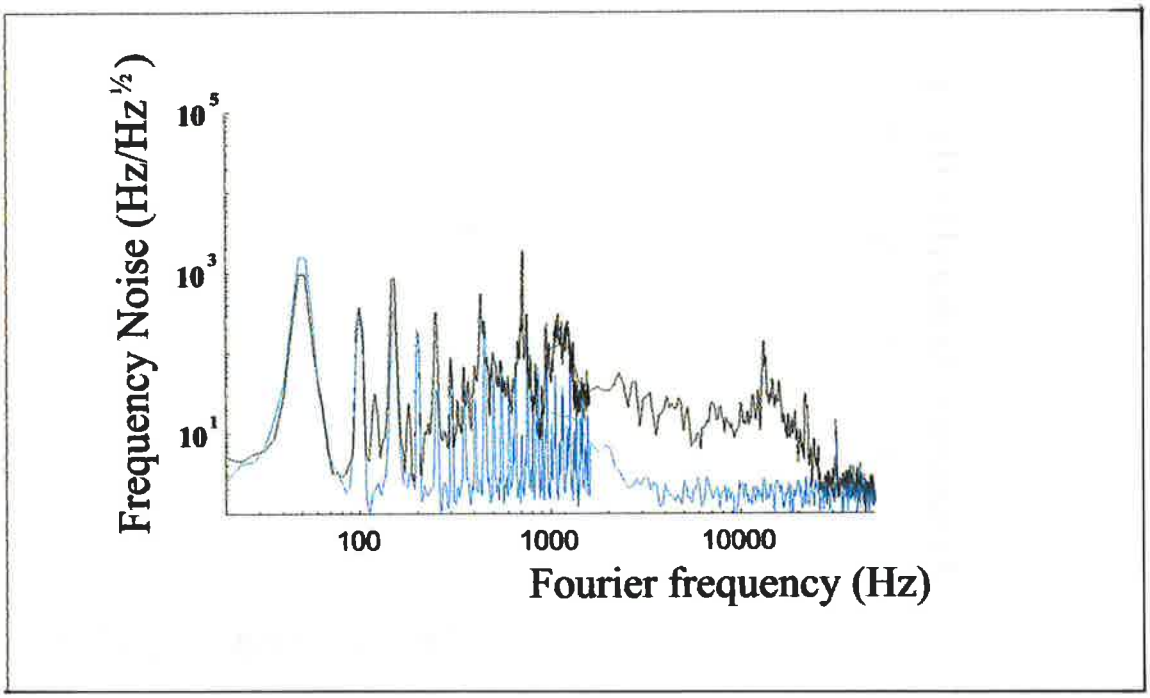

Figure 3.12: The residual slave laser frequency noise with servo noise reduction (black) Noise floor of the discriminator (blue)

noise can be evaluated simply by measuring the signal applied to the PZT actuator. The result is displayed as Fig 3.13.

For a servo with no significant additional noise sources within the servo loop, the reduction in the free-running frequency noise is given by

$$S_{s,servo}^{1/2}(\omega_{\mathrm{mod}}) = \frac{1}{1+G(\omega_{\mathrm{mod}})} S_{s,free\_running}^{1/2}(\omega_{\mathrm{mod}}) \tag{3.17}$$

where $S_{s,free\_running}^{1/2}(\omega_{\mathrm{mod}})$ is the free running frequency noise of the slave laser and ω_{mod} is the frequency of the noise modulation, $G(\omega_{\mathrm{mod}})$ is the loop gain of the servo. $S_{s,servo}^{1/2}(\omega_{\mathrm{mod}})$ is the residual slave laser frequency noise. This term does not include the additional frequency noise suppression due to injection-locking which will be considered in Chapter 4.

The theoretical noise reduction is plotted along with the experimentally determined noise reduction in Fig 3.14. This plot shows good agreement between theory and experiment. This strongly suggests that the residual frequency noise is limited by the magnitude of the free-running slave laser frequency noise and the loop gain,

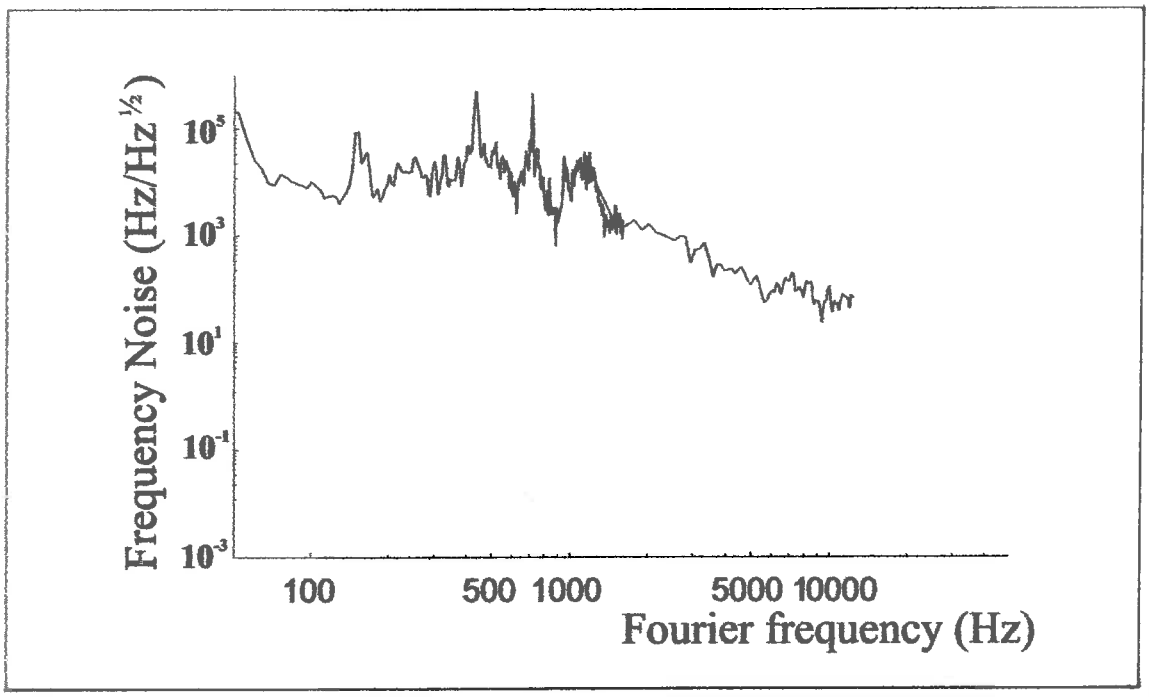

Figure 3.13: The free-running slave laser frequency noise as implied from the servo system actuator signal

and that the servo loop is not significantly polluted by additional noise sources.

With regular lab activity the servo system only loses lock when the limit of the dynamic range of the high voltage amplifier is reached. This limit is caused by the slow drifts of the slave laser frequency due to the thermal expansion and contraction of the optical table on which the resonator components are mounted. This problem could be circumvented by mounting the slave laser resonator components on a temperature stable base.

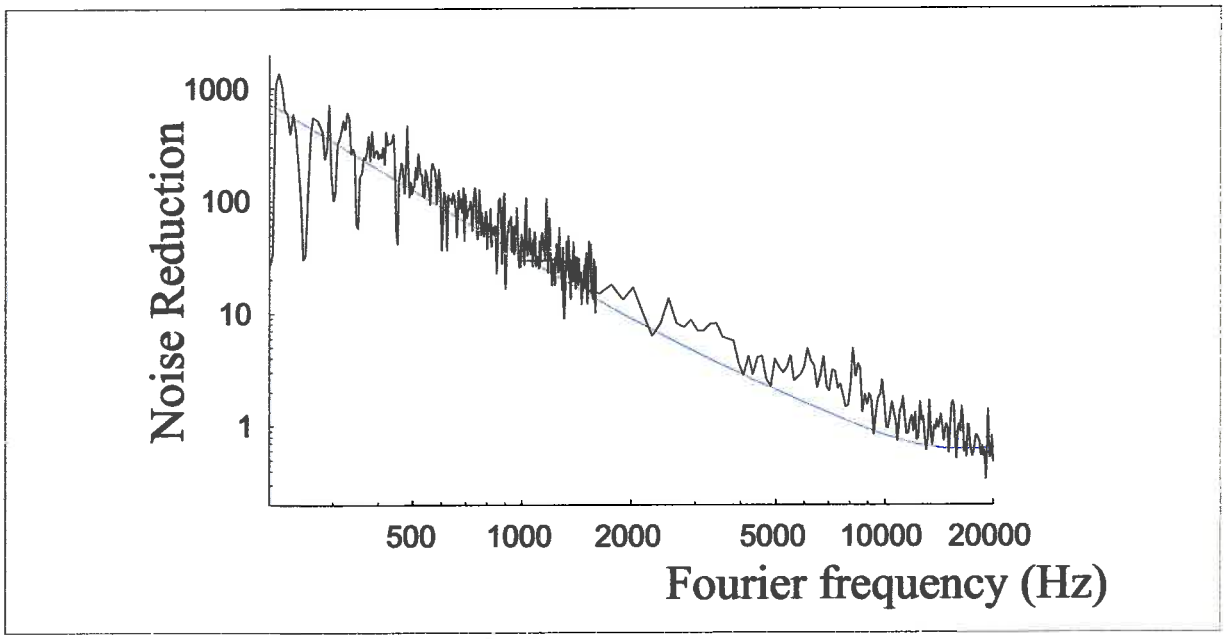

Figure 3.14: Servo sytem noise reduction. Theory (blue) Experimental (Black)

Chapter 4

Frequency and Intensity Noise Measurements

4.1 Introduction

In this chapter the frequency and intensity noise of the injection-locked laser will be discussed. I will start by reviewing the theory of frequency noise reduction by injection-locking as presented by Farinas et al.[62] and Barillet et al.[75]. Next, the contribution of the slave laser's frequency noise to the frequency noise of the injection-locked laser will be discussed. This was found to be insignificant compared to the contribution of the master laser below 30 kHz. The frequency noise contribution due to the slave laser has also been calculated theoretically and good agreement with the experimental data has been obtained.

The intensity noise of the injection-locked laser has been measured both at low frequencies and RF frequencies. We find that the laser is shot-noise limited for frequencies above 5 MHz for 6mA of photocurrent and predominantly limited by the pump noise of the slave laser at low frequencies. We have used feedback to the slave laser pump source to decrease the intensity noise of the injection-locked laser, by over an order of magnitude at low frequencies.

4.2 Theory of Frequency Noise Reduction by Injection-Locking

To describe the various contributions to the frequency noise of an injection-locked laser Farinas followed an approach used for microwave oscillators[62]. By using Laplace transform analysis to solve Equation 3.9, he was able to derive the transfer function for both master and slave frequency noise to the output of the injection-locked laser. The transfer functions are as follows

$$H_m(\omega) = \frac{\phi}{\phi_m} = \frac{1}{1 + j\frac{\omega}{\omega_{lock} Cos[\Delta\phi(t)]}} \tag{4.1}$$

$$H_s(\omega) = \frac{\phi}{\phi_s} = \frac{j\frac{\omega}{\omega_{lock} Cos[\Delta\phi(t)]}}{1 + j\frac{\omega}{\omega_{lock} Cos[\Delta\phi(t)]}} \tag{4.2}$$

where $\omega_{lock} = \pi\Delta\nu_l$ and $\Delta\phi(t)$ =Arcsin $\left[\frac{\omega_m - \omega_s}{\omega_{lock}}\right]$. If it is assumed that the frequency noise of the master and the slave lasers are uncorrelated, then the frequency noise of the injection-locked laser is given by

$$S_{f,il}(\omega) = |H_s(\omega)|^2 S_{f,s}(\omega) + |H_m(\omega)|^2 S_{f,m}(\omega) \tag{4.3}$$

where $S_{f,il}(\omega)$, $S_{f,m}(\omega)$ and $S_{f,s}(\omega)$ are the spectral densities of frequency noise for the injection-locked laser, the master and the slave lasers respectively.

Equations 4.1, 4.2 and 4.3 reveal some important features. For example, the greater the injection-locking range, the greater the range of Fourier frequencies for which the master has control over the injection-locked laser, and the greater the suppression of the frequency noise of the slave laser. When the slave laser is held at the centre of the locking range, the transfer function for the master noise is that of a low pass filter with a corner frequency equal to ω_{lock}. Frequencies higher than the locking range are rejected by the resonator and do not have the opportunity to be amplified.

The transfer function for the slave laser noise is simply that of a high pass filter with its corner frequency at ω_{lock}. This is indeed fortunate as it means that low frequency slave laser frequency noise is heavily attenuated. This is the frequency

region of most interest for gravitational wave detection and is also where slave laser technical noise is greatest in diode pumped solid state lasers.

If the slave laser is not held at the centre of the injection locking range then the effect on the system is the same as an effective reduction in the locking range. This reduces the frequency range in which the master laser effectively controls the phase of the injection locked laser and thus reduces the attenuation of the slave laser frequency noise at low frequencies.

In most practical injection-locked lasers a servo system is required to maintain long term injection-locking. However, the effect of the servo system is not included in Equation 4.2. Barillet et al.[75] expanded on the approach taken by Farinas and considered the frequency noise reducing properties of the servo. The effect of the servo on the frequency noise of the slave laser is given by the equation

$$S_{f,servo}(\omega) = \left|\frac{1}{1+G(\omega)}\right|^2 S_{f,fr(slave)}(\omega) + S_{servo}(\omega) + S_{f,m}(\omega) \qquad (4.4)$$

where S_{servo} is the noise introduced by the servo loop and $G(\omega)$ is the loop gain of the servo. In our laser system the size of the first term is orders of magnitude larger than the second and third term for the frequencies of interest (<50 kHz). Hence for the purpose of this discussion only the first term will be considered. Thus combining Equation 4.4 and Equation 4.2, the contribution to the frequency noise of the injection-locked laser by the free-running slave can be shown to be

$$S_{f,il(slave)}(\omega) = \left|\frac{1}{1+G(\omega)}\frac{j\frac{\omega}{\omega_{lock}Cos\Delta\phi(t)}}{1+j\frac{\omega}{\omega_{lock}Cos\Delta\phi(t)}}\right|^2 S_{f,fr(slave)}(\omega)$$

As the modulations that are of interest to gravitational wave interferometry and field based vibrometry are orders of magnitude smaller than ω_{lock} and the free-running frequency of the slave laser is controlled such that it is close to the frequency of the master laser, the above equation can be simplified to

$$S_{f,il(slave)}(\omega) = \left|j\frac{1}{1+G(\omega)}\frac{\omega}{\omega_{lock}}\right|^2 S_{s,free\_running}(\omega) \qquad (4.5)$$

4.3 Frequency Noise due to the Slave Resonator

Equation 4.5 indicates that the frequency noise of the slave should only be weakly coupled into the frequency noise spectrum of the injection-locked laser. To verify this we set up the experiment shown in Fig ??. This experiment is similar to one performed by Nabors *et al.*[45] for a flash-lamp pumped injection-locked laser system. This set-up uses a beat measurement to measure the fluctuations in the phase difference between the injection-locked laser and the master laser. A sample of the master is frequency shifted by 80 MHz using an Acousto-Optic Modulator (AOM). This beam is combined with a sample of the injection-locked laser using a beam splitter. The resulting beat signal is then detected by a fast photodiode (bandwidth 200 MHz), and the beat note is mixed in quadrature with a sample of the AOM drive frequency.

It can be shown that for small phase variations, the voltage at the IF port of the mixer is related to the phase difference between the injection-locked laser and the master by the following relationship

$$V(t) = \eta_{pd}\eta_{dbm}\eta_{mo}R_f\sqrt{P_{d,m}P_{d,s}}\Delta\phi(t)$$

where η_{pd},η_{dbm}, η_{mo} are the efficiencies of the photodiode, the double balanced mixer and the spatial mode overlap between the frequency shifted master and injection-locked laser respectively, R_f is the transimpedance gain of the photo-detector circuit, $P_{d,m}$, $P_{d,s}$ are the detected power of the frequency shifted master and the injection-locked laser respectively. The above equation is derived in Appendix A5.

The phase difference spectral density plot can be converted to a plot of the additional frequency noise by simply multiplying by the Fourier frequency. Fig 4.2 (black curve) shows the frequency noise that is added to the injection-locked laser by the slave laser resonator and the servo. Also shown in Fig 4.2 for the sake of comparison is the typical frequency noise of a free-running NPRO[62]. This shows that the frequency noise of the injection-locked laser is not limited by the contribution of the slave laser's frequency noise for frequencies below 50 kHz.

The frequency noise contribution from the slave laser can also be inferred using the error signal of the servo loop and is shown in Fig 4.2 (blue curve). It was mentioned in Section 3.4 that the performance of the servo was not limited by the noise of the servo and hence the error signal should be a reasonably accurate representation of the additional frequency noise. It is reassuring that the plots show reasonable agreement.

Also shown in Fig 4.2 (red curve) is the calculated contribution to the frequency noise of the injection-locked slave by the frequency noise of the slave laser. This is derived using the measured free-running slave laser noise (see Fig 3.13) and Equation 4.5. Above 300 Hz all three curves show excellent agreement. It is highly likely that below 300 Hz the measurement using the AOM is limited by the ambient vibrations and the error signal is limited by 50 Hz pickup. The ambient room vibrations are coupled into the beatnote frequency noise measurement via beam jitter caused by vibrations of the beam steering mirrors. Beam jitter causes a time dependent phase-front mis-match between the injection-locked beam and the frequency shifted master laser. This results in time dependent variation of the beatnote. These plots demonstrate that the frequency noise of the injection locked slave is limited by the frequency noise of the NPRO.

Farinas *et al* [62] test the frequency noise performance of their injection-locked laser by beating it against an independent monolithic NPRO and analyzing the resulting beatnote. This demonstrated that the frequency noise of the injection-locked laser was comparable to the frequency noise of the master laser. Barillet *et al.* [75] use the error signal from their Pound-Drever-Hall servo to measure their slave laser's contribution to the frequency noise of their injection-locked laser. From this, they show that the slave laser component of the frequency noise of the injection-locked laser is significantly less than that due to their master laser for frequencies below 50 kHz. Using our technique, however, we can independently show that the contribution due to the slave laser agrees with theoretical predictions.

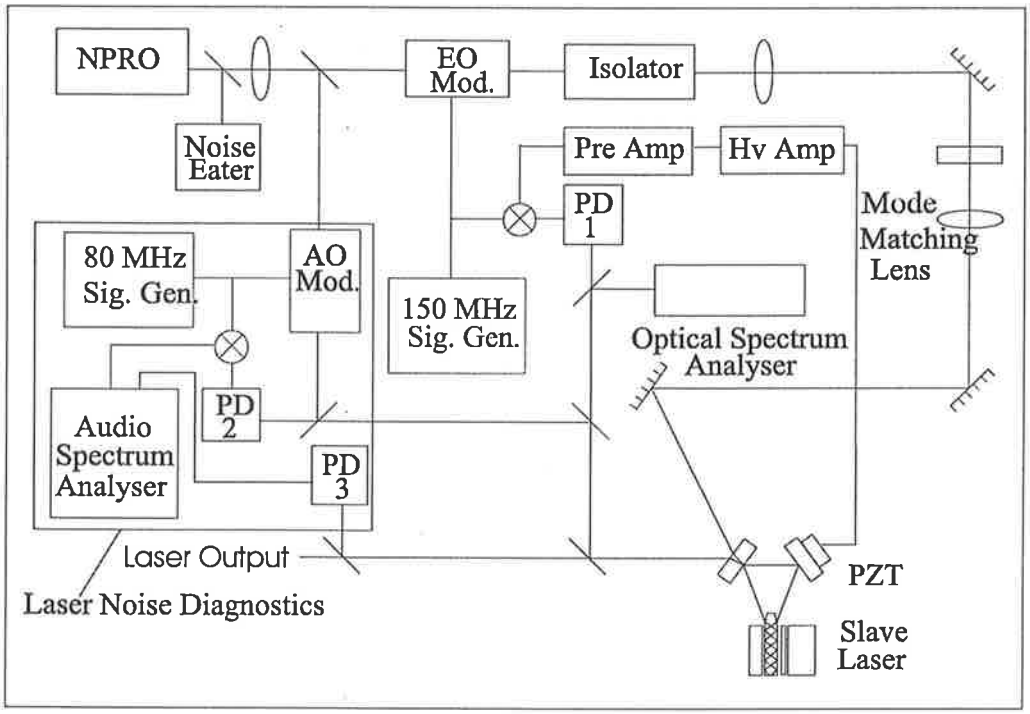

Figure 4.1: A schematic of the experiment used to measure the frequency noise contribution of the slave laser to the injection-locked laser

4.4 Intensity Noise

The intensity noise of injection-locked lasers has been studied extensively using both semi-classical models[62][75] and, more recently, fully quantum mechanical models [61][60][85][58]. Semi-classical models provide an accurate model of the intensity noise spectrum of an injection-locked laser for low to medium frequencies (around the slave laser's relaxation oscillation). As the semi-classical model does not consider the quantum mechanical nature of light, its applicability is limited to the cases where the pump source and the master laser are not quantum noise limited. For high frequencies or when the pump and the master lasers are quantum noise limited the fully quantum mechanical description of Ralph et al.[61][60] must be used.

The intensity noise spectrum has three main contributions

- Pump induced intensity fluctuations
- Master induced intensity fluctuations

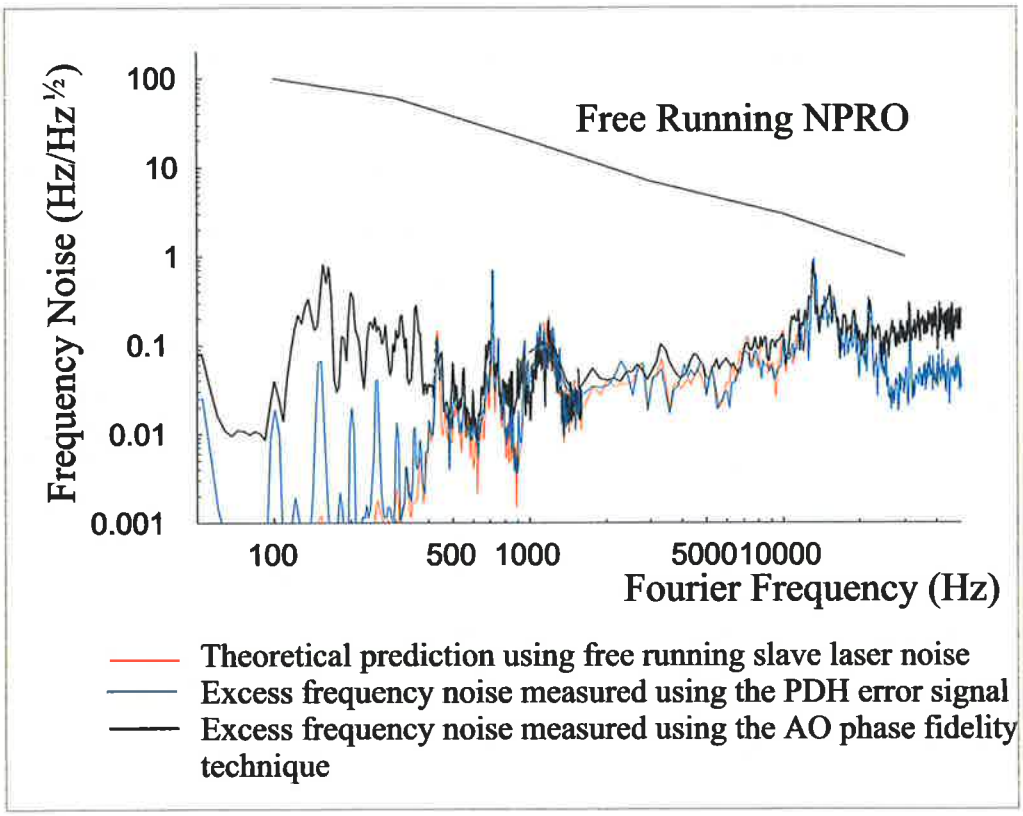

Figure 4.2: The frequency noise contribution of the slave laser to the injection-locked laser

- Conversion of frequency noise to intensity noise

In the following three sub-sections I will provide a summary of the theory of these contributions to the intensity noise of an injection-locked laser.

Effect of Pump Intensity Fluctuations

In a free-running solid-state laser, low frequency (well below the relaxation oscillation frequency) pump noise is directly transferred to the output of the laser. Injection locking does not alter this, which is not surprising as low frequency pump fluctuations directly modulate the available laser gain and hence the output power of the injection-locked laser.

The transfer function of the pump fluctuations to the laser output of a free-running solid-state laser is that of an underdamped second-order filter. The relaxation oscillation caused by the coupling of the lasers intra-cavity light field to the population inversion of the gain medium causes a noise peak in the vicinity of a few hundred kilohertz.

Injection-locking modifies the pump to injection-locked laser transfer function at frequencies around the relaxation oscillation by overdamping the relaxation oscillation. This occurs for all practical slave/master power ratios[62]. Hence the transfer function for the pump to the injection-locked laser is simply an overdamped second second order low pass filter whose roll-off can be as high as 20dB per octave. The corner frequency for this overdamped second order filter is given by[60]

$$\omega_{clow} = \frac{\omega_R^2}{\gamma_L} \cong \frac{\omega_R^2}{\omega_{lock}} \tag{4.6}$$

where γ_L is the damping factor for the relaxation oscillation, ω_R is the frequency of the relaxation oscillation of the free running slave. Thus, slave laser pump noise is a dominant noise term at low frequencies and rapidly looses significance as the frequency of the relaxation oscillation is approached.

Effect of Fluctuations of the Master Laser

The transfer function for the master laser intensity fluctuations to injection-locked laser intensity fluctuations is significantly more complicated than that of the pump

laser transfer function. This transfer function can be broken up into three frequency regions

(1) Low frequency region (frequencies well below the slave laser's relaxation oscillation frequency)

(2) Amplification region (for frequencies around the slave laser's relaxation oscillation frequency)

(3) High frequency region

Low frequency fluctuations of the master laser's intensity cannot be amplified as the slave laser gain is saturated. The intensity noise spectrum of the injection-locked laser at low frequencies is simply the geometric sum of the master and the slave lasers modulations weighted by their respective average powers[61].

For frequencies near the relaxation oscillation of the slave, the slave laser acts like an optical amplifier for master laser intensity fluctuations. In this frequency range, the relative intensity noise of the injection-locked laser will be the same as that of the master[62] if the master laser intensity noise is well above the quantum limit. It is worth noting that even if both the slave laser's pump source and the master laser are quantum noise limited, the injection-locked laser will not be quantum noise limited in this region. This is due to amplification of the master laser quantum noise[61][60].

The last region is the high frequency region, at frequencies that are much greater than the relaxation oscillation frequency. At these high frequencies, fluctuations of the master are simply reflected off the output coupler. Hence the quantum noise of the master laser is neither amplified nor suppressed[61][60].

Conversion of frequency noise to intensity noise

If the slave laser natural resonance is slightly detuned from the master laser frequency, frequency variations between the master and the slave are strongly coupled into the amplitude noise spectrum. Barillet et al. [75] found that when the frequency offset between the natural slave resonance and the master was 84 kHz (locking range=1.6 MHz), a frequency modulation applied to the master at 80kHz with a 126kHz modulation depth produced a relative amplitude modulation of 0.030. When the same frequency modulation was applied with no frequency offset, no additional

amplitude modulation was observed. This effect can be used as a means of tuning out any dc-offset errors in the frequency control servo of the slave laser.

4.4.1 Measurement of Intensity Noise

Low Frequency Intensity Noise

The low frequency intensity noise spectrum of the injection-locked laser was measured using a low noise photo-detector and a low frequency (DC-50kHz) audio-spectrum analyzer. The photo-detector consisted of a reverse biased InGaAs PIN photodiode coupled to a transimpedance amplifier. The InGaAs photodiode was chosen for its high sensitivity at $1\mu m$. A low noise OP27 op-amp was used for the transimpedance circuit, and the ± 9 V rails for this circuit were provided by 9V batteries to eliminate noise from external power supplies. The bandwidth of this photo-detector was 500 kHz. A circuit diagram of a transimpedance photo-diode circuit is shown in Appendix B4. The measurement of the pump diode intensity noise were performed using a similar photo-detector circuit, except a silicon PIN photodiode was used.

The low frequency pump to injection-locked laser transfer function for intensity noise can be derived as follows. The power of an injection-locked laser (P_{il}) is related to the pump power (P_p) by

$$P_{il} = \eta_s \left(P_p - P_{th}\right)$$

where η_s is the slope efficiency of the laser and P_{th} is the power of the pump laser at threshold of the injection-locked laser. Hence at low frequencies the pump relative intensity noise to injection-locked laser relative intensity noise transfer function is given by

$$\frac{\Delta P_{il}/P_{il}}{\Delta P_p/P_p} = \frac{\eta_s \Delta P_p/\left[\eta_s \left(P_p - P_{th}\right)\right]}{\Delta P_p/P_p} = \frac{P_p}{P_p - P_{th}} \tag{4.7}$$

This derivation assumes that the $P_m \ll P_s$ and pump fluctuations do not take the slave laser below threshold. If the slave laser is well above threshold, then Equation

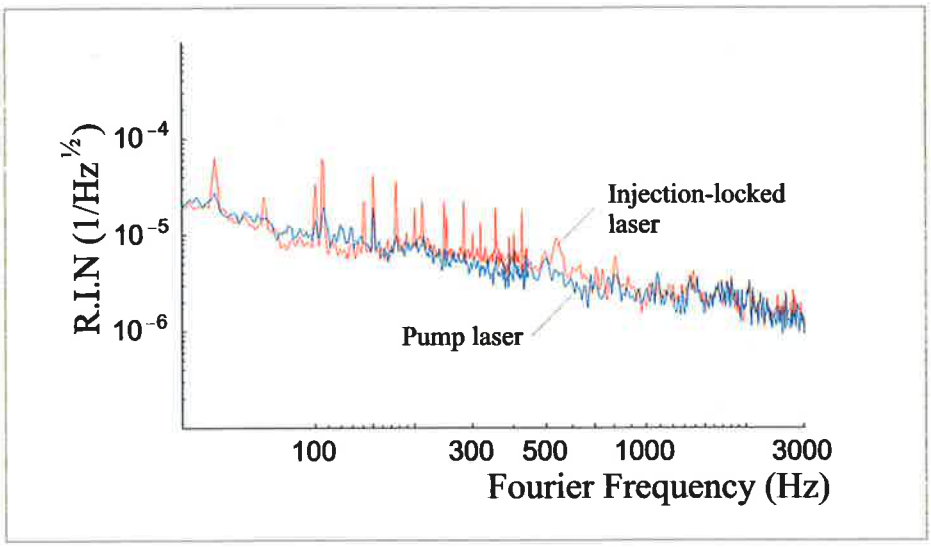

Figure 4.3: Low frequency intensity noise of the pump and injection-locked lasers

4.7 shows that the pump intensity modulation to injection-locked laser intensity modulation transfer function approaches unity. Hence the relative intensity noise of the pump and the injection-locked laser should be the same at low frequencies.

The relative intensity noise of the pump and the injection-locked laser are shown as Fig 4.3. As expected the spectrum of the injection-locked slave is very similar to that of the pump laser with a few exceptions. The peaks that occur in the spectrum of the injection-locked laser have two sources. The 50 Hz harmonics are due to conversion of the 50 Hz harmonics in the slave laser phase noise (this phase noise is illustrated in Fig 3.12) to intensity noise. The 50 Hz harmonics that are observed in the intensity noise spectrum of the master laser are not large enough to cause this effect. The other lines are probably caused by vibrations in the fibre lens used to collimate the laser diode. These bright lines would most likely be eliminated if the pump source was collimated using a micro-lens array attached to the laser diode.

Medium to High Frequency Intensity Noise

The frequency noise beyond 100 kHz was measured using a high bandwidth (DC-200 MHz) photo-detector circuit designed by members of the ANU Quantum Optics group [64]. This photo-detector also uses a photodiode coupled to a transimpedance amplifier. The amplifier uses a very wide bandwidth (gain-bandwidth product=1.9

GHz), low noise op-amp manufactured by Comlinear, model number CLC425. The spectrum was recorded using a Tektronix digital RF spectrum analyzer (model number 497P). The medium to high frequency intensity noise spectra are illustrated as Fig 4.4. In the medium frequency regime, as expected the master laser and the injection-locked laser show reasonable agreement. The noise peak at 650 kHz is an artifact of the servo which suppresses the master laser's relaxation oscillation[55]. Unfortunately the noise floor of this measurement is limited by the spectrum analyzer, and is comparable to the predicted shot noise for this measurement (photo-current = 6 mA). The predicted shot noise power was added to the noise floor power to determine the predicted shot-noise level. It would appear that the injection-locked slave is shot-noise limited beyond 5 MHz when the detected photo-current is 6 mA. The intensity noise spectrum was measured up to 50 MHz and no additional intensity noise peaks were observed.

4.5 Intensity Noise Reduction

As was mentioned in the first chapter, the requirement for the intensity noise at low frequencies for the interferometric detection of gravitational waves is $5\times10^{-8}/\sqrt{Hz}$ at 1 kHz. Active intensity noise reduction is often required to approach this level. Various papers have been published on the intensity stabilization of solid state lasers using active feedback to the pump source[59][57][56][60]. The design of the servo for these systems is made more difficult by the presence of the relaxation oscillation in the pump to laser transfer function. Huntington *et al.*[58] have achieved broadband intensity noise suppression by using injection locking to suppress the relaxation oscillation in an injection-locked monolithic NPRO and multiple feedback loops. Low frequency noise correction was sent to the slave laser's pump source and higher frequency correction was sent to a master laser modulator.

It should be possible in principle to apply this scheme to our higher power device. However, the pump source for our laser is a multi-emitter, multi-mode, high power diode array, while in the work by Huntington et al. the slave laser was pumped using a low power single emitter pump diode. Thus, it was not clear whether feedback

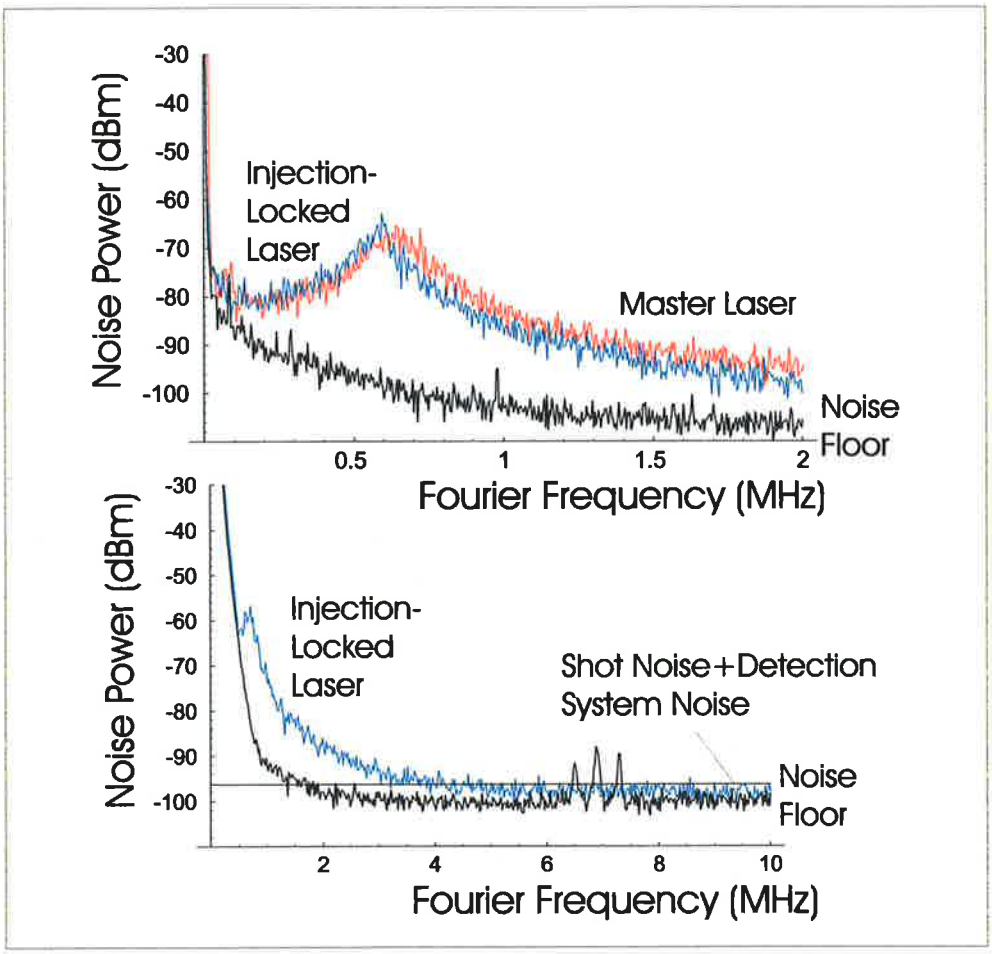

Figure 4.4: The medim to high intensity noise of the injection-locked slave. The detection bandwidths are 10 kHz (Top) and 100 kHz (Bottom) and in both cases the photo-current is 6mA.

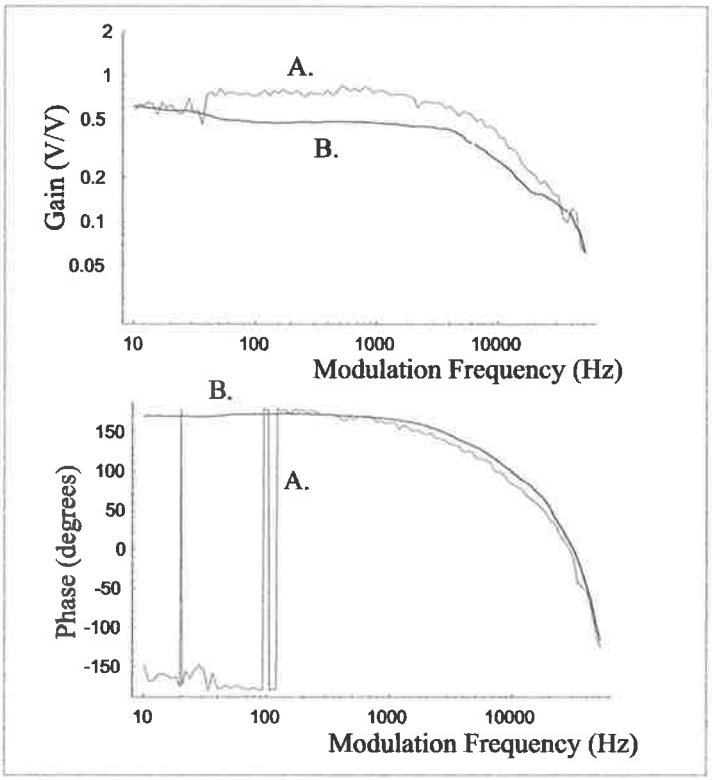

Figure 4.5: The transfer functions for the low frequency modulation port of the laserdiode driver to the laser diode output (B) and the output of the injection-locked laser(A)

to this pump diode array would achieve noise reduction. We have performed this experiment and have achieved significant noise reductions to 8 kHz. Thus, there would appear to no obvious impediment to broad band intensity noise correction being applied to this medium power laser.

The driver for the high power diode array provides a DC-coupled analogue modulation input port. The transfer function for this analogue input to pump intensity modulation is illustrated as Fig 4.5. Also shown is the transfer function of the analogue input to injection-locked laser intensity modulation. This figure shows that the bandwidth is limited by the pump-driver electronics and not by the injection-locking process. We use this port in our proof of principal experiment for convenience. However if greater noise reduction and bandwidth is required, direct injection of the error signal into the laser diode could be used. This would eliminate the phase lag due to the driver electronics.

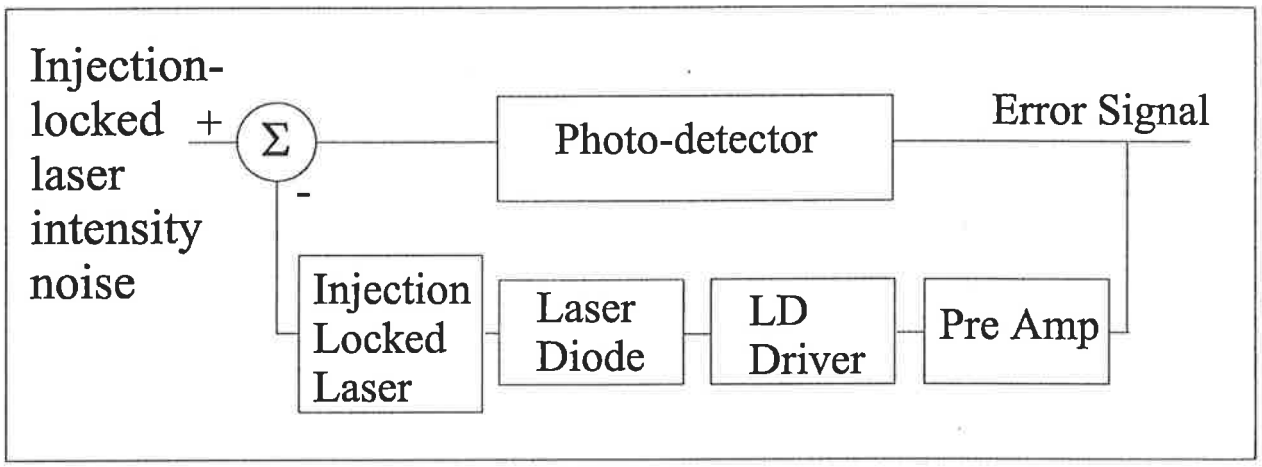

Figure 4.6: A block diagram of the intensity noise reduction servo

The block diagram of the experiment is illustrated as Fig 4.6. The error signal is generated by detecting a small fraction of the injection-locked laser light using the low noise detector that was used in the low frequency intensity noise experiments. A pre-amp is used to optimize the loop gain given the limitations of the diode driver. A circuit diagram for this pre-amp is shown in Appendix B5.

Fluctuations of the pump source directly modulate the temperature of the centre of the lasing crystal and hence the natural frequency of the slave laser mode. Thus,we found it necessary to AC couple the pre-amp as a large amount of loop gain at DC combined with any offset error in the feedback electronics tended to cause the frequency control servo to loose lock. The transfer function of the Pre-Amp is illustrated as Fig 4.7 and the total loop gain is shown as Fig 4.8.

The effectiveness of this technique has be evaluated by measuring the intensity noise of the stabilized laser using an out-of-loop detector. The detector used was the high bandwidth detector that was used in the high frequency intensity noise evaluation. The results of the intensity noise suppression experiment are illustrated as Fig 4.9, and show that feedback to a high power multi-emitter array pump source can be used to significantly reduce the intensity noise of an injection-locked laser. The stabilized intensity noise is limited by the loop gain of the servo above 250 Hz and by electronic noise within the servo below 250 Hz. The slight increase in intensity noise between 9 kHz and 30 kHz is due to lack of phase margin at the unity

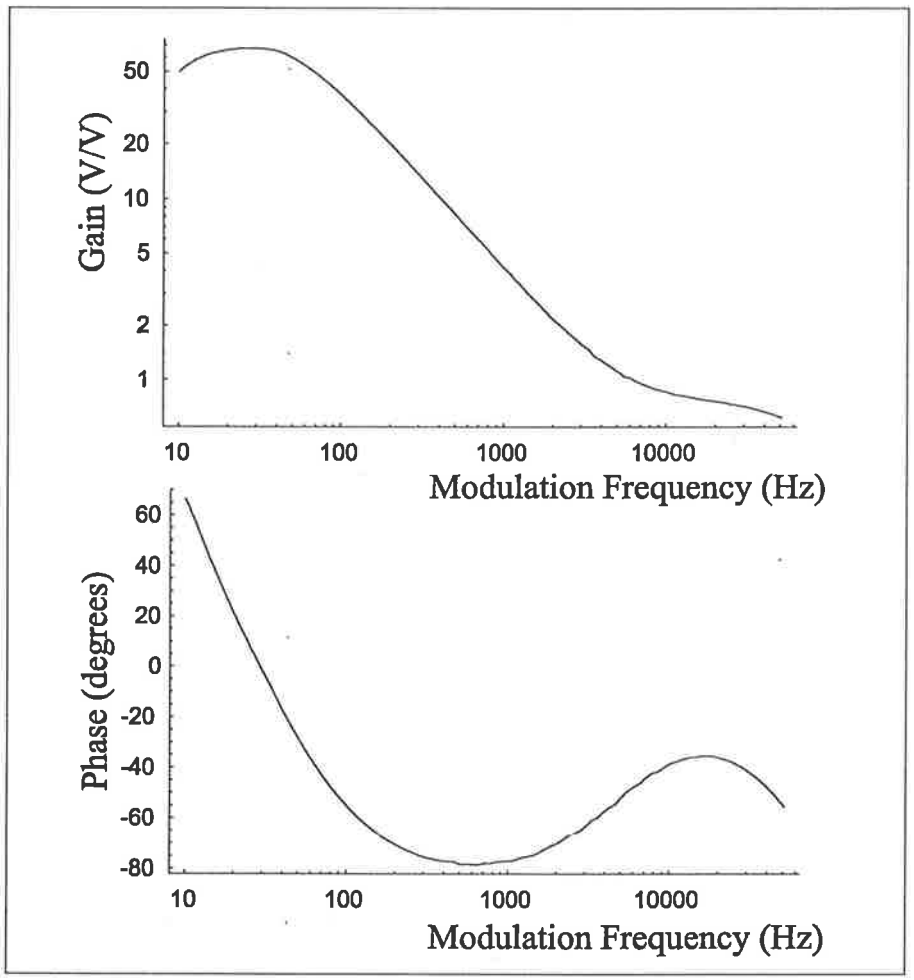

Figure 4.7: The transfer function for the pre-amp used in the intensity noise reduction servo.

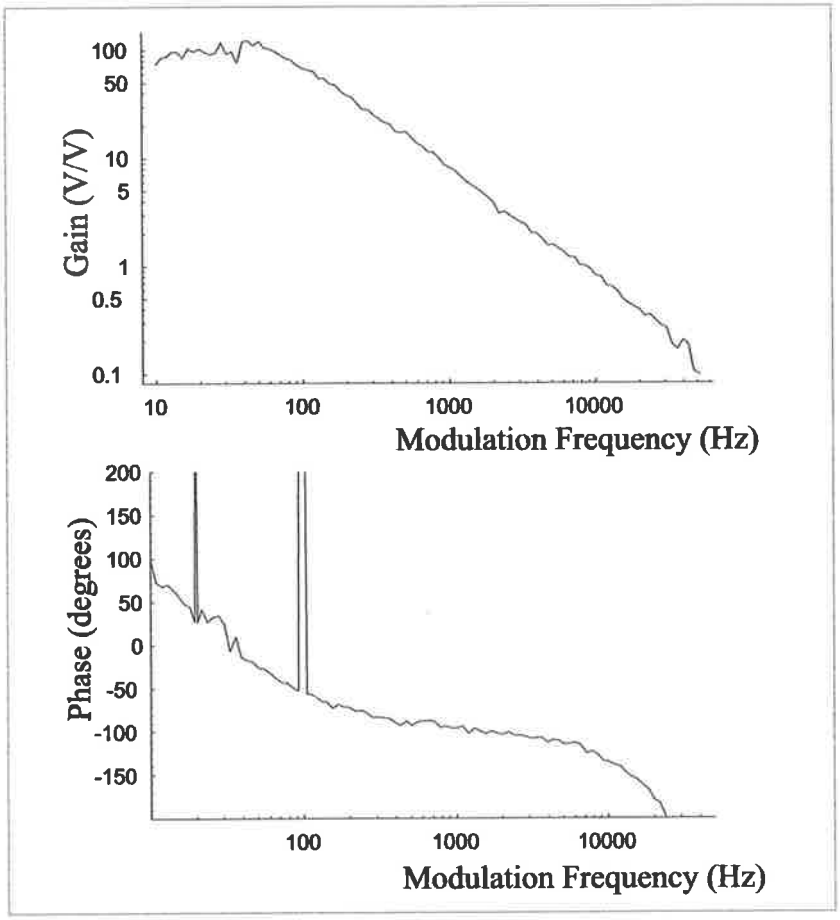

Figure 4.8: The loop gain for the intensity noise reduction servo of the injection-locked slave

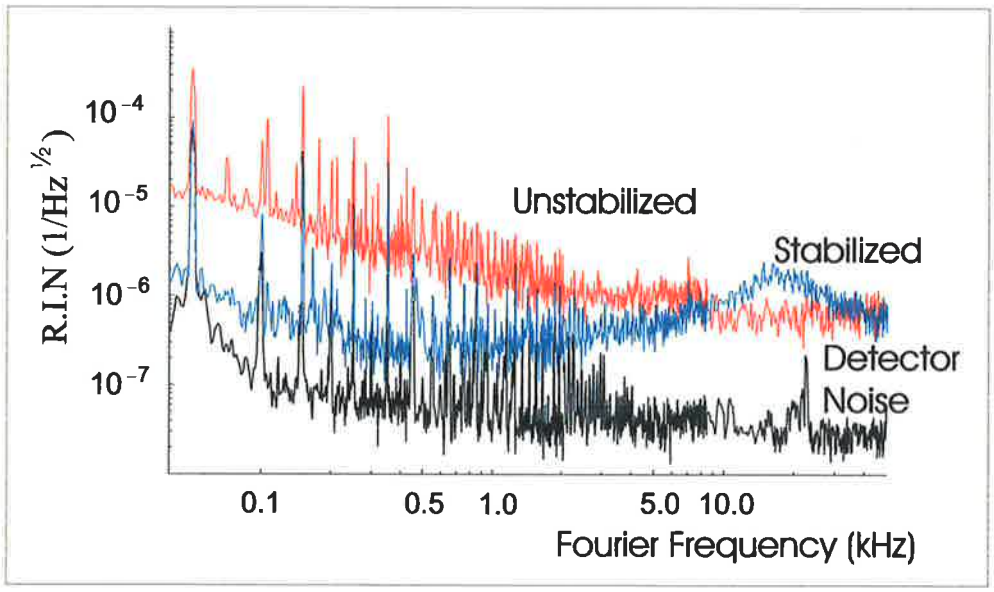

Figure 4.9: The effect of the intensity noise reduction servo on low frequency intensity noise

gain frequency. This could be remedied by using a broad bandwidth current source to directly inject the correction current into the laser diode.

Chapter 5

Conclusions and Further Work

We have developed a laser that is compact, efficient and reliable. The laser produces 5 W of TEM_{00} mode radiation from a single 20 W laser diode array. The output is close to diffraction limited with M^2 values of 1.0 and 1.2 in the horizontal and vertical planes respectively. Single frequency operation and excellent frequency noise performance is obtained by injection-locking the slave laser using 100 mW of master power supplied by a monolithic NPRO.

The slave laser is based on the Co Planar Folded-zig-zag Slab geometry. We have investigated the loss and the gain characteristics of the CPFS geometry. The losses for our crystals were found to be approximately 3% with spatial variations of up to 0.5%. The single pass small signal gain of the crystal when pumped with 20 W was found to be 2.12 ± 0.02 .

The transverse mode properties of the laser were also studied. Mode control in the vertical plane was obtained by adjusting the collimation of the pump source. Horizontal mode confinement was attributed to the residual curvature of the slab sides. Mode control in the horizontal plane was improved by using a convex mirror to expand the size of the fundamental mode. The apertures formed by the Brewster angle faces then provide sufficient mode discrimination to prevent higher order transverse modes from lasing.

The slave laser has good inherent frequency stability: injection-locking was achieved for periods of up to 30 s without a servo system. Long term injection-locking has been achieved using a Pound-Drever-Hall servo system.

The frequency noise of the injection-locked laser has been evaluated. We have shown that the frequency noise performance of the injection-locked laser is limited by the frequency noise of the NPRO master laser for frequencies below 50 kHz, and thus satisfies the specifications for LIGO 1. We therefore are confident that our injection-locked laser can be stabilized by using feedback to the master laser. The frequency noise reducing properties of the injection-locking process and the servo control system have also been studied and excellent agreement with theory has been obtained.

The intensity noise of our injection-locked laser has been measured. The laser meets the specifications for LIGO stage 1 at low frequencies. At high frequencies the laser is shot noise limited above 5 MHz for 6 mA of photo-current. This noise level is within 2 dB of the shot-noise limit for 10 mA of photo-current, and thus satisfies the LIGO stage 1 specifications. Further, we have demonstrated in excess of an order of magnitude of intensity noise reduction at low frequencies by feeding back to the high power pump laser diode.

With a small amount of engineering the laser described here will be ready for use in the Australian gravitational wave detection community's Advanced Research Interferometer (ARI) located in Perth.

Power scaling of the CPFS slab laser is currently being investigated. It was mentioned earlier that 10 Watts of TEM_{00} radiation has already been achieved using two 20 W pump diodes and a standing wave resonator geometry [53]. Further power scaling possibilities are being investigated by Richards *et al.*[53] using transverse cooling techniques and Mudge *et al.*[54] using faced cooled geometries. These advances along with the work presented in this thesis should enable a high power, single frequency injection-locked CPFS laser to be developed.

Further work on frequency stabilization of CPFS injection-locked lasers would be worthwhile. We have recently assembled a moderately high finesse reference cavity (finesse$\approx 2\times 10^3$). The demonstration of frequency noise reduction by locking the injection-locked laser to this reference cavity using feedback to the master laser would further demonstrate the potential of our injection-locked laser.

In the area of intensity noise reduction, it was mentioned earlier that the band-

width of our intensity noise reduction system was limited by the pump laser driver. It would be valuable to investigate the use of direct injection of the correction current into the laser diode, a technique that is frequently used in lower power systems. This along with improved photo-detection circuits should enable the achievement of intensity noise at the level of $5\times10^{-8}\ /\sqrt{Hz}$ across the frequencies of interest for laser interferometric detection of gravitational waves.

Appendix A

Mathematical Derivations of Formulae

A.1 Sensitivity of the Wheastone Bridge Temperature Sensor

The temperature sensor for the temperature controller for the gain medium of the slave laser is shown as Fig A1.

The resistance of the thermistor used in the circuit shown as Fig A1 is related to temperature by

$$R_{therm} = R_0 Exp\left(\frac{B}{T}\right) \tag{A.1}$$

where R_0, B are constants and T is the temperature of the therrmistor in Kelvin

The output voltage of an ideal instrumentation amplifier is the difference of the voltage of its two inputs times the gain of the instrumentation amplifier. Therefore the output voltage of the instrumentation amplifier is given by the following equation

$$V_{out} = \left(\frac{R_{ref}}{R_{ref} + R_{therm}} V_s - V_{ref}\right) G_{instr.} \tag{A.2}$$

where R_{ref} is the resistance of the reference resistor, V_s is the supply voltage of the bridge, V_{ref} is the reference voltage and $G_{instr.}$ is the gain of the instrumentation

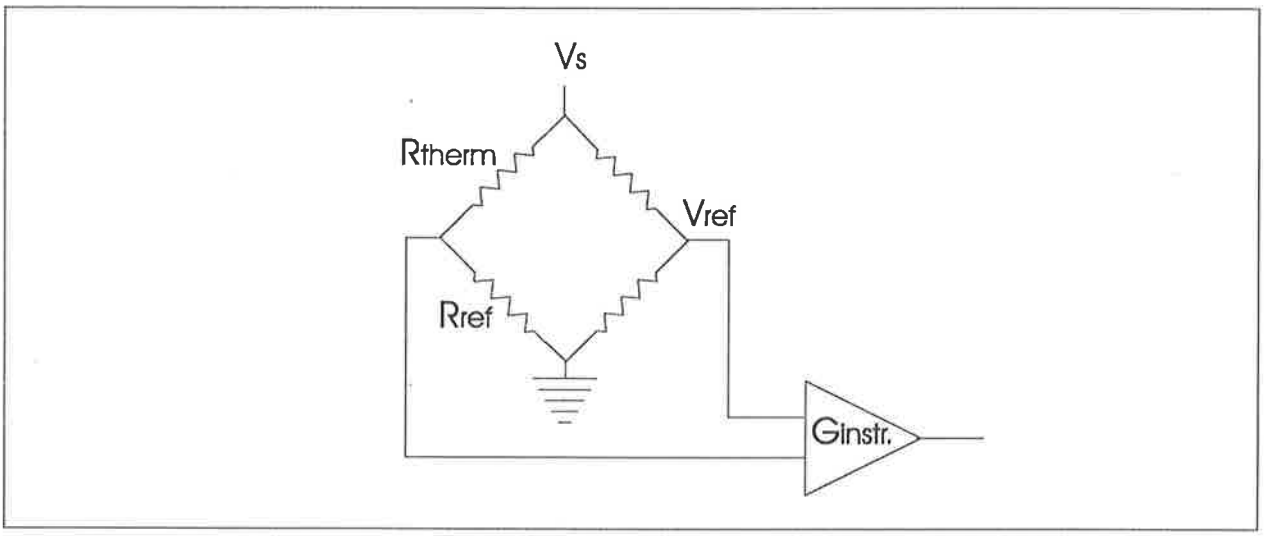

Figure A.1: A schematic of the temperature sensor used in the control system used to regulate the temperature of gain medium in the slave laser

amplifier.

Substituting Equation A.1 into Equation A.2 and taking its derivative with respect to temperature gives

$$\frac{dV_{out}}{dT} = \frac{-T^2 B R_0 Exp\left(\frac{B}{T}\right)}{\left(R_0 Exp\left(\frac{B}{T}\right) + R_{ref}\right)^2} V_s G_{instr.}$$

A.2 Ring Laser as a Regenerative Amplifier

This derivation is included to add some details that are not explicitly stated in Siegman's book[73]. Consider a ring resonator with an external field injected as shown in Fig A.2. In the steady state regime the electric field must be maintained in one round-trip. Hence

$$E_{circ} = jt_{loss}tge^{-j\phi(\omega)}E_{inc} + t_{loss}rge^{-j\phi(\omega)}E_{circ} \tag{A.3}$$

where t is the electric field transmission coefficient of the output coupler, r is the electric field reflection coefficient of the output coupler, t_{loss} is the electric field transmission coefficient of the rest of the cavity ignoring the laser gain medium,g is the magnitude of the amplitude gain from the gain medium and $\phi(\omega) = \omega p/c$ is the

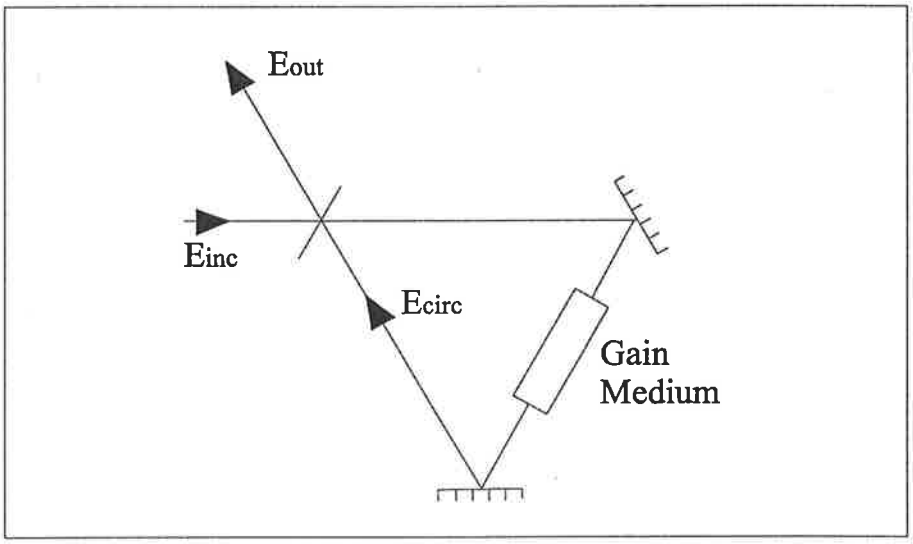

Figure A.2: A schematic of a ring resonator set-up as a regenerative amplifier.

roundtrip phase shift of the resonator (p is the optical round trip distance of the resonator).

Equation A.3 can be rearranged to give the circulating electric field

$$E_{circ} = \frac{jt_{loss}tge^{-j\phi(\omega)}E_{inc}}{1 - t_{loss}rge^{-j\phi(\omega)}} \tag{A.4}$$

The output field of the ring resonator can be expressed as

$$E_{out} = jtE_{circ} + rE_{inc} = rE_{inc} - \frac{t_{loss}ge^{-j\phi(\omega)}t^2E_{inc}}{1 - t_{loss}rge^{-j\phi(\omega)}} \tag{A.5}$$

If the round trip gain is defined as $G_{rt}(\omega) = t_{loss}rge^{-j\phi(\omega)}$ then Equation A.5 can be re-written as

$$E_{out} = \left[r - \frac{t^2G_{rt}(\omega)/r}{1 - G_{rt}(\omega)}\right]E_{inc} \tag{A.6}$$

$$= \frac{1}{\sqrt{R}}\left[R - \frac{(1-R)\,G_{rt}(\omega)}{1 - G_{rt}(\omega)}\right]E_{inc} \tag{A.7}$$

$$= \frac{1}{\sqrt{R}}\frac{R - G_{rt}(\omega)}{1 - G_{rt}(\omega)}E_{inc} \tag{A.8}$$

where R is the reflectivity of the output coupler

A.3 Mode Matching

In this section the effect of slightly incorrect mode matching of the master laser mode into the slave laser fundamental mode will be evaluated. This derivation was done specifically to investigate the fraction of the power that is coupled into an elliptical slave laser fundamental mode when using a circular master mode.

It can be shown[73] that an arbitrary laser field can be expressed as a summation of Hermite Gaussian polynomials ie

$$E(x,y,z) = \sum_n \sum_m c_{nm}\, \mu_{n,m}(x,y,z) \tag{A.9}$$

The values of the constants Cnm are evaluated using the spatial mode overlap integrals

$$c_{nm} = \int_{-\infty}^{\infty} \int_{-\infty}^{\infty} E(x,y,z)\, \mu_{n,m}(x,y,z)\, dxdy \tag{A.10}$$

As the ideal slave laser field or the mode of interest in a mode cleaner is a zeroth order Gaussian. The field that the master laser has to match to can be represented by

$$\begin{aligned} \mu_s(x,y,z) &= \left(\frac{2}{\pi}\right)^{1/2} \sqrt{\frac{Exp\left[-j\psi_s(z)\right]}{w_{sx}(z)\, w_{sy}(z)}} \\ &\quad \times Exp\left[-\frac{jkx^2}{2R_{sx}(z)} - \frac{jky^2}{2R_{sy}(z)} - \frac{x^2}{w_{sx}^2(z)} - \frac{y^2}{w_{sy}^2(z)}\right] \end{aligned} \tag{A.11}$$

The normalized field of the injected master laser is given by

$$\begin{aligned} \mu_m(x,y,z) &= \left(\frac{2}{\pi}\right)^{1/2} \sqrt{\frac{Exp\left[-j\psi_m(z)\right]}{w_{mx}(z)\, w_{my}(z)}} \\ &\quad \times Exp\left[-\frac{jkx^2}{2R_{mx}(z)} - \frac{jky^2}{2R_{my}(z)} - \frac{x^2}{w_{mx}^2(z)} - \frac{y^2}{w_{my}^2(z)}\right] \end{aligned} \tag{A.12}$$

As the master laser beam is circularly symmetric, the waist in the saggital and tangential planes will be located in the same place. To simplify the mode overlap

integral it will evaluated at the location of the waist of the master laser. Hence for the calculation $R_{mx}(z) = R_{my}(z) = \infty$

The mode overlap integral for the master laser and the zeroth order cavity mode is

$$c_{00} = \int\int \mu_m(x,y,z)\,\mu_s{}^*(x,y,z)\,dxdy \tag{A.13}$$

This integral can be evaluated using 'Siegman's Lemma'[73]:

$$\int_{-\infty}^{\infty} Exp\left[-ax^2 - 2bx\right] dx = \sqrt{\frac{\pi}{a}} Exp\frac{b^2}{a} \tag{A.14}$$

Using this lemma assumes that the fields are infinite in transverse dimension and does not allow for truncation of the field by apertures. However in most well designed laser cavities the aperturing affects only the outer few percent of the fundamental mode, hence this is a valid approximation.

The form of the fundamental field that is injected into the zeroth order mode of the slave cavity is

$$E(x,y,z) = c_{00}\mu_m(x,y,z)$$

The fraction of the power (FP) injected into the slave zeroth order field is simply

$$FP = \frac{\iint E(x,y,z)\,E^*(x,y,z)\,dxdy}{\iint \mu_m(x,y,z)\,\mu_m^*(x,y,z)\,dxdy} \tag{A.15}$$

$$= \frac{\iint c_{oo}\mu_m(x,y,z)\,c_{00}^*\mu_m^*(x,y,z)\,dxdy}{\iint \mu_m(x,y,z)\,\mu_m^*(x,y,z)\,dxdy} \tag{A.16}$$

$$= c_{00}c_{00}^* \tag{A.17}$$

Therefore by substituting the Equations A.11, A.12 into the mode overlap integral Equation A.13 and substituting the result into Equation A.15 gives the fractional of power injected into the fundamental mode:

$$FP = \frac{4}{W_{xm}(z)\,W_{ym}(z)\,W_{xs}(z)\,W_{ys}(z)\sqrt{\left[\left(\frac{1}{w_{mx}^2(z)+w_{sx}^2(z)}\right)^2+\frac{k^2}{4R_{sx}^2(z)}\right]}} \times \frac{1}{\sqrt{\left[\left(\frac{1}{w_{my}^2(z)+w_{sy}^2(z)}\right)^2+\frac{k^2}{4R_{sy}^2(z)}\right]}}$$

A.4 Sensitivity of Pound-Drever-Hall Error Signal

This error signal calculation is based on a derivation by Day *et al.* [16]. in which the slope of a Pound-Drever-Hall error signal, used to lock a passive reference cavity to the laser, or visa versa is derived. The difference when this technique is used for injection-locking, is that the reference cavity significantly amplifies the masters power.

In Pound-Drever-Hall locking the beam from the master laser is passed through an electro-optic modulator (EOM) which imposes phase sidebands on the master laser. After the EOM the master laser field may be written as

$$\begin{aligned} E_m(t) &= E_m \exp\left[j\left(\omega t + \beta \sin\left(\omega_m t\right)\right)\right] \\ &\simeq E_m\left[J_0(\beta) + J_1(\beta)\left(e^{j\omega_m t} - e^{-j\omega_m t}\right)\right] e^{j\omega t} \end{aligned}$$

The slave laser field can be written as

$$E_s(t) = E_s \exp\left[j\left(\omega t + \phi(t)\right)\right]$$

where $\phi(t)$ is the time varying phase shift of the slave laser or the slave laser phase noise.

The field at the photodiode is

$$E(t) = E_m(t) + E_s(t)$$

The intensity of the field detected at the photodiode is

$$\begin{aligned} I(t) &\propto E(t)E^*(t) \\ &= E_m E_m^* + E_s E_s^* + E_m^* E_s e^{j\phi(t)}\left[J_0(\beta) + J_1(\beta)\left(e^{j\omega_m t} - e^{-j\omega_m t}\right)\right] + \\ &\quad E_m E_s^* e^{-j\phi(t)}\left[J_0(\beta) + J_1(\beta)\left(e^{-j\omega_m t} - e^{+j\omega_m t}\right)\right] \end{aligned}$$

We are only interested in the time varying terms and hence the first two terms can be ignored, the remaining intensity term is

$$I(t) \propto E_m^* E_s e^{j\phi(t)} J_1(\beta)\left(e^{j\omega_m t} - e^{-j\omega_m t}\right) + E_m E_s^* e^{-j\phi(t)} J_1(\beta)\left(e^{-j\omega_m t} - e^{+j\omega_m t}\right)$$

It can be assumed that E_m, E_s are real, and then the equation immediately above can be written

$$I(t) = 4\sqrt{I_s I_m} J_1(\beta)\sin(\omega_m t)\sin(\phi(t))$$

where I_s and I_m are the intensities of the slave and master fields at the photodiode respectively.

The photo-current of the photo-diode circuit is given by

$$i_{pd}(t) = \eta_d A I(t)$$

where η_d is the detector efficiency and A is the area of the photo-detector. If a fraction of the main beam is η_p of the injection-locked laser is sampled and the photo-detector has a current to voltage gain of R the output of the photo-detector will be given by

$$v(t) = 4R\eta_d\eta_p\sqrt{P_s P_m} J_1(\beta)\sin(\omega_m t)\sin(\phi(t))$$

where P_s, P_m are the power of the slave laser and the master laser respectively.

When this term is mixed in quadrature with a sample of the EOM driver, the voltage measured at the IF port of the double balanced mixer will be

$$\begin{aligned} v(t) &= 4R\eta_d\eta_p\eta_{dbm}\sqrt{P_sP_m}J_1(\beta)\sin(\omega_m t)\sin(\phi(t))\cos(\omega_m t) \\ &= 4R\eta_d\eta_p\eta_{dbm}\sqrt{P_sP_m}J_1(\beta)\sin(\phi(t))\left[-\frac{1}{2}+\frac{1}{2}\cos(2\omega_m t)\right] \end{aligned}$$

where η_{dbm} is the efficiency of the double balanced mixer. The second harmonic term is removed by passing the signal through a low passs filter, leaving

$$v(t) = -2R\eta_d\eta_p\eta_{dbm}\sqrt{P_sP_m}J_1(\beta)\sin(\phi(t))$$

The phase shift $\phi(t)$ is given as Equation 3.10

$$\phi(t) = \text{Arc}\sin\left[\frac{\omega_m - \omega_s(t)}{\omega_{lock}}\right]$$

Hence within the locking range

$$v(t) = -2R\eta_d\eta_p\eta_{dbm}\sqrt{P_sP_m}J_1(\beta)\left[\frac{\omega_m - \omega_s(t)}{\omega_{lock}}\right]$$

Or

$$\frac{\Delta v(t)}{\Delta\omega(t)} = \frac{-2R\eta_d\eta_p\eta_m\sqrt{P_sP_m}J_1(\beta)}{\omega_{lock}}$$

A.5 Sensitivity of the AOM beatnote experiment

The master field after the AOM can be written as

$$E_m(t) = E_m\text{Exp}[j(\omega_m t + \phi_m(t) + \omega_{aom}t)]$$

where $\phi_m(t)$ is the phase noise of the master and $\omega_{aom}t$ is the frequency shift due to the AOM.

The injection-locked laser field can be written as

$$E_{ij}(t) = E_{ij}\mathrm{Exp}[j(\omega_m t + \phi_{il}(t))]$$

where $\phi_{il}(t)$ is the phase noise of the injection-locked laser. Note the time averaged frequency of an injection-locked laser and its master laser are the same, hence the time averaged frequency of the injection-locked laser is $\omega_m t$

The total field at the photodiode is

$$E(t) = E_m(t) + E_{ij}(t)$$

The intensity of the field detected at the photo diode is given by

$$I(t) \propto E(t) E^*(t) \tag{A.18}$$

Substituting the expressions for the master and slave fields into Equation A.18 gives

$$I(t) = I_m + I_{il} + 2\sqrt{I_m I_{il}} \cos[\omega_{am} t + \Delta\phi(t)] \tag{A.19}$$

where I_m, I_{il} are intensity of the master and slave fields respectively, $\Delta\phi = \phi_m(t) - \phi_{il}(t)$ is the phase difference between the injection-locked laser and master fields. The photo-diode produces a photo-current proportional to the intensity incident upon it. Thus the detected beat signal will generate a voltage at the output of the photo-diode given by

$$V(t) = \eta_{pd} R_f 2\sqrt{P_{dm} P_{dil}} \cos[\omega_{aom} t + \Delta\phi(t)] \tag{A.20}$$

where R_f is the transimpedance gain of the photo-detector, η_{pd} is the quantum efficiency of the photodiode and P_{dm}, P_{dil} are the dc detected powers of the frequency-shifted master and the injection-locked lasers respectively.

The above analysis assumes perfect spatial wavefront overlap between the detected master and slave fields. In practice this will not be the case. A wavefront mis-match will manifest itself as a reduction of the magnitude of the detected beat

signal. A time dependent wavefront mis-match will result in additional time variation of the size and phase of the beat signal. It is highly likely that this is responsible for the degraded noise floor of the measurement at low frequencies. To take this into account a mode overlap efficiency factor η_{mo} is required in Equation A.20.

If the beat signal is mixed in quadrature with a sample of the AOM drive the resulting voltage at the IF port is given by

$$V(t) = \eta_{pd}\eta_{mo}\eta_{dbm}R_f\sqrt{P_{dm}P_{dil}}\sin\Delta\phi(t) \tag{A.21}$$

where η_{dbm} is the double balanced mixer efficiency term. This assumes that second harmonic term has been removed.

For phase small fluctuations Equation A.21 can be linearized to the following

$$V(t) = \eta_{pd}\eta_{mo}\eta_{dbm}R_f\sqrt{P_{dm}P_{dil}}\Delta\phi(t)$$

As the beat signal and the reference signal are mixed in quadrature the measurement is relatively insensitive to intensity noise.

Appendix B

Circuit Diagrams

B.1 Pre-Amp for Temperature Control of the Slab

A circuit diagram for the thermal pre-amp is shown as Fig B.1.This circuit consists of a proportional stage, integration stage (for increased low frequency gain) and a differentiation stage (for good higher frequency performance and transient response) in parallel. The Op-Amp on the extreme right is the summing stage.

B.2 Power Amp in the temperature controller of the slab

A schematic of the power-amp used to drive the Peltier cell is shown as Fig B.2

B.3 Pre-Amp for the Frequency Servo for the Slave Laser

A circuit diagram for the pre-amp that was used in the frequency contol servo for the slave laser is shown as Fig B.3. The lock position may be tuned by adding a DC voltage to the error signal offset null point. The high voltage amplifier is only capable of delivering positive voltages. Therefore a voltage must be applied to the high voltage set point so that the zero point occurs in the middle of the dynamic

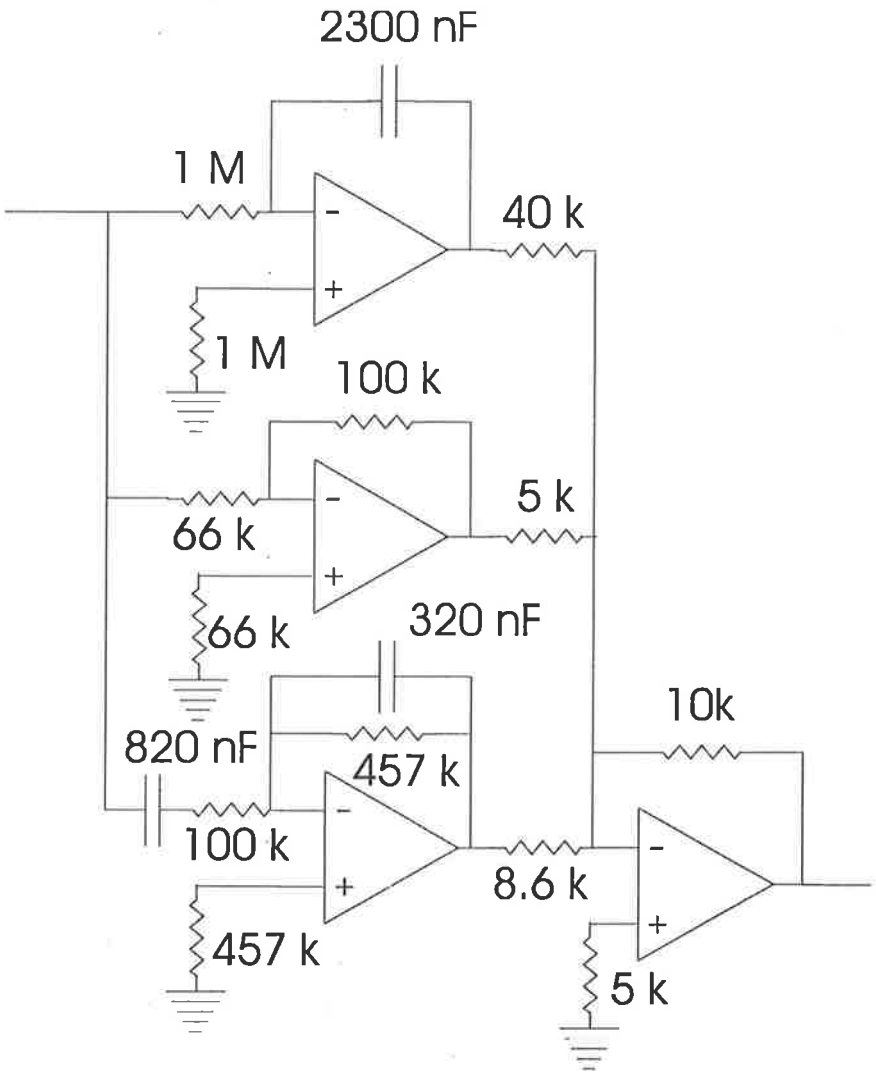

Figure B.1: Pre-amp for the temperature controller of the slab. All values of resistors are in ohms.

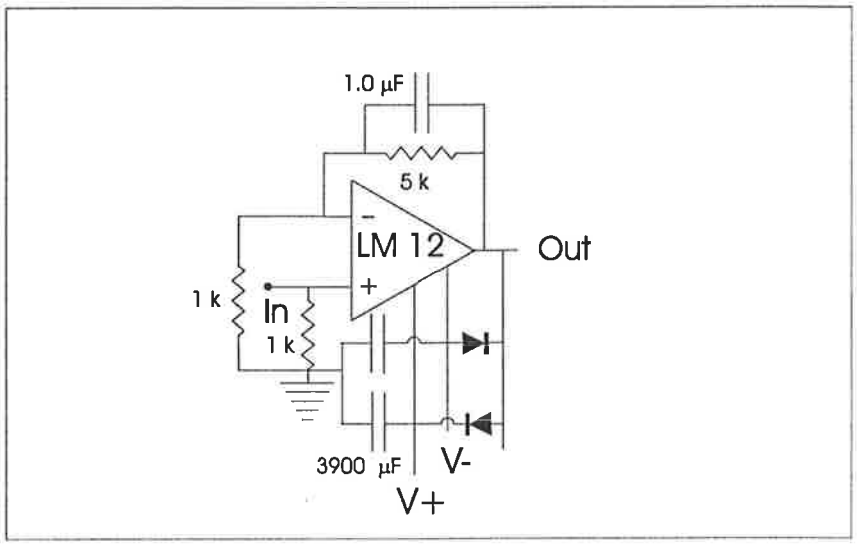

Figure B.2: Power amplifier used to drive the Peltier cell in the slab temperature controller

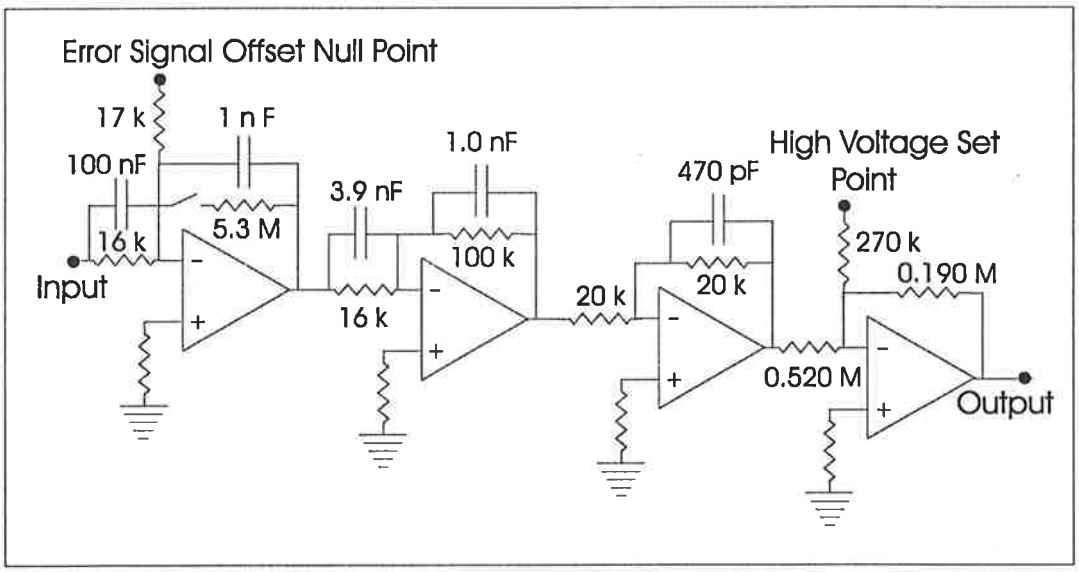

Figure B.3: Pre-Amp for the frequency control servo of the slave laser

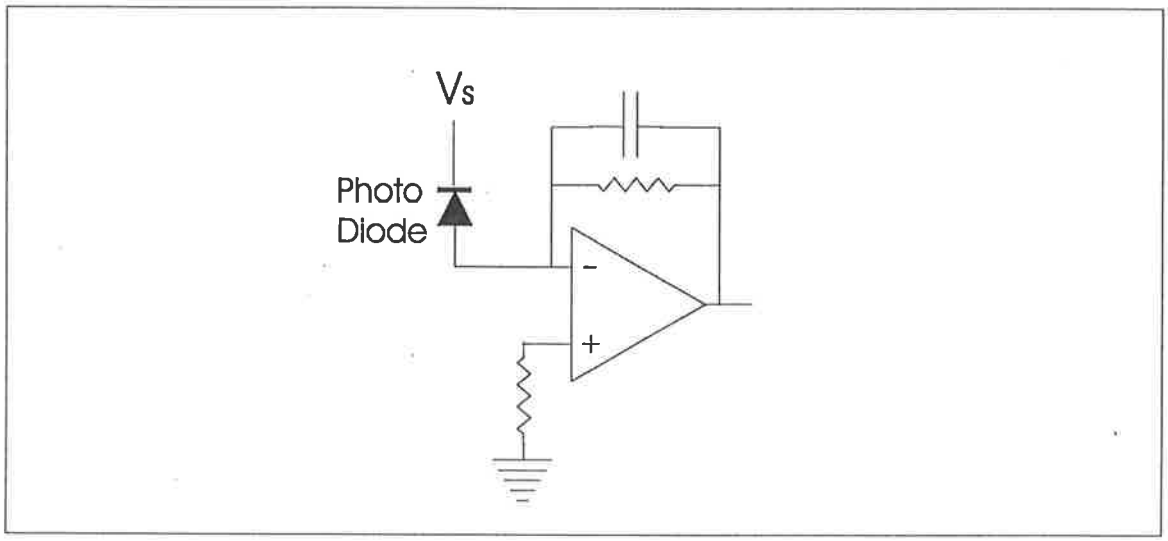

Figure B.4: A photo-detector in transimpedance configuration.

range of the high voltage amplifier.

B.4 Transimpedance Photo-diode Circuit

A typical circuit diagram for a photo-detector using a photo-diode coupled to a transimpedance amplifier is shown as Fig B.4. The transimedance configuration allows high sensitivity and bandwidth, generally limited by the properties of the op-amp used. For maximum sensitivity,. the Op-Amp should be chosen such that noise is limited by the Johnson noise of the feedback resistor.

B.5 Intensity Noise Suppression Pre-Amp

The intensity noise suppression pre-amp circuit diagram is shown as Fig B.5

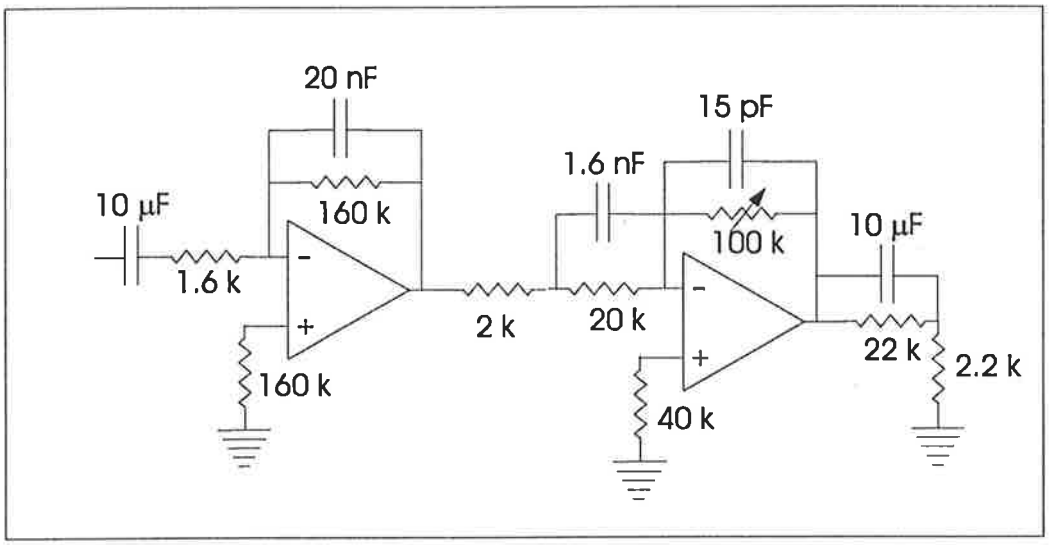

Figure B.5: Pre-Amp circuit diagram for the intensity noise reduction servo.

Appendix C

Publications

Main Publication

- D. J. Ottaway, P. J. Veitch, M. W. Hamilton, C. Hollitt, D. Mudge, and J. Munch "A Compact Injection-Locked Nd:YAG Laser for Gravitational Wave Detection"

  IEEE Journal of Quantum Electronics, Vol 34, No 10 October 1998

  This is reproduced on the following pages

Other Publications assosciated with this work

- Published Papers

- D. Mudge, P.J Veitch, J. Munch, D.J. Ottaway and M.W. Hamilton " High-power diode-laser-pumped CW solid-state lasers using stable-unstable resonators" IEEE Select. Topics Quantum Electron., Vol 3, 1997 pp19-26

- P. J. Veitch, J. Munch, M.W. Hamilton, D.J. Ottaway, A. Greentree and A. Tikhomirov "High Power Lasers and Novel Optics for Laser Interferometric Gravitational Wave Detectors" Aust. J. Phys, Vol 48, 1995, pp 999-1006

Conference Presentations

- D. Ottaway, P. Veitch, M.W. Hamilton, J. Munch, C. Hollitt and D. Mudge "Compact and efficient Nd:YAG laser for field based vibrometry" Verbal presentation at the Defence Science and Technology Organisation (DSTO) Electro-Optics (EO) Hub meeting August 1998

- D. Ottaway, D. Mudge, M.W. Hamilton, J. Munch and P. Veitch "Stable, High Power Nd:YAG Laser for Gravitational Wave Interferometers" IQEC 1996 Oral presentation FE7

- D. Mudge, P.J. Veitch, J. Munch, D.Ottaway, M.W. Hamilton and P Klovekorn "A high power, cw Nd:YAG laser for high precision interferometry" 13th National Congress of the Australian Institute of Physics 1998 Oral presentation

- D. J. Ottaway, P.J. Veitch, M.W. Hamilton, J. Munch, C. Hollit and D. Mudge "A low noise, medium power Nd:YAG laser" 13th National Congress of the Australian Institute of Physics 1998 Oral presentation

- D.J. Ottaway, P.J. Veitch, M.W. Hamilton, J. Munch, C. Hollit and D. Mudge "Compact, Efficient, Nd:YAG Laser Sources for Gravitational Wave Interferometry" 1997 AOS XIConference poster presentation WP1

- D. Mudge, P.J. Veitch, J. Munch, D.Ottaway and M.W. Hamilton "High-power diode-laser-pumped CW Nd:YAG lasers using Stable-Unstable Resonator"1997 AOS XIConference poster presentation WP3

- J. Munch, P.J. Veitch, M.W. Hamilton, D.J. Ottaway, A. Greentree and A. Tikhomirov "A medium power, CW, frequency stable Nd:YAG lasers" AOS X July 1995 Proceedings book of Abstacts (ed) P3

Ottaway, D.J., Veitch, P.J., Hamilton, M.W., Hollitt, C., Mudge, D., and Munch, J., (1998) A compact injection-locked Nd:YAG laser for gravitational wave detection. *IEEE Journal of Quantum Electronics, v. 34 (10), pp. 2006-2009.*

Bibliography

[1] G. Birnbaum, "Frequency Stabilization of Gas Lasers," *Proc. of IEEE*, vol. 55, pp. 1015–1025, 1967.

[2] C. Freed, "Design and Short Term Stability of Single-Frequency CO2 Lasers," *IEEE J. of Quantum Electron.*, vol. 4, pp. 404–408, 1968.

[3] H. Hellwig, H. Bell, P. Kartaschoff, and J. Bergquist, "Frequency Stability of Methane-Stabilized He-Ne Lasers," *Journal of Applied Physics*, vol. 43, pp. 450–452, 1972.

[4] T. Nussmejer and R. Abrams, "Stark Cell Stabilization of CO2 Laser," *Appl. Phys. Lett*, vol. 25, pp. 615–617, 1974.

[5] C. Shank and M. Klein, "Frequency Locking of a CW Dye Laser Near Atomic Absorption Lines in a Gas Discharge," *Appl. Phys. Lett*, vol. 23, pp. 156–157, 1973.

[6] R. Grove, F. Wu, and S. Ezekiel, "Frequency Stabilization of a CW Dye Laser," *Optical Engineering*, vol. 13, pp. 531–533, 1974.

[7] R. Barger, J. West, and T. English, "Fast Frequency Stabilization of a CW Dye Laser," *Appl. Phys. Lett*, vol. 27, pp. 31–33, 1975.

[8] J. Abate, "Long-Term Frequency and Intensity Stabilization of a CW Dye Laser," *Journal of Applied Physics*, vol. 47, pp. 1464–1466, 1976.

[9] S. Rackley and R. Butcher, "Stabilisation of Carbon Dioxide Lasers Using the Stark Effect," *J. Phys D: Appl. Phys*, vol. 16, pp. 505–516, 1983.

[10] R. W. P. Drever, J. L. Hall, F. V. Kowalski, J. Hough, G. M. Ford, A. J. Munley, and H. Ward, "Laser Phase and Frequency Stabilization Using an Optical Resonator," *App. Phys. B*, vol. 31, pp. 97–105, 1983.

[11] J. Hough, D. Hils, M. Rayman, M. L.-S, L. Hollberg, and J. Hall, "Dye-Laser Frequency Stabilization Using Optical Resonators," *Appl. Phys B*, vol. 33, pp. 179–185, 1984.

[12] J. Munch, M. Koplin, and J. Levine, "Frequency Stability and Stabilization of a Chemical Laser," *IEEE J. of Quantum Electron.*, vol. 14, pp. 17–22, 1978.

[13] T. Kane and R. Byer, "Mononlithic, Unidirectional Single Mode Nd:YAG Ring Laser," *Opt. Letters*, vol. 10, pp. 65–67, 1985.

[14] T. Kane, A. Nilsson, and R. Byer, "Frequency Stability and Offset Locking of a Laser-Diode-Pumped Nd:YAG Monolithic Nonplanar Ring Oscillator," *Opt. Letters*, vol. 12, pp. 175–177, 1987.

[15] P. Fritschel, A. Jeffries, and T. Kane, "Frequency Fluctuations of a Diode-Pumped Nd:YAG Ring Laser," *Optics Letters*, vol. 14, pp. 993–995, 1989.

[16] T. Day, E. K. Gustafson, and R. L. Byer, "Sub-Hertz Relative Frequency Stabilization of Two-Diode Laser-Pumped Nd:YAG Lasers Locked to a Fabry-Perot Interferometer," *IEEE J. Quantum Electron.*, vol. 28, no. 4, pp. 1106–1115, 1992.

[17] J. Czarske, R. Philipps, and I. Freitag, "Spectral Properties of Diode-Pumped Non-Planar Monolithic Nd:YAG Ring Lasers," *Appl. Phys*, vol. 61, pp. 243–248, 1995.

[18] T. Day, A. Nilsson, M. Fejer, A. Farinas, E. Gustafon, C. Nabors, and R. Byer, "30 Hz Linewidth, Diode-Laser-Pumped, Nd:GGG Nonplanar Ring Oscillators by Active Frequency Stabilization," *Electron. Lett*, vol. 25, pp. 810–812, 1989.

[19] T. Day, E. Gustafon, and R. Byer, "Active Frequency Stabilzation of a 1.062 um, Nd:GGG, Diode-Laser-Pumped Nonplanar Ring Oscillator to Less Than 3 Hz of Relative Linewidth," *Optics Letters*, vol. 15, pp. 221–223, 1990.

[20] N. Uehara and K. Ueda, "193-mHz Linewidth of Frequency-Stabilized Laser-Diode-Pumped Nd:YAG Ring Lasers," *Optics Letters*, vol. 18, pp. 505–507, 1993.

[21] N. Sampas, E. Gustafson, and R. Byer, "Long-Term Stability of Two Diode-Laser-Pumped Nonplanar Ring Lasers Independently Stabilized to Two Fabry-Perot Interferometers," *Optics Letters*, vol. 18, pp. 947–949, 1993.

[22] N. Uehara and K. Ueda, "Ultrahigh-Frequency Stabilization of a Diode-Pumped Nd:YAG Laser with a High-Power-Acceptance Photodetector," *Optics Letters*, vol. 19, pp. 728–730, 1994.

[23] K. Nakagawa, A. Shelkovnikov, T. Katsuda, and M. Ohtsu, "Absolute Frequency Stability of a Diode-Laser-Pumped Nd:YAG Laser Stabilized to a High-Finesse Optical Cavity," *Applied Optics*, vol. 33, pp. 6383–6386, 1994.

[24] K. Nakagawa, T. Katsuda, and M. Ohtsu, "Short-Term Frequency Stabilzation of Diode-Laser-Pumped Nd:YAG Lasers Using Double-Pendulum Suspended Cavities," *Appl. Phys.*, vol. B 60, pp. 489–494, 1995.

[25] S. Sandford and C. Antill, "Laser Frequency Control Using an Optical Resonator Locked to an Electronic Oscillator," *IEEE J. Quantum Electron.*, vol. 33, pp. 1991–1996, 1997.

[26] G. Ruso, R. Storz, S. Seel, S. Schiller, and J. Mlynek, "Nd:YAG Laser Frequency Stabilization to a Supercavity," *Optics Communications*, vol. 113, pp. 259–262, 1997.

[27] N. Uehara and K. Ueda, "Frequency Stabilization of Two Diode-Pumped Nd:YAG Lasers Locked to Two Fabry-Perot Cavities," *Japanese J. Appl. Phys.*, vol. 33, pp. 1628–1633, 1994.

[28] M. Musha, S. Telada, K. Nakagawa, M. Ohashi, and K. Ueda, "Measurement of Frequency Noise Spectra of Frequency-Stabilized LD-Pumped Nd:YAG Laser by Using a Cavity with Separately Suspended Mirrors," *Optics Communications*, vol. 140, pp. 323–330, 1997.

[29] O. Mor and A. Arie, "Performance Analysis of Drever-Hall Laser Frequency Stabilization Using a Proprtional + Integral Servo," *IEEE J. Quantum Electron.*, vol. 33, pp. 532–540, 1997.

[30] K. Danzmann, J. Chen, P. G. Nelson, T. M. Niebauer, A. Rudiger, R. Schilling, L. Schnupp, K. A. Strain, H. Walther, W. Winkler, J. Hough, A. M. Campbell, C. Cantley, J. E. Logan, B. J. Meers, E. Morrison, G. P. Newton, D. I. Robertson, N. A. Robertson, S. Rowan, K. D. Skeldon, P. J. Veitch, H. Ward, H. Welling, P. Aufmuth, I. Kropke, D. Ristau, J. E. Hall, J. R. J. Bennet, I. F. Corbett, B. W. H. Edwards, R. J. Elsey, R. J. S. Greenhalgh, B. F. Schultz, D. Nicholson, J. R. Shuttleworth, J. Ehlers, P. Kafka, G. Schafer, H. Braun, and V. Kose, "The GEO-Project A Long-Baseline Laser Interferometer for the Detection of Gravitaional Waves," *Lecture Notes in Physics, Springer-Verlag Germany*, vol. 410, 1992.

[31] A. Arie, S. Schiller, E. Gustafson, and R. Byer, "Absolute Frequency Stabilization of Diode-Laser-Pumped Nd:YAG Lasers to Hyperfine Transitions in Molecular Iodine," *Optics Letters*, vol. 17, pp. 1204–1206, 1992.

[32] I. Freitag, A. Tunnermann, and H. Welling, "Power Scaling of Diode-Pumped Monolithic Nd:YAG Lasers to Output Powers of Several Watts," *Optics Communications*, vol. 115, pp. 511–515, 1995.

[33] G. Kerr and J. Hough, "Coherent Addition of Laser Oscillators for Use in Gravitational Wave Antennas," *Appl. Phys.*, vol. B 49, pp. 491–495, 1989.

[34] C. Man and A. Brillet, "Injection Locking of Argon-Ion Lasers," *Optics Letters*, vol. 9, pp. 333–335, 1984.

[35] W. Veldkamp, J. Leger, and G. Swanson, "Coherent Summation of Laser Beams Using Binary Phase Gratings," *Optics Letters*, vol. 11, pp. 303–305, 1986.

[36] J. Leger, G. Swanson, and W. Veldkamp, "Coherent Beam Addition of GaAlAs Lasers by Binary Phase Gratings," *Appl. Phys. Lett.*, vol. 48, pp. 888–890, 1986.

[37] S. Menard, M. Vampouille, B. Colombeau, and C. Froehly, "Highly Efficient Phase Locking and Extracavity Coherent Combination of Two Diode-Pumped Nd:YAG Laser Beams," *Optics Letters*, vol. 21, pp. 1996–1998, 1996.

[38] J. Harrison, G. Rines, P. Moulton, and J. Leger, "Coherent Summation of Injection-Locked, Diode Pumped Nd:YAG Ring Lasers," *Optics Letters*, vol. 13, pp. 111–113, 1988.

[39] W. Weichmann, T. Kane, D. Haserot, F. Adams, G. Truong, and J. Kmetic, *Conference on Optical Society of America.* Washington D.C, 1998 p 432.

[40] A. Abramovici, W. Althouse, R. Drever, Y. Gursel, S. Kawamura, F. Raab, D. Shoemaker, L. Sievers, R. Spero, K. Thorne, R. Vogt, R. Weiss, S. Whitcome, and M. Zucker, "LIGO: The Interferometer Gravitational-Wave Observatory," *Science*, vol. 256, pp. 325–333, 1992.

[41] C. Buczek, R. Freiberg, and M. Skolnick, "Laser Injection Locking," *Proc. IEEE*, vol. 61 (10), pp. 1411–1431, 1973.

[42] H. L. Stover and W. H. Stejer, "Locking of Laser Oscillators by Light Injection," *App. Phys. Letters*, vol. 8, p. 91, 1966.

[43] C. Buczek and R. Freiberg, "Hybrid Injection Locking of Higher Power C02 Lasers," *IEEE J. Quantim Electron.*, vol. 8(7), pp. 641–650, 1972.

[44] M. Ibrahim, "On Injection-Locking of Inhomogeneously Pumped Semiconductor Lasers," *Optical and Quantum Electronics*, vol. 28, pp. 1049–1054, 1996.

[45] C. D. Nabors, A. D. Farinas, T. Day, S. T. Yang, E. K. Gustafon, and R. L. Byer, "Injection Locking of a 13-w CW Nd:YAG Ring Laser," *Optics Letters*, vol. 14, no. 21, pp. 1189–1191, 1989.

[46] D. Golla, I. Freitag, H. Zellmer, W. Schone, I. Kropke, and H. Welling, "15 W Single-Frequency Operation of a CW, Diode Laser-Pumped Nd:YAG Ring Laser," *Optics Communications*, vol. 98, pp. 86–90, 1993.

[47] A. D. Farinas, E. K. Gustafson, and R. L. Byer, "Design and Charactarization of a 5 .5-W, CW, Injection-Locked, Fibre-Coupled, Laser-Diode-Pumped Nd:YAG Minature-Slab Laser," *Optics Letters*, vol. 19, no. 2, pp. 114–116, 1994.

[48] I. Freitag, D. Golla, S. Knoke, W. Schone, H. Zellmer, A. Tunnermann, and H. Welling, "Amplitude and Frequency Stability of a Diode Pumped Nd:YAG Laser Operating at a Single-Frequency Continuous-Wave Output Power of 20 W," *Optics Letters*, vol. 20, no. 5, pp. 462–464, 1995.

[49] S. T. Yang, Y. Imai, M. Oka, N. Eguchi, and S. Kubota, "Frequency- Stabilized, 10-W Continuous-Wave, Laser-Diode End Pumped, Injection-Locked Nd:YAG Laser," *Optics Letters*, vol. 21, no. 20, pp. 1676–1678, 1996.

[50] O. Crecut, C. N. Man, D. Shoemaker, A. Brillet, A. Menhert, P. Peuser, N. P. Schmitt, P. Zeller, and K. Wallmeroth, "18 W Single-Frequency Operation of An Injection-Locked, CW, Nd:YAG Laser," *Physics Letters A*, vol. 140, no. 6, pp. 294–298, 1989.

[51] J. Richards and A. McInnes, "Versatile,Efficient,Diode-Pumped Minature Slab, Laser," *Optics Letters*, vol. 20, no. 4, pp. 371–373, 1995.

[52] W. Koechner, *Solid State Laser Engineering 3rd Edition.* Springer-Verlag, 1992.

[53] J. Richards *Personal Communication.*

[54] D. Mudge, P. J. Veitch, J. Munch, D. Ottaway, and M. W. Hamilton, "High-Power Diode-Laser-Pumped CW Solid-State Lasers Using Stable-Unstable Resonators," *IEEE Selected Topics in Quantum Electronics*, vol. 3, no. 1, pp. 19–26, 1997.

[55] C. C. Harb, M. B. Gray, H. A. Bachor, R. Schilling, P. Rottengatter, I. Freitag, and H. Welling, "Suppression of the Intensity Noise in a Diode-Pumped Neodymium:YAG Nonplanar Ring Laser," *IEEE J. Quantum Electron.*, vol. 30, no. 12, pp. 2907–2913, 1994.

[56] S. Rowan, A. M. Cambell, K. Skeldon, and J. Hough, "Broadband Intensity Stabilization of a Diode-Pumped Monolithic Minature Nd:YAG Ring Laser," *Journal of Modern Optics*, vol. 41, no. 6, pp. 1263–1269, 1994.

[57] K. Tsubono and S. Moiwaki, "Shot-Noise Limited Low-Frequency Intensity Noise of a Nd:YAG Laser," *Jpn. J. Appl. Phys*, vol. 31, pp. 1241–1242, 1992.

[58] E. Huntington, B. Buchler, C. Harb, T.Ralph, D. McClelland, and H. Bachor, "Feedback Control of the Intensity Noise of Injection Locked Lasers," *Optics Communications*, vol. 145, pp. 359–366, 1998.

[59] T. J. Kane, "Intensity Noise in Diode-Pumped Single Frequency Nd:YAG Lasers and its Control by Electronic Feedback," *IEEE Photonics Technology Letters*, vol. 2, no. 4, pp. 244–245, 1990.

[60] C. C. Harb, T. C. Ralph, E. Huntington, I. Freitag, D. McClelland, and H. A. Bachor, "Intensity-Noise Properties of Injection-Locked Lasers," *Phys Rev A*, vol. 54, no. 5, pp. 4370–4382, 1996.

[61] T. C. Ralph, C. C. Harb, and H. A. Bachor, "Intensity Noise Injection-Locked Lasers: Quantum Theory Using a Linearized Input Output Method," *Phys. Rev. A*, vol. 54, no. 5, p. 4359, 1996.

[62] A. D. Farinas, E. K. Gustafson, and R. L. Byer, "Frequency and Intensity Noise in an Injection-Locked, Solid State Laser," *J. Opt. Soc. Am. B*, vol. 12, pp. 328–334, 1995.

[63] H. Layer, "Acoustooptic Modulator Intensity Servo," *Applied Optics*, vol. 18, pp. 2947–2949, 1979.

[64] C. Harb, *PhD Thesis.* Australian National University (Canberra): Unpublished, 1996.

[65] M. Hamilton, "An Introduction to Stabilized Lasers," *Contemporary Physics*, vol. 30, pp. 21–33, 1989.

[66] A. Yariv, *Optical Electronics.* Saunders College Publishing, 1991.

[67] P. Saulson, *Fundumentals of Interferometric Gravitational Wave Detectors.* World Scientific, 1994.

[68] S. Whitcomb *Personal Communication.*

[69] R. Lerou, "Long Range Vibration Sensing by Lasers," *9th Conference on Coherent Laser Radar*, Jun 23-27, 1997.

[70] W. Bosenberg, A. Drobshoff, J. Alexander, L. Myers, and R. Byer, "Continuous-Wave Singly Resonant Optical Parametric Oscillator Based on Periodically Poled LiNbO3," *Optics Letters*, vol. 21, pp. 713–715, 1996.

[71] R. Dorf and R. Bishop, *Modern Control Systems 7th Edition.* Addison-Wesley, 1995.

[72] K. Ogata, *Modern Control Engineering 2nd Edition.* Prentice-Hall, 1990.

[73] A. E. Siegman, *Lasers.* University Science Books, 1986.

[74] I. Freitag and H. Welling, "Investigation on Amplitude and Frequency Noise of Injection-Locked Diode-Pumped Nd:YAG Lasers," *Appl. Phys. B*, vol. 58, pp. 537–543, 1994.

[75] R. Barrilet, A. Brillet, R. Chiche, F. Cleva, L. Latrach, and C. N. Man, "An Injection-Locked Nd:YAG Laser for the Interferometric Detection of Gravitational Waves," *Meas.Sci.Technol*, vol. 7, pp. 162–169, 1996.

[76] *Opto-Power Corporation, Tucson, Arizona.*

[77] "Doric Lenses Inc, St-Clement, Ancienne-Lorette, Canada,"

[78] *British Aerospace Australia, Holden Hill, South Australia.*

[79] *Thermoelectric Cooling Systems Design Guide.* Dallas, Texas: Marlow Industries Inc.

[80] E. Kreyszig, *Advanced Engineering Mathematics.* Wiley Sons, 1988.

[81] A. McInnes and J. Richards, "Thermal Effects in a Coplanar-Pumped Folded-Zigzag Slab Laser," *IEEE J. Quantum Electron.*, vol. 32, no. 7, pp. 1243–1252, 1996.

[82] J. Lortscher, J. Steffen, and G. Herziger, "Dynamic Stable Resonators: A Design Procedure," *Optical and Quantum Electronics*, vol. 7, pp. 505–514, 1975.

[83] R. Adler, "A Study of Locking Phenonema in Oscillators," *Proc. IRE*, vol. 34, pp. 351–357, 1946.

[84] W. Chow, "Theory of Line Narrowing and Frequency Selection in an Injection Locked Laser," *IEEE J. Quantum Electron.*, vol. 19, pp. 243–249, 1983.

[85] E. H. Huntington, C. C. Harb, T. C. Ralph, H. A. Bachor, and D. E. McClelland, "Investigation of Polarisation Effects in Injection Locked Lasers," *Appl. Phys. B*, vol. 64, pp. 507–514, 1997.

[86] N. Lesage, G. Mullot, Y. Andre, and G. Bourdet, "Servo-Loop Based on Heterodyne Interferometry for Injection Locking of CW Nd:YAG Lasers," *Optics Communications*, vol. 115, pp. 291–296, 1995.

[87] D. Anderson, "Alignment of Resonant Optical Cavities," *Applied Optics*, vol. 23, pp. 2944–2949, 1984.

[88] H. Kolgelnik and T.Li, "Laser Beams and Resonators," *Applied Optics*, vol. 5, pp. 1550–1566, 1966.

[89] G. Cantatore, F. D. Valle, E. Milotti, P. Pace, E. Zavattini, E. Polacco, F. Perrone, C. Rizzo, G. Zavattini, and G. Ruoso, "Frequency Locking of a Nd:YAG Laser Using the laser itself as the Optical Phase Modulator," *Rev. Sci. Instrum.*, vol. 66, pp. 2785–2787, 1995.

[90] *Piezo Ceramics.* Denmark: Ferroperm.

[91] *Guide to Modern Piezoelectric Ceramics.* Morgan Matroc, Bedford, Ohio.

[92] *Data Sheet for PA 85A.* Apex Microtechnology Corporation, Tucson, Arizona.